



# Quantum Gates for Electronics Engineers

Mattia Borgarino <sup>1,2,\*</sup>  and Alessandro Badiali <sup>1,3</sup> 

- <sup>1</sup> Enzo Ferrari Engineering Department, University of Modena and Reggio Emilia, 41125 Modena, Italy; alessandro.badiali01@universitadipavia.it
- <sup>2</sup> Consorzio Nazionale Interuniversitario per le Telecomunicazioni (CNIT), 43124 Parma, Italy
- <sup>3</sup> Department of Electrical, Computer and Biomedical Engineering, University of Pavia, 27100 Pavia, Italy
- \* Correspondence: mattia.borgarino@unimore.it; Tel.: +39-059-2056168

**Abstract:** The design of a solid-state quantum processor is nowadays a hot research topic in micro-electronics. Like the logic gates in a classical processor, quantum gates serve as the fundamental building blocks for quantum processors. The main goal of the present paper is to deduce the matrix of the main one- and two-qubit quantum gates from the Schrödinger equation. The mathematical formalism is kept as comfortable as possible for electronics engineers. This paper does not cover topics such as dissipations, state density, coherence, and state purity. In a similar manner, this paper also deals with the quantum nature of a quantum processor by leveraging the concept of a finite-state machine, which is a background notion for any electronics engineer.

**Keywords:** quantum gates; matrix; Schrödinger equation; electron spin qubits

## 1. Introduction

Despite the traditional dominance of a hydrocarbon-based global economy, the first two decades of the XXI century witnessed a substantial influence of information technology on the geopolitical scale. According to the Forbes survey of June 2023, three out of the top five global companies in terms of market capitalization (MCAP) operate within the information and communication technology (ICT) sector, with a collective consolidated MCAP of about USD 6300 billion [1]. One company only, positioned third in the ranking with an MCAP of about USD 2000 billion, operates in the field of fossil energy resources. The fifth company is involved in the field of online retail, with an MCAP of about USD 1100 billion.

The dawn of the silicon-based digital information era can be conventionally marked in 1971, with the release of the first commercial poly-silicon gate, self-aligned MOSFET microprocessor [2]. Since that year, the strong synergy between microelectronics and computer science has fundamentally reshaped the technological landscape.

Data and artificial intelligence (AI) are the main drivers of actual information technology. AI algorithms, in their various flavors, are only a side of the equation. The other side is specialized AI chips (e.g., neuromorphic processors), tailored to specific software and business requirements. In this area of AI-oriented microelectronics, quantum processing units (QPUs) are gaining increasing interest. Indeed, they enable the actual execution of quantum algorithms. These algorithms, leveraging the laws of quantum mechanics (QM), pave the way to efficient solutions of mathematical or optimization problems, which, due to their non-deterministic polynomial nature, are not attackable even by the best classical algorithms, because the solution time or the required resources increase exponentially with the problem size [3]. This is exemplified by the world-famous Shor algorithm for prime number factorization [4]. Quantum algorithms offer the possibility to speed up calculations that would require a prohibitive amount of time using a classical approach. For instance, the Harrow–Hassidim–Lloyd (HHL) quantum algorithm promises exponential speed-ups in solving linear equation systems [5]. In 2023, the historical company Rolls-Royce signed



**Citation:** Borgarino, M.; Badiali, A. Quantum Gates for Electronics Engineers. *Electronics* **2023**, *12*, 4664. <https://doi.org/10.3390/electronics12224664>

Academic Editor: Jian-Qiang You

Received: 6 October 2023

Revised: 7 November 2023

Accepted: 13 November 2023

Published: 15 November 2023



**Copyright:** © 2023 by the authors. Licensee MDPI, Basel, Switzerland. This article is an open access article distributed under the terms and conditions of the Creative Commons Attribution (CC BY) license (<https://creativecommons.org/licenses/by/4.0/>).

agreements with ICT companies to develop quantum algorithms aimed at addressing the notably hard differential fluid dynamic equations crucial for the design of efficient avionic turbojet engines [6]. Quantum algorithms also hold the potential to speed up AI software technologies like deep learning and machine learning when applied to massive datasets [7]. It is worth noting that quantum algorithms can be emulated on traditional microprocessors but at the cost of a significant loss of efficiency [8]. Consequently, major players in the ICT sector, including IBM [9–13], Honeywell [14], Intel [9,15–18], Google [9,19–21], IonQ [22,23], and Rigetti [24], are investing significant efforts in gaining expertise and capabilities to fabricate their own QPU. Figure 1 shows that these endeavors have led to an exponential increase over time in the quantum bits (or qubits), the quantum counterparts of the traditional bits, hosted in a single QPU. The IBM roadmap envisions a QPU with 4158 qubits in the near future and approximately 100,000 qubits in the next decade [25]. Regardless of the more or less rigorous definition of quantum supremacy, a 100,000-qubit QPU is estimated as a landmark for the addressing of engineering problems of practical relevance.

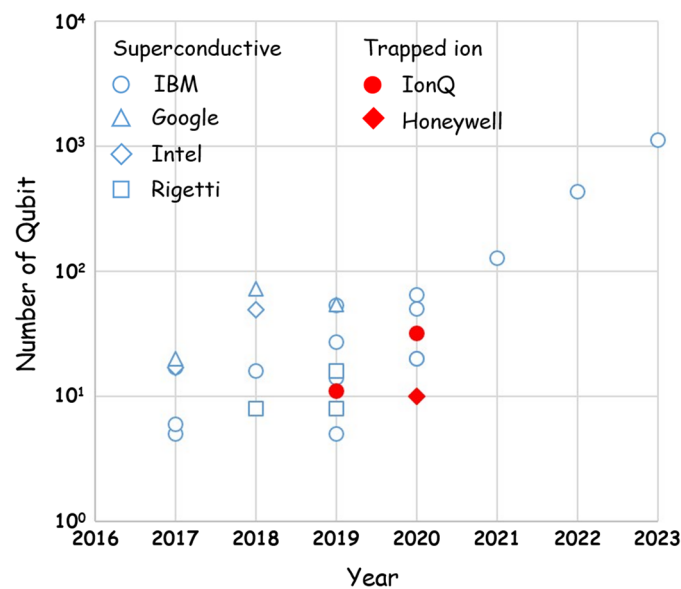


Figure 1. Number of qubits in a single QPU versus time [9–24].

Any two-state quantum-mechanical system can encode a qubit. Examples include the presence/absence of charge in a couple of quantum dots (QDs) (charge qubit) [26], the spin orientation of an electron confined in a QD (electron spin qubit) [27], the presence/absence of a Cooper pair in a superconductive island (transmon qubit), the clockwise/counter-clockwise current flow around a superconductive loop (flux qubit) [28], or the ground/excited states of a radio frequency (RF)-trapped ion (trapped ion qubit) [29]. All these qubits need to work at cryogenic temperatures to preserve their quantum properties. Figure 1 reveals that the superconductive qubit is the current predominant choice. Often fashioned as transmons, superconductive qubits offer several compelling advantages, including lower sensitivity to charge noise, greater tolerance against fabrication variations, engineerable properties, and compatibility with the current complementary metal oxide semiconductor (CMOS) microelectronics manufacturing processes. The size is the main drawback of the transmon qubits. Essentially, a transmon is an anharmonic oscillator designed with capacitors, inductors, and Josephson junctions acting as a non-linear inductor. Because of all these inductors and capacitors, transmons exhibit a footprint that is orders of magnitude larger than that of QDs. On the other hand, charge qubits offer both small footprints and CMOS compatibility, but they suffer from a sensitivity to charge noise. Lower sensitivity can be achieved by magnetically coupling the qubit, as in the case of the electron spin qubit, which also offers small footprints and CMOS compatibility. The drawback of the spin qubit is a slower operating speed compared to the charge qubit, mainly because the magnetic coupling is weaker than the electric one [26].

Here, it is worth remarking that, in light of Figure 1, the IBM prediction of achieving a 100,000-qubit QPU by 2033 may sound excessively conservative. The exponential trend in Figure 1, with its slope of about 1dec/2 years, could indicate that this milestone could be achieved in about 4–5 years from the present. The necessity for the individual addressing of each qubit within the QPU may partially support this conservative position.

The current practice, widely adopted in several research labs, involves generating the control and readout signals using off-QPU room temperature circuitry. This approach is conceivable only for a limited number of qubits. When dealing with a large number of qubits (e.g., 100,000), it is mandatory to envisage a solution based on a chipset constituted by, at least, a quantum chip for the QPU and a classical chip for the control and readout circuitry. The classical chip should stay as close as possible to the QPU. It should thus operate at cryogenic temperatures. Moreover, the number of cables connecting the quantum microprocessor to the classical microprocessor running the software should be kept as low as possible.

In this perspective, CMOS integrated circuits offer a promising solution, as Reilly suggested in 2015 [30] and Charbon investigated in 2017 [31]. Presently, several high-tech companies are investing in cryogenic CMOS integrated chipsets for their quantum microprocessors [32]. Consequently, they also share the need for electronics engineers for the design of cryogenic CMOS chipsets. This situation is reminiscent of the early years of the XXI century, when the proliferation of radio frequency mobile devices for telecommunications induced the need for radio frequency integrated circuit (RFIC) designers. The above-presented overview emphasizes the dynamic nature of the field, necessitating a quantitatively and qualitatively more advanced migration of quantum concepts from physics to electronics engineering. The fundamentals of electron devices for electronics engineers typically do not require systematically resorting to QM. Once the origin of the conduction and valence bands is explained by means of the simple 1931 Kronig–Penney model and the Fermi–Dirac statistics are introduced, QM concepts are no longer necessary. However, this is not the case for electronics engineers in charge of designing cryogenic CMOS chips for a quantum microprocessor. These cryogenic circuits should control and read out devices that are intrinsically single quantum objects, not reducible to a semi-classical collective behavior. To design them effectively, electronics engineers need to grasp quantum physics concepts and communicate effectively with physicists. In the current early development phase of quantum computing hardware, a close and rigorous collaboration between physicists and electronics engineers is indeed mandatory, similar to the cooperation that occurred in the fifties and sixties of the past century during the growth of microelectronics [33,34].

The aim of the present paper is to introduce the fundamental components of a QPU, specifically the quantum gates, using a mathematical formalism as accessible as possible for electronics engineers. Section 2 addresses the nature of a quantum microprocessor by leveraging the notion of a finite-state machine, a concept familiar to electronics engineers. Section 3 introduces the Bloch sphere together with other generalities about a qubit. Section 4 focuses on the physics of the single-electron-spin qubit and Section 5 deduces the main one-qubit quantum gates. In the same way, Section 6 addresses the physics of the two-electron-spin qubit, and Section 7 deduces the main two-qubit quantum gates. The electron spin qubit has been chosen, in virtue of its potential as an attractive option for future QPUs, given its advantages such as lower charge noise sensitivity, a small footprint, and compatibility with CMOS technology. Here, it is worth reminding the reader that the electron spin qubit was the first qubit suggested for quantum computation in 1998 by DiVincenzo [27]. Charge qubits have been ruled out as they currently appear less appealing. Superconductive qubits and trapped ion qubits have also been excluded, despite their presence in Figure 1, due to their more complex mathematical treatment, which does not well fit the goals of the present paper. Section 8 reports on the Deutsch quantum algorithm with the aim of giving evidence that a quantum microprocessor may speed up the solution of mathematical problems. Eventually, Section 9 ends the paper by summarizing key points and by drawing some conclusions.

## 2. On the Nature of a Quantum Microprocessor

From a general point of view, a microprocessor can be described as a finite-state machine whose behavior is controlled by a program that implements an algorithm. In the case of a classical microprocessor, the machine state can be stored in a bank of latches, each memorizing a single bit.

In the simple case of the four-state machine in Figure 2, this bank, and thus, the state of the finite-state machine, can be mathematically represented as a vector. Meanwhile, a matrix, dubbed the transition state matrix, describes how the state evolves over time after the execution of each step in the algorithm. The entries of the matrix can be either 1 or 0. Programming the machine means specifying the entries in the transition state matrix. For each column, the sum of all entries should be 1, ensuring that the machine always has a path to transition from its current state to a future one. For instance, the red dashed line in the figure shows that the current state  $S_2$  leads to the future state  $S_4$ . It is worth remarking that, for a finite-state machine, it is praxis to introduce the terms of current and future states because the microprocessor is a clocked electronics system. In the frame of quantum physics, it is more common to use the terms input and output state.

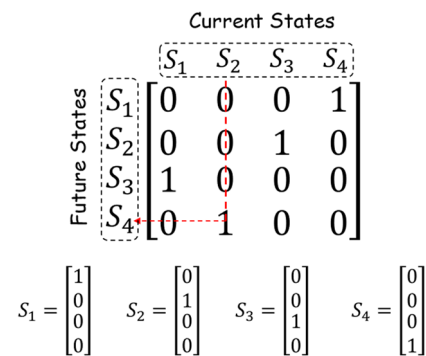


Figure 2. Transition matrix for a deterministic four-state microprocessor.

The future state vector can be calculated by multiplying the transition state matrix by the current vector state.

$$\begin{bmatrix} 0 & 0 & 0 & 1 \\ 0 & 0 & 1 & 0 \\ 1 & 0 & 0 & 0 \\ 0 & 1 & 0 & 0 \end{bmatrix} \begin{bmatrix} 0 \\ 1 \\ 0 \\ 0 \end{bmatrix} = \begin{bmatrix} 0 \\ 0 \\ 0 \\ 1 \end{bmatrix} = S_4$$

Similarly, by assuming that  $S_1$  is the initial state and that the algorithm ends after three steps, one can calculate the final state  $S_{Final}$  by means of three products carried out from the right to the left:

$$S_{Final} = \begin{bmatrix} 0 & 0 & 0 & 1 \\ 0 & 0 & 1 & 0 \\ 1 & 0 & 0 & 0 \\ 0 & 1 & 0 & 0 \end{bmatrix} \begin{bmatrix} 0 & 0 & 0 & 1 \\ 0 & 0 & 1 & 0 \\ 1 & 0 & 0 & 0 \\ 0 & 1 & 0 & 0 \end{bmatrix} \begin{bmatrix} 0 & 0 & 0 & 1 \\ 0 & 0 & 1 & 0 \\ 1 & 0 & 0 & 0 \\ 0 & 1 & 0 & 0 \end{bmatrix} \begin{bmatrix} 1 \\ 0 \\ 0 \\ 0 \end{bmatrix} = \begin{bmatrix} 0 \\ 0 \\ 0 \\ 1 \end{bmatrix} = S_4 \quad (1)$$

Considering the deterministic nature of the final result, it is sufficient to execute the algorithm only once to determine the output of the algorithm.

Now, let us shift the perspective slightly by interpreting the 1 and 0 values of the entries of the matrix in Figure 2 as transition probabilities of 100% and 0%, respectively. If you enter the matrix with the state  $S_2$ , you have a 100% probability (certain event) of reaching the state  $S_4$  and a 0% probability (impossible event) of reaching any other state. Under this probabilistic interpretation, Figure 3 shows that the entries of the transition matrix can also assume fractional values while still fulfilling the constraint that the sum of their values in each column should be 1. This means that the microprocessor evolves

certainly from the current state to some future state, reachable with a given probability. The finite-state machine therefore proceeds as a Markov process.

		Current States			
		S <sub>1</sub>	S <sub>2</sub>	S <sub>3</sub>	S <sub>4</sub>
Future States	S <sub>1</sub>	0	1/2	0	1/8
	S <sub>2</sub>	1/2	0	1/3	1/8
	S <sub>3</sub>	1/2	1/4	1/3	0
	S <sub>4</sub>	0	1/4	1/3	3/4

Figure 3. Transition matrix for a stochastic four-state microprocessor.

Using the example in Figure 3, the transition probability from the current state S<sub>1</sub> to the future states S<sub>2</sub> and S<sub>3</sub> is 50% with a consolidated probability of 100%. Even when the current state is certain, the future state is not deterministic. The future state vector is therefore a vector of probabilities, with its entries summing to 1, indicating that the future state of the machine is certainly one out of the possible four states.

Like the previous case, the future state vector can be calculated by multiplying the current state vector by the transition matrix. Assuming that S<sub>1</sub> in Figure 2 is the initial state of the microprocessor and that the algorithm ends after three steps, the final state S<sub>Final</sub> is as follows:

$$S_{Final} = \begin{bmatrix} 0 & 1/2 & 0 & 1/8 \\ 1/2 & 0 & 1/3 & 1/8 \\ 1/2 & 1/4 & 1/3 & 0 \\ 0 & 1/4 & 1/3 & 3/4 \end{bmatrix} \begin{bmatrix} 0 & 1/2 & 0 & 1/8 \\ 1/2 & 0 & 1/3 & 1/8 \\ 1/2 & 1/4 & 1/3 & 0 \\ 0 & 1/4 & 1/3 & 3/4 \end{bmatrix} \begin{bmatrix} 0 & 1/2 & 0 & 1/8 \\ 1/2 & 0 & 1/3 & 1/8 \\ 1/2 & 1/4 & 1/3 & 0 \\ 0 & 1/4 & 1/3 & 3/4 \end{bmatrix} \begin{bmatrix} 1 \\ 0 \\ 0 \\ 0 \end{bmatrix} = \begin{bmatrix} 23/192 \\ 149/576 \\ 19/72 \\ 103/288 \end{bmatrix} \cong \begin{bmatrix} 0.120 \\ 0.259 \\ 0.264 \\ 0.358 \end{bmatrix} \quad (2)$$

Please note that the sum of all the entries in the probability vector for the final state equals 1. As in the case in Figure 2, at the end of each algorithm execution, you observe only one of the four possible states. Nevertheless, since the microprocessor behaves like a random state machine, you cannot predict the output state. If you desire to observe the output of the algorithm, that is, the final state vector in Equation (2), you need to run the algorithm several times and calculate the resulting statistics. If the algorithm addresses some specific problem, the most reliable solution is the one with the highest probability state; for instance, the state S<sub>4</sub> in Equation (2). A higher difference in probability among the possible states implies a higher confidence in the achieved solution. In the simple examples addressed above, Equations (1) and (2) show that the deterministic and the stochastic algorithms yield the same solution. Nevertheless, in principle, the random algorithm may offer solutions that are not conceivable with a deterministic algorithm.

The entries of the state transition matrix in Figure 3 are real-valued, classical probabilities. Now, let us assume that they are complex-valued, as depicted in Figure 4. In QM, the complex-valued entries are probability amplitudes, and according to the 1926 Born interpretation [35], their squared modules represent probabilities. Consequently, the constraint on the entries is that the sum of their squared modules should be 1 for each column.

		Current States			
		S <sub>1</sub>	S <sub>2</sub>	S <sub>3</sub>	S <sub>4</sub>
Future States	S <sub>1</sub>	-0.3524 + 0.0359j	0.6290 - 0.3030j	0.5198 - 0.0076j	0.2036 + 0.2746j
	S <sub>2</sub>	0.1989 + 0.0150j	0.2807 + 0.5593j	-0.0576 - 0.4693j	0.5779 - 0.1050j
	S <sub>3</sub>	0.3541 - 0.2112j	-0.1506 - 0.1889j	0.1971 + 0.5831j	0.5994 - 0.1830j
	S <sub>4</sub>	-0.7994 + 0.1603j	0.2409 - 0.0675j	0.3407 - 0.1063j	-0.3810 + 0.0134j

Figure 4. Transition matrix U for a quantum four-state microprocessor.

The matrix U in Figure 4 describes a quantum microprocessor. As for the matrix in Figure 3, the above constraint guarantees that the microprocessor evolves certainly from the current state to some future state, reachable with a given probability. The probabilities

of reaching the future states  $S_1, S_2, S_3,$  and  $S_4$  from the current state  $S_1$  are  $|-0.3524 + j0.0359|^2 \cong 0.1255, |0.1989 + j0.0150|^2 \cong 0.0398, |0.3541 - j0.2112|^2 \cong 0.1700,$  and  $|0.7994 + j0.1603|^2 \cong 0.6647,$  respectively, with an aggregate probability of 100%. Note that  $j$  is the imaginary unit.

The final state  $S_{Final}$  reached by a quantum algorithm still can be calculated by means of matrix products. Still assuming that  $S_1$  is the initial state and the algorithm envisages three steps,  $S_{Final}$  is as follows:

$$\begin{aligned}
 S_{Final} &= UUU S_1 = UUU \begin{bmatrix} 1 \\ 0 \\ 0 \\ 0 \end{bmatrix} \\
 &= \begin{bmatrix} 0.2596 - 0.205j & 0.3306 - 0.109j & 0.4538 - 0.3492j & -0.044 + 0.6631j \\ -0.016 - 0.1369j & -0.1716 - 0.1268j & 0.6743 + 0.4339j & 0.5133 - 0.1702j \\ -0.1352 + 0.1664j & 0.8948 + 0.0864j & -0.0099 + 0.0336j & 0.2503 - 0.2865j \\ 0.8916 + 0.1754j & -0.0537 + 0.1494j & -0.1182 - 0.1184j & 0.2804 - 0.2064j \end{bmatrix} \begin{bmatrix} 1 \\ 0 \\ 0 \\ 0 \end{bmatrix} \\
 &= \begin{bmatrix} 0.2596 - 0.205j \\ -0.016 - 0.1369j \\ -0.1352 + 0.1664j \\ 0.8916 + 0.1754j \end{bmatrix}
 \end{aligned} \tag{3}$$

Also in the present case, the algorithm yields  $S_4$  as the solution to the problem because its probability of  $|0.8916 + 0.1754j|^2 \cong 0.8257$  is the highest one. Here, it is worth noting that, in the frame of the QM, the probability vector and the state transition matrix correspond to the state vector  $|\psi\rangle$  and the operator  $\hat{A}$ , respectively [36]. Following John Wheeler, in QM, an operator  $\hat{A}$  can be considered as an engine that receives an input state vector  $|\psi_{IN}\rangle$  and generates an output state  $|\psi_{OUT}\rangle$  [37]. By adopting this physics lexicon, Equation (3) should be commented on in terms of input and output states, corresponding to the current and future state terms, respectively, in the electronics engineering lexicon.

For a better understanding of the nature of the quantum microprocessor, it may be useful to compare the above description with the historical experiment involving fringe patterns generated on a photographic plate by electrons passing through a double slit [38]. In this experiment, the same patterns were obtained by exposing a photographic plate, for a short time, to an electron beam or, for a longer time, to single electrons. In the analogy proposed here, each single execution of the algorithm corresponds to the launch of a single electron through the double slit. The single electron strikes the photographic plate at an unpredictable position, much like the outcome of a single algorithm execution. On the other hand, the final fringe pattern corresponds to the final probability state vector in Equation (3). The final fringe pattern results from averaging the positions where electrons struck the plate after numerous single-electron launches. Similarly, the final probability state vector is calculated by averaging across multiple single outcomes. This highlights that the quantum microprocessor shares with QM the fact of being inductive with respect to single events but predictive for collective events [39].

Although similar considerations could also be carried out for the stochastic microprocessor in Figure 3, the relevant difference between the stochastic and the quantum microprocessors is that only in Equation (3) can destructive interferences occur in the various sums of products, because  $j^2 = -1$ . On the other hand, in Equation (2), the sums can only be additive, because the entries of the matrix are all positive, real-valued probabilities. By referring to the double-slit experiment, since the pattern generated in this experiment is equivalent to the output of the quantum algorithm, it is possible to conclude that, for a given problem, there are solutions attainable (attainable patterns) only when probabilities carry a phase.

### 3. The Bloch Sphere

In his book, Dirac introduced the so-dubbed “ket” notation  $|\psi\rangle$  for the state vector [40]. So, for the four states in Figure 2, you can write  $|\psi_i\rangle = S_i$  for  $i = 1..4$ . For a qubit, which exhibits two possible basis states, you can formulate the following:

$$|\psi_0\rangle = \begin{bmatrix} 1 \\ 0 \end{bmatrix} \tag{4}$$

$$|\psi_1\rangle = \begin{bmatrix} 0 \\ 1 \end{bmatrix} \tag{5}$$

Unlike the classical bit, which can be in only one of the two possible states, in force of the QM Postulates (see, for instance, [36]), the qubit can be in a state  $|\psi\rangle$ , which is the superposition of the two basis states  $|\psi_0\rangle$  and  $|\psi_1\rangle$ :

$$|\psi\rangle = \alpha(t)|\psi_0\rangle + \beta(t)|\psi_1\rangle = \alpha(t) \begin{bmatrix} 1 \\ 0 \end{bmatrix} + \beta(t) \begin{bmatrix} 0 \\ 1 \end{bmatrix} = \begin{bmatrix} \alpha(t) \\ \beta(t) \end{bmatrix} \tag{6}$$

where  $\alpha(t)$  and  $\beta(t)$  are time-variant, complex-valued probability amplitudes. The QM Postulates require also that  $|\alpha(t)|^2 + |\beta(t)|^2 = 1$ . With  $\alpha(t)$  and  $\beta(t)$  in the polar form, you obtain the following:

$$\alpha(t) = r_\alpha(t)e^{j\Phi_\alpha(t)}$$

$$\beta(t) = r_\beta(t)e^{j\Phi_\beta(t)}$$

Equation (6) takes the following form:

$$|\psi\rangle = r_\alpha(t)e^{j\Phi_\alpha(t)}|\psi_0\rangle + r_\beta(t)e^{j\Phi_\beta(t)}|\psi_1\rangle \tag{7}$$

Equation (7) can be split into two mathematical forms depending on the gathered phase:

$$\begin{aligned} |\psi\rangle &= e^{j\Phi_\alpha(t)} \left\{ r_\alpha(t)|\psi_0\rangle + r_\beta(t)e^{j[\Phi_\beta(t) - \Phi_\alpha(t)]}|\psi_1\rangle \right\} \\ |\psi\rangle &= e^{j\Phi_\beta(t)} \left\{ r_\alpha(t)e^{j[\Phi_\alpha(t) - \Phi_\beta(t)]}|\psi_0\rangle + r_\beta(t)|\psi_1\rangle \right\} \end{aligned}$$

Because of Euler’s formula  $e^{jy} = \cos(y) + jsin(y)$ , the two above mathematical expressions can be rewritten as follows:

$$|\psi\rangle = e^{j\Phi_\alpha(t)} \left\{ r_\alpha(t)|\psi_0\rangle + r_\beta(t) \left\{ \cos[\Phi_\beta(t) - \Phi_\alpha(t)] + jsin[\Phi_\beta(t) - \Phi_\alpha(t)] \right\} |\psi_1\rangle \right\} \tag{8}$$

$$|\psi\rangle = e^{j\Phi_\beta(t)} \left\{ r_\alpha(t) \left\{ \cos[\Phi_\alpha(t) - \Phi_\beta(t)] + jsin[\Phi_\alpha(t) - \Phi_\beta(t)] \right\} |\psi_0\rangle + r_\beta(t)|\psi_1\rangle \right\} \tag{9}$$

Since  $|\alpha|^2 + |\beta|^2 = 1$  should be true, Equations (8) and (9), respectively, yield

$$\begin{aligned} \left| e^{j\Phi_\alpha(t)} \right|^2 |r_\alpha(t)|^2 + \left| e^{j\Phi_\alpha(t)} \right|^2 |r_\beta(t)|^2 \left| \cos[\Phi_\beta(t) - \Phi_\alpha(t)] + jsin[\Phi_\beta(t) - \Phi_\alpha(t)] \right|^2 \\ = |r_\alpha(t)|^2 + |r_\beta(t)|^2 \left\{ \cos^2[\Phi_\beta(t) - \Phi_\alpha(t)] + \sin^2[\Phi_\beta(t) - \Phi_\alpha(t)] \right\} \\ = |r_\alpha(t)|^2 + |r_\beta(t)|^2 = \left| r_\alpha(t)e^{j\Phi_\alpha(t)} \right|^2 + \left| r_\beta(t)e^{j\Phi_\beta(t)} \right|^2 \\ = |\alpha(t)|^2 + |\beta(t)|^2 = 1 \end{aligned}$$

$$\begin{aligned}
 & \left| e^{j\Phi_\beta(t)} \right|^2 |r_\alpha(t)|^2 \left| \cos[\Phi_\alpha(t) - \Phi_\beta(t)] + j\sin[\Phi_\alpha(t) - \Phi_\beta(t)] \right|^2 + \left| e^{j\Phi_\beta(t)} \right|^2 |r_\beta(t)|^2 \\
 &= |r_\alpha(t)|^2 \{ \cos^2[\Phi_\alpha(t) - \Phi_\beta(t)] + \sin^2[\Phi_\alpha(t) - \Phi_\beta(t)] \} + |r_\beta(t)|^2 \\
 &= |r_\alpha(t)|^2 + |r_\beta(t)|^2 = \left| r_\alpha(t) e^{j\Phi_\alpha(t)} \right|^2 + \left| r_\beta(t) e^{j\Phi_\beta(t)} \right|^2 \\
 &= |\alpha(t)|^2 + |\beta(t)|^2 = 1
 \end{aligned}$$

where it is accounted that  $\cos^2(x) + \sin^2(x) = 1$ . From Equations (8) and (9), respectively, it is thus possible to write

$$|r_\alpha(t)|^2 + |r_\beta(t)|^2 \cos^2[\Phi_\beta(t) - \Phi_\alpha(t)] + |r_\beta(t)|^2 \sin^2[\Phi_\beta(t) - \Phi_\alpha(t)] = 1 \tag{10}$$

$$|r_\alpha(t)|^2 \cos^2[\Phi_\alpha(t) - \Phi_\beta(t)] + |r_\alpha(t)|^2 \sin^2[\Phi_\alpha(t) - \Phi_\beta(t)] + |r_\beta(t)|^2 = 1 \tag{11}$$

When  $z(t) = r_\alpha(t)$ ,  $x(t) = r_\beta(t)\cos[\Phi_\beta(t) - \Phi_\alpha(t)]$ , and  $y(t) = r_\beta(t)\sin[\Phi_\beta(t) - \Phi_\alpha(t)]$  are defined for Equation (10) and, in the same way,  $z(t) = r_\beta(t)$ ,  $x(t) = r_\alpha(t)\cos[\Phi_\alpha(t) - \Phi_\beta(t)]$ , and  $y(t) = r_\alpha(t)\sin[\Phi_\alpha(t) - \Phi_\beta(t)]$  are defined for Equation (11), Equations (10) and (11) assume the compact form  $x(t)^2 + y(t)^2 + z(t)^2 = 1$ , which describes a unitary sphere in the three-dimensional Cartesian space (x, y, z), dubbed the Bloch sphere. On the other hand, by remembering the relationship of the Cartesian coordinates with the spherical ones in Figure 5 with  $r = 1$ , that is,  $x = \sin\theta\cos\Phi$ ,  $y = \sin\theta\sin\Phi$ , and  $z = \cos\theta$ , for Equation (10), you obtain the following:

$$\begin{aligned}
 x(t) &= r_\beta(t)\cos[\Phi_\beta(t) - \Phi_\alpha(t)] = \sin[\theta(t)]\cos[\Phi(t)] \\
 y(t) &= r_\beta(t)\sin[\Phi_\beta(t) - \Phi_\alpha(t)] = \sin[\theta(t)]\sin[\Phi(t)] \\
 z(t) &= r_\alpha(t) = \cos[\theta(t)]
 \end{aligned}$$

from which

$$r_\alpha(t) = \cos[\theta(t)] \tag{12}$$

$$r_\beta(t) = \sin[\theta(t)] \tag{13}$$

$$\Phi_\beta(t) - \Phi_\alpha(t) = \Phi(t) \tag{14}$$

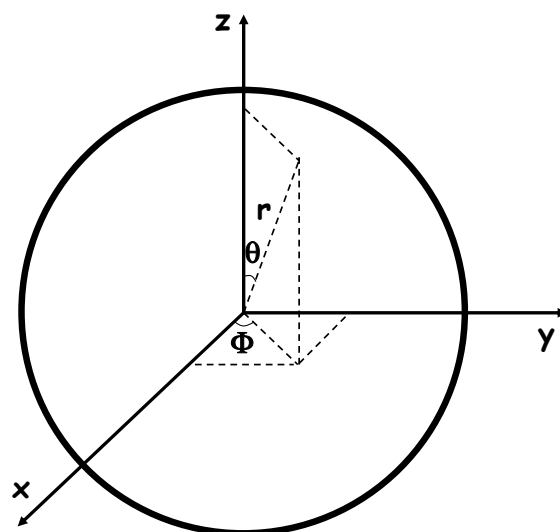


Figure 5. The Bloch sphere.



Similarly, for Equation (11), you obtain the following:

$$\begin{aligned} x(t) &= r_\alpha(t)\cos[\Phi_\alpha(t) - \Phi_\beta(t)] = \sin[\theta(t)]\cos[\Phi(t)] \\ y(t) &= r_\alpha(t)\sin[\Phi_\alpha(t) - \Phi_\beta(t)] = \sin[\theta(t)]\sin[\Phi(t)] \\ z(t) &= r_\beta(t) = \cos[\theta(t)] \end{aligned}$$

from which

$$r_\alpha(t) = \sin[\theta(t)] \tag{15}$$

$$r_\beta(t) = \cos[\theta(t)] \tag{16}$$

$$\Phi_\alpha(t) - \Phi_\beta(t) = \Phi(t) \tag{17}$$

Equations (12)–(17) allow for writing Equations (8) and (9) by means of the angles  $\theta$  and  $\Phi$ :

$$|\psi\rangle = e^{j\Phi_\alpha(t)}\{\cos[\theta(t)]|\psi_0\rangle + \sin[\theta(t)]\{\cos[\Phi(t)] + jsin[\Phi(t)]\}|\psi_1\rangle\} = e^{j\Phi_\alpha(t)}\{\cos[\theta(t)]|\psi_0\rangle + \sin[\theta(t)]e^{j\Phi(t)}|\psi_1\rangle\} \tag{18}$$

$$|\psi\rangle = e^{j\Phi_\beta(t)}\{\sin[\theta(t)]\{\cos[\Phi(t)] + jsin[\Phi(t)]\}|\psi_0\rangle + \cos[\theta(t)]|\psi_1\rangle\} = e^{j\Phi_\beta(t)}\{\sin[\theta(t)]e^{j\Phi(t)}|\psi_0\rangle + \cos[\theta(t)]|\psi_1\rangle\} \tag{19}$$

where the Euler formula has been applied again.

It is now worth noting that for  $\theta = 0$ , you obtain the following:

$$|\psi\rangle = e^{j\Phi_\alpha(t)}|\psi_0\rangle \tag{20}$$

$$|\psi\rangle = e^{j\Phi_\beta(t)}|\psi_1\rangle \tag{21}$$

while for  $\theta = \pi/2$ , you obtain the following:

$$|\psi\rangle = e^{j\Phi_\alpha(t)}e^{j\Phi(t)}|\psi_1\rangle = e^{j[\Phi_\alpha(t)+\Phi(t)]}|\psi_1\rangle \tag{22}$$

$$|\psi\rangle = e^{j\Phi_\beta(t)}e^{j\Phi(t)}|\psi_0\rangle = e^{j[\Phi_\beta(t)+\Phi(t)]}|\psi_0\rangle \tag{23}$$

Since the complex exponential multiplying the states does not impact the module of the probability amplitudes, because their module is 1, Equations (20)–(23) suggest that the possible states of the qubit can be described with  $\theta$  spanning the interval  $[0 \dots \pi/2]$ . On the Bloch sphere, this can be accounted for by reformulating Equations (18) and (19) as follows:

$$|\psi\rangle = e^{j\Phi_\alpha(t)}\left\{\cos\frac{\theta(t)}{2}|\psi_0\rangle + e^{j\Phi(t)}\sin\frac{\theta(t)}{2}|\psi_1\rangle\right\} \tag{24}$$

$$|\psi\rangle = e^{j\Phi_\beta(t)}\left\{e^{j\Phi(t)}\sin\frac{\theta(t)}{2}|\psi_0\rangle + \cos\frac{\theta(t)}{2}|\psi_1\rangle\right\} \tag{25}$$

The two angles  $\theta$  and  $\Phi$  allow for representing all the qubit states on the Bloch sphere.

Equations (24) and (25) show that the qubit state vector is, in general, a complex-valued vector, of which Equations (4) and (5) are special cases. In Dirac’s notation, the complex transposed state is symbolized with  $\langle l$ , dubbed the “bra” [40]. So, for instance, the bras for Equations (4) and (5) are as follows:

$$\langle\psi_0| = \begin{bmatrix} 1 \\ 0 \end{bmatrix}^\dagger = [1 \quad 0] \tag{26}$$

$$\langle \psi_1 | = \begin{bmatrix} 0 \\ 1 \end{bmatrix}^\dagger = [0 \quad 1] \tag{27}$$

It is straightforward to observe that  $\langle \psi_i | \psi_j \rangle$  is 1 if  $i = j$  and 0 otherwise. Mathematically speaking, the states  $|\psi_0\rangle$  and  $|\psi_1\rangle$  are orthonormal with respect to the product  $\langle \cdot | \cdot \rangle$ . Physically speaking, the two states are distinguishable.

Eventually, it is worth noting that the complex transposed of  $z|\psi\rangle$  is  $\langle \psi | z^*$ , with  $z^*$  being the complex conjugate of the complex number  $z$ . As a consequence, when taking into consideration Equations (26) and (27), the bra of Equation (6) is as follows:

$$\langle \psi | = \langle \psi_0 | \alpha^*(t) + \langle \psi_1 | \beta^*(t) = [1 \quad 0] \alpha^*(t) + [0 \quad 1] \beta^*(t) = [\alpha^*(t) \quad \beta^*(t)] \tag{28}$$

#### 4. Physics of the One-Electron-Spin Qubit

In the semi-classical description of the atom, the electron revolves in a circular orbit around the nucleus. It thus possesses an orbital angular moment  $L$  and, since it carries charge, also an orbital magnetic moment  $\mu_L = -g_L qL/2m$ , where  $q$  and  $m$  are the charge and the mass of the electron, respectively [36]. The term  $g_L$  is the electron orbital g-factor about equal to 1. In their effort to explain the Stern–Gerlach experiment [36], in 1925, Goudsmit and Uhlenbeck assigned an intrinsic spin angular moment  $S$  to the electron. Here, it is worth quoting Uhlenbeck’s words from [41]: “It was then that it occurred to me that, since (as I have learned) each quantum number corresponds to a degree of freedom of the electron, the fourth quantum number must mean that the electron had an additional degree of freedom, in other words the electron must be rotating.” In analogy to  $L$  and  $\mu_L$ , Goudsmit and Uhlenbeck associated an intrinsic magnetic moment  $\mu_S$  with  $S$  [36]:

$$\vec{\mu}_S = -g_S \frac{q}{2m} \vec{S} = -g \frac{q}{2m} (S_X \vec{x} + S_Y \vec{y} + S_Z \vec{z}) \tag{29}$$

where  $g_S$  is the electron spin g-factor, about equal to 2, and  $S_X, S_Y,$  and  $S_Z$  are the components of  $S$  in a Cartesian reference system. Since the components of  $S$  are physical observables, the QM Postulates (see, for instance, [36]) associate the operators  $\hat{S}_X, \hat{S}_Y,$  and  $\hat{S}_Z$  with them:

$$\hat{S}_X = \frac{\hbar}{2} \begin{pmatrix} 0 & 1 \\ 1 & 0 \end{pmatrix} \tag{30}$$

$$\hat{S}_Y = \frac{\hbar}{2} \begin{pmatrix} 0 & -j \\ j & 0 \end{pmatrix} \tag{31}$$

$$\hat{S}_Z = \frac{\hbar}{2} \begin{pmatrix} 1 & 0 \\ 0 & -1 \end{pmatrix} \tag{32}$$

where  $\hbar$  is the reduced Planck’s constant and  $j$  is the imaginary unit. As in Figure 4, Equations (30)–(32) describe the operators  $\hat{S}_X, \hat{S}_Y,$  and  $\hat{S}_Z$  in a matrix notation. These matrices are known as the X, Y, and Z Pauli matrices. The substitution of Equations (30)–(32) into Equation (29) yields

$$\hat{\mu}_S = -g \frac{q}{2m} \frac{\hbar}{2} \left[ \begin{pmatrix} 0 & 1 \\ 1 & 0 \end{pmatrix} \vec{x} + \begin{pmatrix} 0 & -j \\ j & 0 \end{pmatrix} \vec{y} + \begin{pmatrix} 1 & 0 \\ 0 & -1 \end{pmatrix} \vec{z} \right] \tag{33}$$

where  $x, y,$  and  $z$  are the unitary vectors of the Cartesian axis. As in the Stern–Gerlach experiment, you need a magnetic field to make the quantization observable. The potential energy  $-\mu_S \cdot \mathbf{B}$  is the total energy of an electron with an intrinsic magnetic moment  $\mu_S$ , confined in a QD, and in the presence of a magnetic field  $\mathbf{B}$ . In virtue of Equation (33)

and of the QM Postulates (see, for instance, [36]), to this energy corresponds the following Hamiltonian operator  $\hat{H}$ :

$$\hat{H} = \frac{g\mu_B}{2} \left[ \begin{pmatrix} 0 & 1 \\ 1 & 0 \end{pmatrix} \vec{x} + \begin{pmatrix} 0 & -j \\ j & 0 \end{pmatrix} \vec{y} + \begin{pmatrix} 1 & 0 \\ 0 & -1 \end{pmatrix} \vec{z} \right] \cdot (B_x \vec{x} + B_y \vec{y} + B_z \vec{z}) \tag{34}$$

where  $B_x$ ,  $B_y$ , and  $B_z$  are the components of  $\mathbf{B}$  and  $\mu_B = q\hbar/2m$  is the Bohr magneton. Still after the QM Postulates, the electron spin qubit evolves in obedience to the following Schrödinger equation:

$$j\hbar \begin{bmatrix} \frac{\partial \alpha(t)}{\partial t} \\ \frac{\partial \beta(t)}{\partial t} \end{bmatrix} = \frac{g\mu_B}{2} \begin{bmatrix} B_z & B_x - jB_y \\ B_x + jB_y & -B_z \end{bmatrix} \begin{bmatrix} \alpha(t) \\ \beta(t) \end{bmatrix} \tag{35}$$

where the state of the electron has been described after Equation (6). Equation (35) is equivalent to the following system of differential equations:

$$\begin{cases} j\hbar \frac{\partial \alpha(t)}{\partial t} = \frac{g\mu_B}{2} [B_z \alpha(t) + B_x \beta(t) - jB_y \beta(t)] \\ j\hbar \frac{\partial \beta(t)}{\partial t} = \frac{g\mu_B}{2} [B_x \alpha(t) + jB_y \alpha(t) - B_z \beta(t)] \end{cases} \tag{36}$$

The component  $B_z$  is a DC large value  $B_0$  corresponding to the strong magnet used by Stern and Gerlach to induce the spatial quantization. On the other hand, the other two components  $B_x$  and  $B_y$  are time-variant and have an amplitude value of  $B_1$  much lower than  $B_0$ . In this way, you can write

$$\begin{aligned} B_z &= B_0 \\ B_x &= B_1 \cos(\omega t) \\ B_y &= B_1 \sin(\omega t) \end{aligned} \tag{37}$$

Note that  $B_x$  and  $B_y$  describe a magnetic field rotating on a plane normal to the  $z$  axis. The substitution of Equation (37) into Equation (36) yields

$$\begin{cases} \frac{\partial \alpha(t)}{\partial t} = -j \frac{g\mu_B B_0}{2\hbar} \alpha(t) - j \frac{g\mu_B B_1}{2\hbar} [\cos(\omega t) - j \sin(\omega t)] \beta(t) \\ \frac{\partial \beta(t)}{\partial t} = -j \frac{g\mu_B B_1}{2\hbar} [\cos(\omega t) + j \sin(\omega t)] \alpha(t) + j \frac{g\mu_B B_0}{2\hbar} \beta(t) \end{cases} \tag{38}$$

The mathematical form of Equation (38) can be simplified by remembering the Euler formula and by introducing the frequencies  $\omega_0 = g\mu_B B_0/2\hbar$  and  $\omega_1 = g\mu_B B_1/2\hbar$ :

$$\begin{cases} \frac{\partial \alpha(t)}{\partial t} = -j\omega_0 \alpha(t) - j\omega_1 e^{-j\omega t} \beta(t) \\ \frac{\partial \beta(t)}{\partial t} = -j\omega_1 e^{j\omega t} \alpha(t) + j\omega_0 \beta(t) \end{cases} \tag{39}$$

The frequencies  $2\omega_0$  and  $2\omega_1$  are known as the Larmor and Rabi frequencies, respectively. The writing of Equation (39) in matrix form reveals the two frequencies  $-\omega_0$  and  $\omega_0$  on the main diagonal, corresponding, respectively, to the two energy levels  $-\hbar\omega_0$  and  $\hbar\omega_0$  exhibited by the qubit:

$$\begin{bmatrix} \frac{\partial \alpha(t)}{\partial t} \\ \frac{\partial \beta(t)}{\partial t} \end{bmatrix} = j \begin{bmatrix} -\omega_0 & -\omega_1 e^{-j\omega t} \\ -\omega_1 e^{j\omega t} & \omega_0 \end{bmatrix} \begin{bmatrix} \alpha(t) \\ \beta(t) \end{bmatrix} \tag{40}$$

A quantum of electromagnetic energy of frequency  $\omega = 2\omega_0$  thus stimulates the transition from one state to the other. The condition  $\omega = 2\omega_0$  is known as the resonance condition.

For the initial conditions  $\alpha(t=0) = 0$  and  $\beta(t=0) = 1$  and under the condition  $\omega = 2\omega_0$ , the solution of Equation (39) is as follows (see Appendix A):

$$|\psi\rangle = e^{-j\omega_0 t} \left[ e^{-j\frac{\pi}{2}} \sin(\omega_1 t) |\psi_0\rangle + \cos(\omega_1 t) |\psi_1\rangle \right] \tag{41}$$

A comparison of Equation (41) with Equations (24) and (25) shows that Equation (25) is most apt to describe on the Bloch sphere the effect of the rotating magnetic field on the state  $|\psi\rangle$ . The state vector of the qubit rotates around the x axis ( $\Phi = -\pi/2$ ), as depicted on the left in Figure 6, at an angular speed equal to the Rabi frequency  $2\omega_1$ .

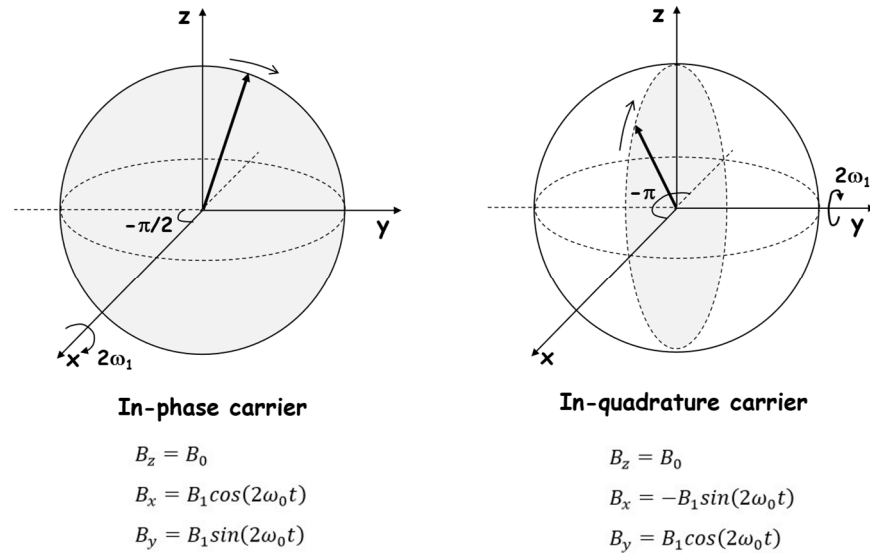


**Figure 6.** Rotation on the Bloch sphere of the qubit state vector for an in-phase (on the left) and an in-quadrature (on the right) carrier at frequency  $\omega = 2\omega_0$ .

On the other hand, for the initial conditions  $\alpha(t = 0) = 1$  and  $\beta(t = 0) = 0$ , still under the condition  $\omega = 2\omega_0$ , the solution of Equation (39) is as follows (see Appendix A):

$$|\psi\rangle = e^{-j\omega_0 t} \left[ \cos\omega_1 t |\psi_0\rangle + e^{-j\frac{\pi}{2}} \sin\omega_1 t |\psi_1\rangle \right] \tag{42}$$

In this case, Equation (24) well depicts the effect of the rotating magnetic field on  $|\psi\rangle$ . Like Equation (41), Equation (42) also shows that the state vector of the qubit rotates around the x axis ( $\Phi = -\pi/2$ ) at an angular speed equal to the Rabi frequency  $2\omega_1$ .

Let us assume a magnetic field with the following components:

$$\begin{aligned} B_z &= B_0 \\ B_x &= B_1 \cos\left(\omega t + \frac{\pi}{2}\right) = -B_1 \sin(\omega t) \\ B_y &= B_1 \sin\left(\omega t + \frac{\pi}{2}\right) = B_1 \cos(\omega t) \end{aligned} \tag{43}$$

The difference between Equations (43) and (37) is in the  $B_x$  and  $B_y$  components, with  $B_x$  ( $B_y$ ) in Equation (37) being in quadrature with  $B_x$  ( $B_y$ ) in Equation (43).

The substitution of Equation (43) into Equation (36) yields

$$\begin{cases} \frac{\partial \alpha(t)}{\partial t} = -j\omega_0 \alpha(t) + \omega_1 [j \sin(\omega t) - \cos(\omega t)] \beta(t) \\ \frac{\partial \beta(t)}{\partial t} = \omega_1 [j \sin(\omega t) + \cos(\omega t)] \alpha(t) + j\omega_0 \beta(t) \end{cases} \tag{44}$$

where the reader is reminded that  $\omega_0 = g\mu_B B_0 / 2\hbar$  and  $\omega_1 = g\mu_B B_1 / 2\hbar$ . As for Equation (40), the matrix form of Equation (44) highlights the two frequencies  $-\omega_0$  and  $\omega_0$  on the main diagonal, corresponding to the two energy levels of the qubit.

For the initial conditions  $\alpha(t = 0) = 0$  and  $\beta(t = 0) = 1$  and under the resonance condition  $\omega = 2\omega_0$ , the solution of Equation (44) is as follows (see Appendix B):

$$|\psi\rangle = e^{-j\omega_0 t} \left[ e^{-j\pi} \sin(\omega_1 t) |\psi_0\rangle + \cos(\omega_1 t) |\psi_1\rangle \right] \tag{45}$$

A comparison of Equation (45) with Equations (24) and (25) shows that Equation (25) is the most proper to describe on the Bloch sphere the effect of the rotating magnetic field on  $|\psi\rangle$ . The state vector of the qubit rotates around the y axis ( $\Phi = -\pi$ ), as depicted on the right in Figure 6, at an angular speed equal to the Rabi frequency  $2\omega_1$ .

On the other hand, for the initial conditions  $\alpha(t = 0) = 1$  and  $\beta(t = 0) = 0$ , still under the resonance condition  $\omega = 2\omega_0$ , the solution of Equation (44) is as follows (see Appendix B):

$$|\psi\rangle = e^{-j\omega_0 t} [\cos\omega_1 t |\psi_0\rangle + \sin\omega_1 t |\psi_1\rangle] \tag{46}$$

In this case, Equation (24) better captures the effect of the rotating magnetic field on  $|\psi\rangle$ . As in Equation (45), the state vector of the qubit rotates around the y axis ( $\Phi = 0$ ) at an angular speed equal to the Rabi frequency  $2\omega_1$ .

Table 1 collects Equations (41), (42), (45), and (46) by clearly showing the dependence of the time evolution law of  $|\psi\rangle$  on the carrier phase and the initial condition.

**Table 1.** Time evolution of the qubit state as a function of the carrier phase and the initial condition for an electromagnetic frequency  $\omega = 2\omega_0$ .

<b>In-phase carrier (Rotation around x-axis)</b>	Initial qubit state $ \psi_0\rangle$	$ \psi\rangle = e^{-j\omega_0 t} [\cos(\omega_1 t)  \psi_0\rangle + e^{-j\frac{\pi}{2}} \sin(\omega_1 t)  \psi_1\rangle]$
	Initial qubit state $ \psi_1\rangle$	$ \psi\rangle = e^{-j\omega_0 t} [e^{-j\frac{\pi}{2}} \sin(\omega_1 t)  \psi_0\rangle + \cos(\omega_1 t)  \psi_1\rangle]$
<b>In-quadrature carrier (Rotation around y-axis)</b>	Initial qubit state $ \psi_0\rangle$	$ \psi\rangle = e^{-j\omega_0 t} [\cos(\omega_1 t)  \psi_0\rangle + \sin(\omega_1 t)  \psi_1\rangle]$
	Initial qubit state $ \psi_1\rangle$	$ \psi\rangle = e^{-j\omega_0 t} [e^{-j\pi} \sin(\omega_1 t)  \psi_0\rangle + \cos(\omega_1 t)  \psi_1\rangle]$

### 5. One-Qubit Quantum Gates

As the qubit is the quantum counterpart of the classical bit, a quantum logic gate in a quantum processor is the counterpart of a logic gate in a classical processor. For the electron spin qubit addressed in the previous section, a quantum gate is obtained by applying a transversal magnetic field of components  $B_x$  and  $B_y$  at the resonance frequency to the qubit for a given precise duration. Since this frequency is in the microwave range, the transversal magnetic pulse is a microwave pulse. Several envelopes, such as rectangular, Gaussian, and sinusoidal, are possible for the microwave pulse. If on the one hand, it is desirable that the largest amount of the RF energy is centered around the resonance frequency of the qubit, on the other hand, different envelopes imply different spectral contents of the microwave pulse. For the sake of straightforwardness, the rectangular envelope has been adopted in the present paper even though it leads to a broader spectral content (see Appendix C).

#### 5.1. $R_X$ and Pauli X Quantum Gates

On the Bloch sphere, the quantum gate  $R_X$  is defined by a rotation of an angle  $\theta$  around the x axis of the qubit state vector. After Figure 6, it is obtained by the application of a microwave in-phase carrier pulse at frequency  $2\omega_0$  for a time duration  $t$ . Since the rotation speed of the qubit state vector is  $2\omega_1$ , you obtain  $2\omega_1 t = \theta$ . In virtue of the equations in Table 1, if the initial qubit state is  $|\psi_0\rangle$ , the mathematical expression of the qubit state  $|\psi\rangle$  after the application of the microwave pulse is as follows:

$$|\psi\rangle = e^{-j\omega_0 \frac{\theta}{2\omega_1}} \left[ \cos\frac{\theta}{2} |\psi_0\rangle + e^{-j\frac{\pi}{2}} \sin\frac{\theta}{2} |\psi_1\rangle \right] = e^{-j\omega_0 \frac{\theta}{2\omega_1}} \left[ \cos\frac{\theta}{2} |\psi_0\rangle - j \sin\frac{\theta}{2} |\psi_1\rangle \right] \tag{47}$$

Similarly, if the initial qubit state is  $|\psi_1\rangle$ , the mathematical expression of the qubit state  $|\psi\rangle$  after the application of the microwave pulse is as follows:

$$|\psi\rangle = e^{-j\omega_0 \frac{\theta}{2\omega_1}} \left[ e^{-j\frac{\pi}{2}} \sin\frac{\theta}{2} |\psi_0\rangle + \cos\frac{\theta}{2} |\psi_1\rangle \right] = e^{-j\omega_0 \frac{\theta}{2\omega_1}} \left[ -j \sin\frac{\theta}{2} |\psi_0\rangle + \cos\frac{\theta}{2} |\psi_1\rangle \right] \tag{48}$$

The  $R_X$  quantum gate thus transforms the state  $|\psi_0\rangle$  into the state  $|\psi\rangle = \cos\theta/2|\psi_0\rangle - j\sin\theta/2|\psi_1\rangle$  and the state  $|\psi_1\rangle$  into the state  $|\psi\rangle = -j\sin\theta/2|\psi_0\rangle + \cos\theta/2|\psi_1\rangle$ . Since  $\langle\psi_i|\psi_j\rangle$  is 1 if  $i = j$  and 0 otherwise, the operator  $\hat{A}_{RX}$  associated with the  $R_X$  quantum gate is therefore given by

$$\hat{A}_{RX} = \left[ \cos\frac{\theta}{2}|\psi_0\rangle - j\sin\frac{\theta}{2}|\psi_1\rangle \right] \langle\psi_0| + \left[ -j\sin\frac{\theta}{2}|\psi_0\rangle + \cos\frac{\theta}{2}|\psi_1\rangle \right] \langle\psi_1| \tag{49}$$

The following calculations yield its matrix formulation:

$$\begin{aligned} \hat{A}_{RX} &= \cos\frac{\theta}{2}|\psi_0\rangle\langle\psi_0| - j\sin\frac{\theta}{2}|\psi_1\rangle\langle\psi_0| - j\sin\frac{\theta}{2}|\psi_0\rangle\langle\psi_1| + \cos\frac{\theta}{2}|\psi_1\rangle\langle\psi_1| \\ \hat{A}_{RX} &= \cos\frac{\theta}{2} \begin{bmatrix} 1 & 0 \\ 0 & 0 \end{bmatrix} - j\sin\frac{\theta}{2} \begin{bmatrix} 0 & 1 \\ 1 & 0 \end{bmatrix} - j\sin\frac{\theta}{2} \begin{bmatrix} 1 & 0 \\ 0 & 1 \end{bmatrix} + \cos\frac{\theta}{2} \begin{bmatrix} 0 & 0 \\ 0 & 1 \end{bmatrix} \\ \hat{A}_{RX} &= \cos\frac{\theta}{2} \begin{bmatrix} 1 & 0 \\ 0 & 0 \end{bmatrix} - j\sin\frac{\theta}{2} \begin{bmatrix} 0 & 0 \\ 1 & 0 \end{bmatrix} - j\sin\frac{\theta}{2} \begin{bmatrix} 0 & 1 \\ 0 & 0 \end{bmatrix} + \cos\frac{\theta}{2} \begin{bmatrix} 0 & 0 \\ 0 & 1 \end{bmatrix} \\ \hat{A}_{RX} &= \begin{bmatrix} \cos\frac{\theta}{2} & -j\sin\frac{\theta}{2} \\ -j\sin\frac{\theta}{2} & \cos\frac{\theta}{2} \end{bmatrix} \end{aligned} \tag{50}$$

In the case  $\theta = \pi$ , the operator reduces to

$$\hat{A}_{RX}|_{\theta=\pi} = \begin{bmatrix} 0 & -j \\ -j & 0 \end{bmatrix} = -j \begin{bmatrix} 0 & 1 \\ 1 & 0 \end{bmatrix} = e^{-j\frac{\pi}{2}} \begin{bmatrix} 0 & 1 \\ 1 & 0 \end{bmatrix} = e^{-j\frac{\pi}{2}} \hat{A}_X \tag{51}$$

where

$$\hat{A}_X = \begin{bmatrix} 0 & 1 \\ 1 & 0 \end{bmatrix} \tag{52}$$

is the operator describing a quantum gate, which is dubbed Pauli X, because the matrix in Equation (52) is identical to the X Pauli matrix in Equation (30). It is simple to show, by means of the following multiplication, that the Pauli X quantum gate transforms an input state  $|\psi_{IN}\rangle = |\psi_0\rangle$  ( $|\psi_1\rangle$ ) into the output state  $|\psi_{OUT}\rangle = |\psi_1\rangle$  ( $|\psi_0\rangle$ ):

$$|\psi_{OUT}\rangle = \hat{A}_X|\psi_0\rangle = \begin{bmatrix} 0 & 1 \\ 1 & 0 \end{bmatrix} \begin{bmatrix} 1 \\ 0 \end{bmatrix} = \begin{bmatrix} 0 \\ 1 \end{bmatrix} = |\psi_1\rangle$$

$$|\psi_{OUT}\rangle = \hat{A}_X|\psi_1\rangle = \begin{bmatrix} 0 & 1 \\ 1 & 0 \end{bmatrix} \begin{bmatrix} 0 \\ 1 \end{bmatrix} = \begin{bmatrix} 1 \\ 0 \end{bmatrix} = |\psi_0\rangle$$

Figure 7 depicts the truth table and the symbol of the Pauli X quantum gate.

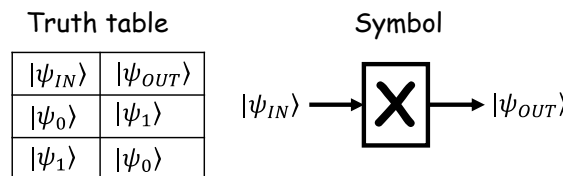


Figure 7. Truth table and symbol of the Pauli X quantum gate.

The Pauli X gate is the quantum equivalent of the classical NOT gate with respect to the basis states  $|\psi_0\rangle$  and  $|\psi_1\rangle$ , since it maps  $|\psi_0\rangle$  to  $|\psi_1\rangle$  and  $|\psi_1\rangle$  to  $|\psi_0\rangle$ .

### 5.2. $R_Y$ and Pauli Y Quantum Gates

On the Bloch sphere, the quantum gate  $R_Y$  is defined by a rotation of an angle  $\theta$  around the y axis of the qubit state vector. Figure 6 shows that it can be obtained by applying a

microwave in-quadrature carrier pulse at frequency  $2\omega_0$  for a time duration  $t$ , where, as in the previous case,  $2\omega_1 t = \theta$ . From the equations in Table 1, the mathematical expression of the qubit state  $|\psi\rangle$  after the application of the microwave pulse is

$$|\psi\rangle = e^{-j\omega_0 \frac{\theta}{2\omega_1}} \left[ \cos\frac{\theta}{2}|\psi_0\rangle + \sin\frac{\theta}{2}|\psi_1\rangle \right] \tag{53}$$

if the initial qubit state is  $|\psi_0\rangle$ , or the following one if the initial qubit state is  $|\psi_1\rangle$ :

$$|\psi\rangle = e^{-j\omega_0 \frac{\theta}{2\omega_1}} \left[ -\sin\frac{\theta}{2}|\psi_0\rangle + \cos\frac{\theta}{2}|\psi_1\rangle \right] \tag{54}$$

The  $R_Y$  quantum gate therefore transforms the state  $|\psi_0\rangle$  into the state  $|\psi\rangle = \cos\theta/2|\psi_0\rangle + \sin\theta/2|\psi_1\rangle$  and the state  $|\psi_1\rangle$  into the state  $|\psi\rangle = -\sin\theta/2|\psi_0\rangle + \cos\theta/2|\psi_1\rangle$ . Since  $\langle\psi_i|\psi_j\rangle$  is 1 if  $i = j$  and 0 otherwise, the operator  $\hat{A}_{RY}$  associated with the  $R_Y$  quantum gate is therefore given by

$$\hat{A}_{RY} = \left( \cos\frac{\theta}{2}|\psi_0\rangle + \sin\frac{\theta}{2}|\psi_1\rangle \right) \langle\psi_0| + \left( -\sin\frac{\theta}{2}|\psi_0\rangle + \cos\frac{\theta}{2}|\psi_1\rangle \right) \langle\psi_1| \tag{55}$$

The following calculations yield the matrix formulation of Equation (55):

$$\begin{aligned} \hat{A}_{RY} &= \cos\frac{\theta}{2}|\psi_0\rangle\langle\psi_0| + \sin\frac{\theta}{2}|\psi_1\rangle\langle\psi_0| - \sin\frac{\theta}{2}|\psi_0\rangle\langle\psi_1| + \cos\frac{\theta}{2}|\psi_1\rangle\langle\psi_1| \\ \hat{A}_{RY} &= \cos\frac{\theta}{2} \begin{bmatrix} 1 & 0 \\ 0 & 0 \end{bmatrix} + \sin\frac{\theta}{2} \begin{bmatrix} 0 & 1 \\ 0 & 0 \end{bmatrix} - \sin\frac{\theta}{2} \begin{bmatrix} 0 & 0 \\ 1 & 0 \end{bmatrix} + \cos\frac{\theta}{2} \begin{bmatrix} 0 & 0 \\ 0 & 1 \end{bmatrix} \\ \hat{A}_{RY} &= \cos\frac{\theta}{2} \begin{bmatrix} 1 & 0 \\ 0 & 0 \end{bmatrix} + \sin\frac{\theta}{2} \begin{bmatrix} 0 & 1 \\ 1 & 0 \end{bmatrix} - \sin\frac{\theta}{2} \begin{bmatrix} 0 & 1 \\ 0 & 0 \end{bmatrix} + \cos\frac{\theta}{2} \begin{bmatrix} 0 & 0 \\ 0 & 1 \end{bmatrix} \\ \hat{A}_{RY} &= \begin{bmatrix} \cos\frac{\theta}{2} & -\sin\frac{\theta}{2} \\ \sin\frac{\theta}{2} & \cos\frac{\theta}{2} \end{bmatrix} \end{aligned} \tag{56}$$

In the case  $\theta = \pi$ , the operator reduces to

$$\hat{A}_{RY}|_{\theta=\pi} = \begin{bmatrix} 0 & -1 \\ 1 & 0 \end{bmatrix} = \begin{bmatrix} 0 & e^{-j\pi} \\ 1 & 0 \end{bmatrix} = e^{-j\frac{\pi}{2}} \begin{bmatrix} 0 & e^{-j\frac{\pi}{2}} \\ e^{j\frac{\pi}{2}} & 0 \end{bmatrix} = e^{-j\frac{\pi}{2}} \begin{bmatrix} 0 & -j \\ j & 0 \end{bmatrix} = e^{-j\frac{\pi}{2}} \hat{A}_Y \tag{57}$$

where

$$\hat{A}_Y = \begin{bmatrix} 0 & -j \\ j & 0 \end{bmatrix} \tag{58}$$

is the operator describing a quantum gate, which is dubbed Pauli Y, because the matrix in Equation (58) is identical to the Y Pauli matrix in Equation (31). Figure 8 depicts the truth table and the symbol of the Pauli Y quantum gate.

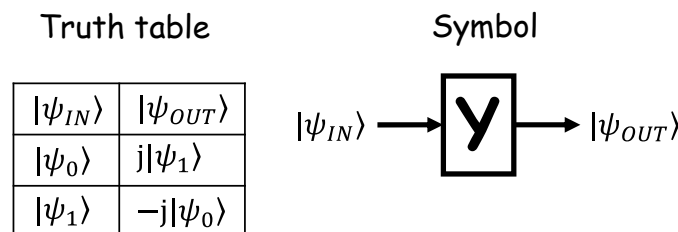


Figure 8. Truth table and symbol of the Pauli Y quantum gate.

The truth table can be calculated still following the mathematical approach used in Section 2. For instance, for  $|\psi_{IN}\rangle = |\psi_0\rangle$  you obtain the following:

$$|\psi_{OUT}\rangle = \hat{A}_Y|\psi_0\rangle = \begin{bmatrix} 0 & -j \\ j & 0 \end{bmatrix} \begin{bmatrix} 1 \\ 0 \end{bmatrix} = j \begin{bmatrix} 0 \\ 1 \end{bmatrix} = j|\psi_1\rangle$$

Therefore, the Pauli Y gate maps the basis states  $|\psi_0\rangle$  to  $j|\psi_1\rangle$  and  $|\psi_1\rangle$  to  $-j|\psi_0\rangle$ .

### 5.3. $R_Z$ and Pauli Z Quantum Gates

On the Bloch sphere, the quantum gate  $R_Z$  is defined by a rotation of an angle  $\theta$  around the z axis of the qubit state vector. Looking at Figure 6, it can be obtained by a rotation of  $-\pi/2$  around the x axis, followed by a rotation of  $\theta$  around the y axis, followed by a final rotation of  $\pi/2$  around the x axis. In this case, a microwave in-phase carrier pulse at frequency  $2\omega_0$  is applied for a time duration  $t_1$ , such that  $2\omega_1 t_1 = 3\pi/2$  (since the rotation speed of the qubit state vector is  $2\omega_1$ ). Then, a microwave in-quadrature carrier pulse at frequency  $2\omega_0$  is applied for a time duration  $t_2$ , such that  $2\omega_1 t_2 = \theta$ , and finally, a microwave in-phase carrier pulse at frequency  $2\omega_0$  is applied for a time duration  $t_3$ , such that  $2\omega_1 t_3 = \pi/2$ . Its operator  $\hat{A}_{RZ}$  can be thus computed as follows:

$$\hat{A}_{RZ} = \hat{A}_{RX}|_{\theta=\frac{\pi}{2}} \hat{A}_{RY} \hat{A}_{RX}|_{\theta=-\frac{\pi}{2}} \tag{59}$$

and, from Equation (50),

$$\hat{A}_{RX}|_{\theta=\frac{\pi}{2}} = \begin{bmatrix} \frac{1}{\sqrt{2}} & -j\frac{1}{\sqrt{2}} \\ -j\frac{1}{\sqrt{2}} & \frac{1}{\sqrt{2}} \end{bmatrix} = \frac{1}{\sqrt{2}} \begin{bmatrix} 1 & -j \\ -j & 1 \end{bmatrix} \tag{60}$$

$$\hat{A}_{RX}|_{\theta=-\frac{\pi}{2}} = \begin{bmatrix} \frac{1}{\sqrt{2}} & j\frac{1}{\sqrt{2}} \\ j\frac{1}{\sqrt{2}} & \frac{1}{\sqrt{2}} \end{bmatrix} = \frac{1}{\sqrt{2}} \begin{bmatrix} 1 & j \\ j & 1 \end{bmatrix} \tag{61}$$

The substitution of Equations (56), (60) and (61) into Equation (59) yields

$$\hat{A}_{RZ} = \frac{1}{2} \begin{bmatrix} 1 & -j \\ -j & 1 \end{bmatrix} \begin{bmatrix} \cos\frac{\theta}{2} & -\sin\frac{\theta}{2} \\ \sin\frac{\theta}{2} & \cos\frac{\theta}{2} \end{bmatrix} \begin{bmatrix} 1 & j \\ j & 1 \end{bmatrix} = \begin{bmatrix} e^{-j\frac{\theta}{2}} & 0 \\ 0 & e^{j\frac{\theta}{2}} \end{bmatrix} \tag{62}$$

In the case  $\theta = \pi$ , the operator reduces to

$$\hat{A}_{RZ}|_{\theta=\pi} = \begin{bmatrix} e^{-j\frac{\pi}{2}} & 0 \\ 0 & e^{j\frac{\pi}{2}} \end{bmatrix} = e^{-j\frac{\pi}{2}} \begin{bmatrix} 1 & 0 \\ 0 & -1 \end{bmatrix} = e^{-j\frac{\pi}{2}} \hat{A}_Z \tag{63}$$

where

$$\hat{A}_Z = \begin{bmatrix} 1 & 0 \\ 0 & -1 \end{bmatrix} \tag{64}$$

is the operator describing a quantum gate, which is dubbed Pauli Z, because the matrix in Equation (64) is identical to the Z Pauli matrix in Equation (32). Figure 9 depicts the truth table and the symbol of the Pauli Z quantum gate.

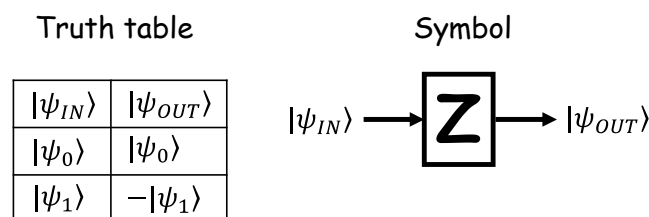


Figure 9. Truth table and symbol of the Pauli Z quantum gate.



The Pauli Z gate leaves the basis state  $|\psi_0\rangle$  unchanged, while it maps  $|\psi_1\rangle$  to  $-|\psi_1\rangle$ .

#### 5.4. Hadamard Quantum Gate

On the Bloch sphere, the Hadamard quantum gate H is defined by a qubit state vector rotation of  $\pi/2$  around the y axis, followed by a rotation of  $\pi$  around the x axis. Its operator  $\hat{A}_H$  is thus calculated as follows:

$$\hat{A}_H = \hat{A}_{RX}|_{\theta=\pi} \hat{A}_{RY}|_{\theta=\frac{\pi}{2}} \tag{65}$$

Since Equations (50) and (56) yield

$$\hat{A}_{RX}|_{\theta=\pi} = \begin{bmatrix} 0 & -j \\ -j & 0 \end{bmatrix} = -j \begin{bmatrix} 0 & 1 \\ 1 & 0 \end{bmatrix} \tag{66}$$

$$\hat{A}_{RY}|_{\theta=\frac{\pi}{2}} = \begin{bmatrix} \frac{1}{\sqrt{2}} & -\frac{1}{\sqrt{2}} \\ \frac{1}{\sqrt{2}} & \frac{1}{\sqrt{2}} \end{bmatrix} = \frac{1}{\sqrt{2}} \begin{bmatrix} 1 & -1 \\ 1 & 1 \end{bmatrix} \tag{67}$$

from Equation (65) you obtain the following:

$$\hat{A}_H = -\frac{j}{\sqrt{2}} \begin{bmatrix} 1 & 1 \\ 1 & -1 \end{bmatrix} \tag{68}$$

Since  $-j$  is a global phase, Equation (68) can be rewritten by neglecting  $-j$ :

$$\hat{A}_H = \frac{1}{\sqrt{2}} \begin{bmatrix} 1 & 1 \\ 1 & -1 \end{bmatrix} \tag{69}$$

Figure 10 depicts the truth table and the symbol of the Hadamard quantum gate.

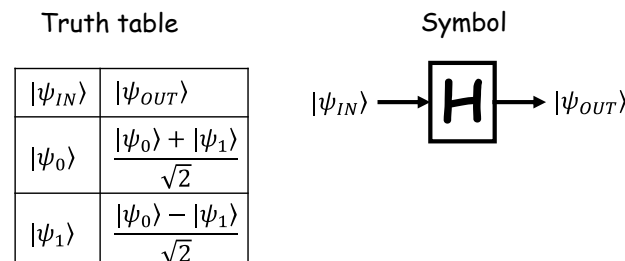


Figure 10. Truth table and symbol of the Hadamard quantum gate.

The Hadamard gate H maps the basis states  $|\psi_0\rangle$  and  $|\psi_1\rangle$  into a superposition state.

#### 5.5. Decomposition of One-Qubit Quantum Gates

Sections 5.3 and 5.4 suggest that any one-qubit quantum gate can be decomposed into X and Y quantum gates. They can thus be obtained by applying an opportune sequence of microwave pulses to the electron spin qubit. It is worth inclosing this remark in a more general framework. The operators  $\hat{A}_{RX}$ ,  $\hat{A}_{RY}$ , and  $\hat{A}_{RZ}$  describe the evolution of the qubit state in time; that is, they are time evolution operators. In classical mechanics, the physics laws are reversible, entailing that two different states should remain different during the time evolution. The preservation of the distinguishability of different states remains valid in the context of quantum mechanics as well. It implies that any time evolution operators  $\hat{A}(t)$  should be unitary; that is,  $\hat{A}^\dagger(t)\hat{A}(t) = I$ , where I is the unit matrix [37]. It is straightforward to verify that the operators  $\hat{A}_{RX}$ ,  $\hat{A}_{RY}$ , and  $\hat{A}_{RZ}$  are unitary. For instance,

$$\hat{A}_{RZ}^\dagger \hat{A}_{RZ} = \begin{bmatrix} e^{j\frac{\theta}{2}} & 0 \\ 0 & e^{-j\frac{\theta}{2}} \end{bmatrix} \begin{bmatrix} e^{-j\frac{\theta}{2}} & 0 \\ 0 & e^{j\frac{\theta}{2}} \end{bmatrix} = \begin{bmatrix} 1 & 0 \\ 0 & 1 \end{bmatrix} = I$$

Equation (65) is a particular case of the X-Y decomposition theorem. This theorem states that given a unitary operator  $\hat{U}$  on a single qubit, it is possible to find out four real-valued numbers  $a, b, c,$  and  $d$  such that  $\hat{U} = e^{j\hat{a}t} \hat{A}_{RX} |_{t=b} \hat{A}_{RY} |_{t=c} \hat{A}_{RX} |_{t=d}$  [3]. Similarly, the Z-Y decomposition theorem also exists [3].

### 6. Physics of Two-Electron-Spin Qubits

Let us consider a couple of electrons, both confined in a QD. After Equation (29), the intrinsic spin magnetic dipole moments  $\mu_{S1}$  and  $\mu_{S2}$  of the two electrons can be expressed as follows:

$$\vec{\mu}_{S1} = -g \frac{q}{2m} \vec{S}_1 = -g \frac{q}{2m} (S_{1X} \vec{x} + S_{1Y} \vec{y} + S_{1Z} \vec{z}) \tag{70}$$

$$\vec{\mu}_{S2} = -g \frac{q}{2m} \vec{S}_2 = -g \frac{q}{2m} (S_{2X} \vec{x} + S_{2Y} \vec{y} + S_{2Z} \vec{z}) \tag{71}$$

where  $S_{1X}, S_{1Y},$  and  $S_{1Z}$  ( $S_{2X}, S_{2Y},$  and  $S_{2Z}$ ) are the components of the electron spin  $S_1$  ( $S_2$ ) along the axis of an  $(x, y, z)$  Cartesian reference system.

Let us assume that the two electron spins are in the presence of a magnetic field and they interact. As the electrons are confined in a QD, the total energy of the physical system coincides with its potential energy, which is equal to  $\sum_{i,j=x,y,z} J_{ij} S_{1i} S_{2j} - \mu_{S1} \cdot B_1 - \mu_{S2} \cdot B_2,$  where  $J_{ij}$  is the coupling between the two spins. The QM Postulates (see, for instance, [36]) lead to the following quantum Hamiltonian of the system:

$$\hat{H} = \sum_{i,j=x,y,z} J_{ij} \vec{S}_{1i} \cdot \vec{S}_{2j} - \sum_{i=1,2} \vec{\mu}_i \cdot \vec{B}_i = \sum_{i,j=x,y,z} J_{ij} \vec{S}_{1i} \cdot \vec{S}_{2j} + g \frac{q}{2m} \sum_{i=1,2} \vec{S}_i \cdot \vec{B}_i$$

By adopting an isotropic Heisenberg interaction as in [42], for which  $J_{ij} \neq 0$  if  $i = j$  and  $J_{ij} = 0$  otherwise, the above Hamiltonian becomes simpler, and the resulting Schrödinger equation is as follows:

$$j\hbar \frac{\partial |\psi\rangle}{\partial t} = \left[ \sum_{i=x,y,z} J_{ii} S_{1i} S_{2i} + g \frac{q}{2m} \sum_{i=x,y,z} S_{1i} B_{1i} + g \frac{q}{2m} \sum_{i=x,y,z} S_{2i} B_{2i} \right] |\psi\rangle \tag{72}$$

Since two coupled qubits form the physical system, there are four basis states. As in Figure 2 and by extension of Equations (4) and (5), you can write

$$|\psi_1\rangle = \begin{bmatrix} 1 \\ 0 \\ 0 \\ 0 \end{bmatrix} \tag{73}$$

$$|\psi_2\rangle = \begin{bmatrix} 0 \\ 1 \\ 0 \\ 0 \end{bmatrix} \tag{74}$$

$$|\psi_3\rangle = \begin{bmatrix} 0 \\ 0 \\ 1 \\ 0 \end{bmatrix} \tag{75}$$

$$|\psi_4\rangle = \begin{bmatrix} 0 \\ 0 \\ 0 \\ 1 \end{bmatrix} \tag{76}$$

Similarly, by extension of Equations (26) and (27), you can write

$$\langle \psi_1 | = \begin{bmatrix} 1 \\ 0 \\ 0 \\ 0 \end{bmatrix}^\dagger = [1 \ 0 \ 0 \ 0] \quad (77)$$

$$\langle \psi_2 | = \begin{bmatrix} 0 \\ 1 \\ 0 \\ 0 \end{bmatrix}^\dagger = [0 \ 1 \ 0 \ 0] \quad (78)$$

$$\langle \psi_3 | = \begin{bmatrix} 0 \\ 0 \\ 1 \\ 0 \end{bmatrix}^\dagger = [0 \ 0 \ 1 \ 0] \quad (79)$$

$$\langle \psi_4 | = \begin{bmatrix} 0 \\ 0 \\ 0 \\ 1 \end{bmatrix}^\dagger = [0 \ 0 \ 0 \ 1] \quad (80)$$

As in the case of the single qubit, the four states are also distinguishable, because they are orthonormal; that is,  $\langle \psi_i | \psi_j \rangle$  is 1 if  $i = j$  and 0 otherwise.

In virtue of the QM Postulates (see, for instance, [36]), the generic state  $|\psi\rangle$  of the two interacting qubits is the superposition of the four states  $|\psi_1\rangle$ ,  $|\psi_2\rangle$ ,  $|\psi_3\rangle$ , and  $|\psi_4\rangle$ :

$$|\psi\rangle = \alpha(t)|\psi_1\rangle + \beta(t)|\psi_2\rangle + \gamma(t)|\psi_3\rangle + \delta(t)|\psi_4\rangle = \begin{bmatrix} \alpha(t) \\ \beta(t) \\ \gamma(t) \\ \delta(t) \end{bmatrix} \quad (81)$$

where  $\alpha(t)$ ,  $\beta(t)$ ,  $\gamma(t)$ , and  $\delta(t)$  are time-variant, complex-valued probability amplitudes. Equation (81) is an extension of Equation (6). In addition, the QM Postulates also require  $|\alpha(t)|^2 + |\beta(t)|^2 + |\gamma(t)|^2 + |\delta(t)|^2 = 1$ . As an extension of Equations (30)–(32), the components of the spin operators  $\hat{S}_1$  and  $\hat{S}_2$  are given by the following tensorial products between the Pauli matrix and the identity matrix I:

$$\hat{S}_{1x} = \frac{\hbar}{2} \begin{bmatrix} 0 & 1 \\ 1 & 0 \end{bmatrix} \otimes \begin{bmatrix} 1 & 0 \\ 0 & 1 \end{bmatrix} = \frac{\hbar}{2} \begin{bmatrix} 0 & 0 & 1 & 0 \\ 0 & 0 & 0 & 1 \\ 1 & 0 & 0 & 0 \\ 0 & 1 & 0 & 0 \end{bmatrix} \quad (82)$$

$$\hat{S}_{1y} = \frac{\hbar}{2} \begin{bmatrix} 0 & -j \\ +j & 0 \end{bmatrix} \otimes \begin{bmatrix} 1 & 0 \\ 0 & 1 \end{bmatrix} = \frac{\hbar}{2} \begin{bmatrix} 0 & 0 & -j & 0 \\ 0 & 0 & 0 & -j \\ +j & 0 & 0 & 0 \\ 0 & +j & 0 & 0 \end{bmatrix} \quad (83)$$

$$\hat{S}_{1z} = \frac{\hbar}{2} \begin{bmatrix} 1 & 0 \\ 0 & -1 \end{bmatrix} \otimes \begin{bmatrix} 1 & 0 \\ 0 & 1 \end{bmatrix} = \frac{\hbar}{2} \begin{bmatrix} 1 & 0 & 0 & 0 \\ 0 & 1 & 0 & 0 \\ 0 & 0 & -1 & 0 \\ 0 & 0 & 0 & -1 \end{bmatrix} \quad (84)$$

$$\hat{S}_{2x} = \frac{\hbar}{2} \begin{bmatrix} 1 & 0 \\ 0 & 1 \end{bmatrix} \otimes \begin{bmatrix} 0 & 1 \\ 1 & 0 \end{bmatrix} = \frac{\hbar}{2} \begin{bmatrix} 0 & 1 & 0 & 0 \\ 1 & 0 & 0 & 0 \\ 0 & 0 & 0 & 1 \\ 0 & 0 & 1 & 0 \end{bmatrix} \tag{85}$$

$$\hat{S}_{2y} = \frac{\hbar}{2} \begin{bmatrix} 1 & 0 \\ 0 & 1 \end{bmatrix} \otimes \begin{bmatrix} 0 & -j \\ +j & 0 \end{bmatrix} = \frac{\hbar}{2} \begin{bmatrix} 0 & -j & 0 & 0 \\ +j & 0 & 0 & 0 \\ 0 & 0 & 0 & -j \\ 0 & 0 & +j & 0 \end{bmatrix} \tag{86}$$

$$\hat{S}_{2z} = \frac{\hbar}{2} \begin{bmatrix} 1 & 0 \\ 0 & 1 \end{bmatrix} \otimes \begin{bmatrix} 1 & 0 \\ 0 & -1 \end{bmatrix} = \frac{\hbar}{2} \begin{bmatrix} 1 & 0 & 0 & 0 \\ 0 & -1 & 0 & 0 \\ 0 & 0 & 1 & 0 \\ 0 & 0 & 0 & -1 \end{bmatrix} \tag{87}$$

As the vectors of a tensorial product space are calculated from vectors of a lower-dimensional space, higher-dimensional operators are calculated as tensorial products of lower-dimensional operators [37]. In particular, in Equation (82), the tensorial product of the operator  $\hat{A}_x$  with the unitary operator I describes a higher-dimensional operator acting on the x component of the first (left) spin but not on the second (right) spin. Similarly, in Equation (85) the tensorial product of the operators I and  $\hat{A}_x$  describes a higher-dimensional operator acting on the x component of the second (right) spin but not on the first (left) spin. In the same way, you can comment on the remaining equations.

The substitution of Equations (82)–(87) into Equation (72) yields

$$j\hbar \begin{bmatrix} \frac{\partial \alpha(t)}{\partial t} \\ \frac{\partial \beta(t)}{\partial t} \\ \frac{\partial \gamma(t)}{\partial t} \\ \frac{\partial \delta(t)}{\partial t} \end{bmatrix} = \left\{ \begin{aligned} & J_{xx} \left(\frac{\hbar}{2}\right)^2 \begin{bmatrix} 0 & 0 & 1 & 0 \\ 0 & 0 & 0 & 1 \\ 1 & 0 & 0 & 0 \\ 0 & 1 & 0 & 0 \end{bmatrix} \begin{bmatrix} 0 & 1 & 0 & 0 \\ 1 & 0 & 0 & 0 \\ 0 & 0 & 0 & 1 \\ 0 & 0 & 1 & 0 \end{bmatrix} \\ & + J_{yy} \left(\frac{\hbar}{2}\right)^2 \begin{bmatrix} 0 & 0 & -j & 0 \\ 0 & 0 & 0 & -j \\ +j & 0 & 0 & 0 \\ 0 & +j & 0 & 0 \end{bmatrix} \begin{bmatrix} 0 & -j & 0 & 0 \\ +j & 0 & 0 & 0 \\ 0 & 0 & 0 & -j \\ 0 & 0 & +j & 0 \end{bmatrix} \\ & + J_{zz} \left(\frac{\hbar}{2}\right)^2 \begin{bmatrix} 1 & 0 & 0 & 0 \\ 0 & 1 & 0 & 0 \\ 0 & 0 & -1 & 0 \\ 0 & 0 & 0 & -1 \end{bmatrix} \begin{bmatrix} 1 & 0 & 0 & 0 \\ 0 & -1 & 0 & 0 \\ 0 & 0 & 1 & 0 \\ 0 & 0 & 0 & -1 \end{bmatrix} \\ & + g \frac{q}{2m} \frac{\hbar}{2} \left[ \begin{bmatrix} 0 & 0 & 1 & 0 \\ 0 & 0 & 0 & 1 \\ 1 & 0 & 0 & 0 \\ 0 & 1 & 0 & 0 \end{bmatrix} B_{1x} + \begin{bmatrix} 0 & 0 & -j & 0 \\ 0 & 0 & 0 & -j \\ +j & 0 & 0 & 0 \\ 0 & +j & 0 & 0 \end{bmatrix} B_{1y} \right. \\ & + \begin{bmatrix} 1 & 0 & 0 & 0 \\ 0 & 1 & 0 & 0 \\ 0 & 0 & -1 & 0 \\ 0 & 0 & 0 & -1 \end{bmatrix} B_{1z} + \begin{bmatrix} 0 & 1 & 0 & 0 \\ 1 & 0 & 0 & 0 \\ 0 & 0 & 0 & 1 \\ 0 & 0 & 1 & 0 \end{bmatrix} B_{2x} \\ & \left. + \begin{bmatrix} 0 & -j & 0 & 0 \\ +j & 0 & 0 & 0 \\ 0 & 0 & 0 & -j \\ 0 & 0 & +j & 0 \end{bmatrix} B_{2y} + \begin{bmatrix} 1 & 0 & 0 & 0 \\ 0 & -1 & 0 & 0 \\ 0 & 0 & 1 & 0 \\ 0 & 0 & 0 & -1 \end{bmatrix} B_{2z} \right] \begin{bmatrix} \alpha(t) \\ \beta(t) \\ \gamma(t) \\ \delta(t) \end{bmatrix} \end{aligned} \right\}$$

Once the matrix products and sums are calculated, remembering that  $\hbar/2m$  is the Bohr magneton  $\mu_B$ , the above equation takes the following form:

$$j\hbar \begin{bmatrix} \frac{\partial \alpha(t)}{\partial t} \\ \frac{\partial \beta(t)}{\partial t} \\ \frac{\partial \gamma(t)}{\partial t} \\ \frac{\partial \delta(t)}{\partial t} \end{bmatrix} = \left\{ \left(\frac{\hbar}{2}\right)^2 \begin{bmatrix} J_{zz} & 0 & 0 & J_{xx} - J_{yy} \\ 0 & -J_{zz} & J_{xx} + J_{yy} & 0 \\ 0 & J_{xx} + J_{yy} & -J_{zz} & 0 \\ J_{xx} - J_{yy} & 0 & 0 & J_{zz} \end{bmatrix} + g\frac{\mu_B}{2} \begin{bmatrix} B_{1z} + B_{2z} & B_{2x} - jB_{2y} & B_{1x} - jB_{1y} & 0 \\ B_{2x} + jB_{2y} & B_{1z} - B_{2z} & 0 & B_{1x} - jB_{1y} \\ B_{1x} + jB_{1y} & 0 & -B_{1z} + B_{2z} & B_{2x} - jB_{2y} \\ 0 & B_{1x} + jB_{1y} & B_{2x} + jB_{2y} & -B_{1z} - B_{2z} \end{bmatrix} \right\} \begin{bmatrix} \alpha(t) \\ \beta(t) \\ \gamma(t) \\ \delta(t) \end{bmatrix} \tag{88}$$

It is worth noting that Equation (88) matches with the Hamiltonian reported in [42] for  $\hbar = 1$ ;  $g\mu_B = 1$ ; and  $B_{1x} = B_{2x} = B_x$ ,  $B_{1y} = B_{2y} = B_y$ ,  $B_{1z} = B_{2z} = B_z$ ,  $J_{xx} = J_x$ ,  $J_{yy} = J_y$ , and  $J_{zz} = J_z$ . By assuming, for the sake of straightforwardness,  $J_{zz} \neq 0$  and  $J_{xx} = J_{yy} = 0$ , one can reduce Equation (88) to

$$j\hbar \begin{bmatrix} \frac{\partial \alpha(t)}{\partial t} \\ \frac{\partial \beta(t)}{\partial t} \\ \frac{\partial \gamma(t)}{\partial t} \\ \frac{\partial \delta(t)}{\partial t} \end{bmatrix} = \left\{ \left(\frac{\hbar}{2}\right)^2 \begin{bmatrix} J_{zz} & 0 & 0 & 0 \\ 0 & -J_{zz} & 0 & 0 \\ 0 & 0 & -J_{zz} & 0 \\ 0 & 0 & 0 & J_{zz} \end{bmatrix} + g\frac{\mu_B}{2} \begin{bmatrix} B_{1z} + B_{2z} & B_{2x} - jB_{2y} & B_{1x} - jB_{1y} & 0 \\ B_{2x} + jB_{2y} & B_{1z} - B_{2z} & 0 & B_{1x} - jB_{1y} \\ B_{1x} + jB_{1y} & 0 & -B_{1z} + B_{2z} & B_{2x} - jB_{2y} \\ 0 & B_{1x} + jB_{1y} & B_{2x} + jB_{2y} & -B_{1z} - B_{2z} \end{bmatrix} \right\} \begin{bmatrix} \alpha(t) \\ \beta(t) \\ \gamma(t) \\ \delta(t) \end{bmatrix} \tag{89}$$

It is worth noting that the above conditions on the coupling describe the Ising interaction, which is another typical interaction addressed in the literature for interacting spin systems [43]. To make the two qubits addressable singularly with a microwave pulse of the proper frequency, the DC large magnetic field  $B_z$  component should be different for the two qubits; that is,  $B_{1z} = B_{01}$  and  $B_{2z} = B_{02}$ . The integration of a Cobalt micro-magnet close to the QD makes that possible [44]. In addition, since the two qubits are usually irradiated with the same microantenna [45], it is reasonable to assume that the components  $B_x$  and  $B_y$  of the magnetic field rotating on the  $xy$  plane are the same for the two qubits, so  $B_{1x} = B_{2x} = B_1 \cos \omega t$  and  $B_{1y} = B_{2y} = B_1 \sin \omega t$ . Under the above assumptions, Equation (89) takes the following form:

$$j \begin{bmatrix} \frac{\partial \alpha(t)}{\partial t} \\ \frac{\partial \beta(t)}{\partial t} \\ \frac{\partial \gamma(t)}{\partial t} \\ \frac{\partial \delta(t)}{\partial t} \end{bmatrix} = \begin{bmatrix} \hbar \frac{J_{zz}}{4} + \frac{g\mu_B}{2\hbar} (B_{01} + B_{02}) & \frac{g\mu_B}{2\hbar} B_1 e^{-j\omega t} & \frac{g\mu_B}{2\hbar} B_1 e^{-j\omega t} & 0 \\ \frac{g\mu_B B_1}{2\hbar} e^{j\omega t} & -\hbar \frac{J_{zz}}{4} + \frac{g\mu_B}{2\hbar} (B_{01} - B_{02}) & 0 & \frac{g\mu_B}{2\hbar} B_1 e^{-j\omega t} \\ \frac{g\mu_B B_1}{2\hbar} e^{j\omega t} & 0 & -\hbar \frac{J_{zz}}{4} - (B_{01} - B_{02}) & \frac{g\mu_B}{2\hbar} B_1 e^{-j\omega t} \\ 0 & \frac{g\mu_B B_1}{2\hbar} e^{j\omega t} & \frac{g\mu_B B_1}{2\hbar} e^{j\omega t} & \hbar \frac{J_{zz}}{4} - \frac{g\mu_B}{2\hbar} (B_{01} + B_{02}) \end{bmatrix} \begin{bmatrix} \alpha(t) \\ \beta(t) \\ \gamma(t) \\ \delta(t) \end{bmatrix}$$

where it was noticed that

$$B_x - jB_y = B_1(\cos \omega t - j \sin \omega t) = B_1 \left( \frac{e^{j\omega t} + e^{-j\omega t}}{2} - j \frac{e^{j\omega t} - e^{-j\omega t}}{2j} \right) = B_1 e^{-j\omega t}$$

$$B_x + jB_y = B_1(\cos \omega t + j \sin \omega t) = B_1 \left( \frac{e^{j\omega t} + e^{-j\omega t}}{2} + j \frac{e^{j\omega t} - e^{-j\omega t}}{2j} \right) = B_1 e^{j\omega t}$$

By spotting the two Larmor frequencies  $2\omega_{01} = g\mu_B B_{01}/\hbar$  and  $2\omega_{02} = g\mu_B B_{02}/\hbar$ , and the Rabi frequency  $2\omega_1 = g\mu_B B_1/\hbar$ , the above equation can be rewritten as follows:

$$j \begin{bmatrix} \frac{\partial \alpha(t)}{\partial t} \\ \frac{\partial \beta(t)}{\partial t} \\ \frac{\partial \gamma(t)}{\partial t} \\ \frac{\partial \delta(t)}{\partial t} \end{bmatrix} = \begin{bmatrix} \omega_{01} + \omega_{02} + J & \omega_1 e^{-j\omega t} & \omega_1 e^{-j\omega t} & 0 \\ \omega_1 e^{j\omega t} & \omega_{01} - \omega_{02} - J & 0 & \omega_1 e^{-j\omega t} \\ \omega_1 e^{j\omega t} & 0 & \omega_{02} - \omega_{01} - J & \omega_1 e^{-j\omega t} \\ 0 & \omega_1 e^{j\omega t} & \omega_1 e^{j\omega t} & -\omega_{01} - \omega_{02} + J \end{bmatrix} \begin{bmatrix} \alpha(t) \\ \beta(t) \\ \gamma(t) \\ \delta(t) \end{bmatrix} \tag{90}$$

where  $J = \hbar J_{zz}/4$ . As in Equation (40), Equation (90) also exhibits on the main diagonal the frequencies corresponding to the energy levels of the system, of which are four. Figure 11

shows that, like in the case of the single qubit, the differences between the energy levels identify four resonance frequencies:  $\omega_{R1} = 2(\omega_{02} - J)$ ,  $\omega_{R2} = 2(\omega_{01} - J)$ ,  $\omega_{R3} = 2(\omega_{01} + J)$ , and  $\omega_{R4} = 2(\omega_{02} + J)$ .

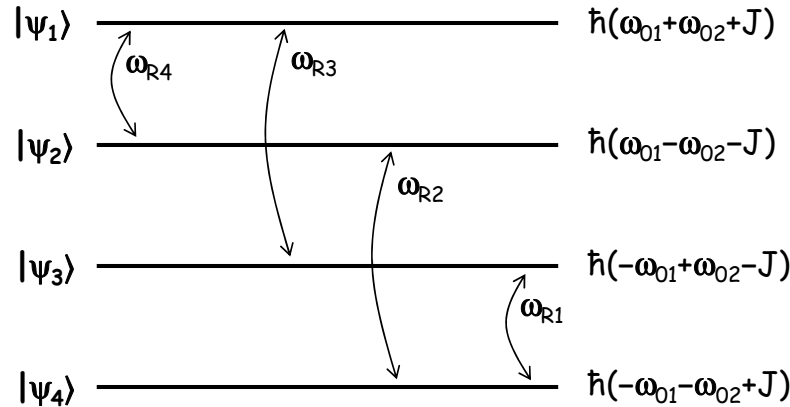


Figure 11. Energy levels of the two-qubit system.

These resonance frequencies can be put into evidence in Equation (90) by means of the following definitions:

$$\begin{aligned}
 \alpha(t) &= x(t)e^{-j(\omega_{01}+\omega_{02}+J)t} \\
 \beta(t) &= y(t)e^{-j(\omega_{01}-\omega_{02}-J)t} \\
 \gamma(t) &= z(t)e^{-j(\omega_{02}-\omega_{01}-J)t} \\
 \delta(t) &= w(t)e^{-j(-\omega_{01}-\omega_{02}+J)t}
 \end{aligned}
 \tag{91}$$

from which

$$\frac{\partial \alpha(t)}{\partial t} = \frac{\partial x(t)}{\partial t} e^{-j(\omega_{01}+\omega_{02}+J)t} - j(\omega_{01} + \omega_{02} + J)\alpha(t)
 \tag{92}$$

$$\frac{\partial \beta(t)}{\partial t} = \frac{\partial y(t)}{\partial t} e^{-j(\omega_{01}-\omega_{02}-J)t} - j(\omega_{01} - \omega_{02} - J)\beta(t)
 \tag{93}$$

$$\frac{\partial \gamma(t)}{\partial t} = \frac{\partial z(t)}{\partial t} e^{-j(\omega_{02}-\omega_{01}-J)t} - j(\omega_{02} - \omega_{01} - J)\gamma(t)
 \tag{94}$$

$$\frac{\partial \delta(t)}{\partial t} = \frac{\partial w(t)}{\partial t} e^{-j(-\omega_{01}-\omega_{02}+J)t} - j(-\omega_{01} - \omega_{02} + J)\delta(t)
 \tag{95}$$

The substitution of Equations (92)–(95) into Equation (90) leads to a more compact form:

$$\begin{bmatrix} \frac{\partial x(t)}{\partial t} \\ \frac{\partial y(t)}{\partial t} \\ \frac{\partial z(t)}{\partial t} \\ \frac{\partial w(t)}{\partial t} \end{bmatrix} = -j\omega_1 \begin{bmatrix} 0 & e^{-j(\omega-\omega_{R4})t} & e^{-j(\omega-\omega_{R3})t} & 0 \\ e^{j(\omega-\omega_{R4})t} & 0 & 0 & e^{-j(\omega-\omega_{R2})t} \\ e^{j(\omega-\omega_{R3})t} & 0 & 0 & e^{-j(\omega-\omega_{R1})t} \\ 0 & e^{j(\omega-\omega_{R2})t} & e^{j(\omega-\omega_{R1})t} & 0 \end{bmatrix} \begin{bmatrix} x(t) \\ y(t) \\ z(t) \\ w(t) \end{bmatrix}$$

or, equivalently, to the following system of differential equations:

$$\begin{cases} \frac{\partial x(t)}{\partial t} = -j\omega_1 \left\{ y(t)e^{-j(\omega-\omega_{R4})t} + z(t)e^{-j(\omega-\omega_{R3})t} \right\} \\ \frac{\partial y(t)}{\partial t} = -j\omega_1 \left\{ x(t)e^{j(\omega-\omega_{R4})t} + w(t)e^{-j(\omega-\omega_{R2})t} \right\} \\ \frac{\partial z(t)}{\partial t} = -j\omega_1 \left\{ x(t)e^{j(\omega-\omega_{R3})t} + w(t)e^{-j(\omega-\omega_{R1})t} \right\} \\ \frac{\partial w(t)}{\partial t} = -j\omega_1 \left\{ y(t)e^{j(\omega-\omega_{R2})t} + z(t)e^{j(\omega-\omega_{R1})t} \right\} \end{cases}
 \tag{96}$$

Unlike the system of coupled differential equations for the one qubit in Equations (39) and (44), the coefficients in Equation (96) are time-dependent, making it hard to find a solution [46].

Nevertheless, Section 5 pointed out that the one-qubit quantum gates are obtained by exciting the qubit with an electromagnetic field oscillating at the resonance frequency, by which the qubit is stimulated to transit between the two states. Figure 11 thus suggests that the two-qubit system also transits between two out of the four states, when excited with an electromagnetic field at a frequency  $\omega$  equal to one out of the four resonance frequencies. For instance, the system transits between the two states  $|\psi_4\rangle$  and  $|\psi_3\rangle$  when  $\omega = \omega_{R1}$ . Numerical solutions, obtained by means of Matlab, support these conclusions. Figure 12 shows the results obtained for  $\omega_{01} = 0.6$  GHz,  $\omega_{02} = 0.5$  GHz, and  $J = 0.3$  GHz, corresponding to  $\omega_{R1} = 0.4$  GHz,  $\omega_{R2} = 0.6$  GHz,  $\omega_{R3} = 1.8$  GHz, and  $\omega_{R4} = 1.6$  GHz.

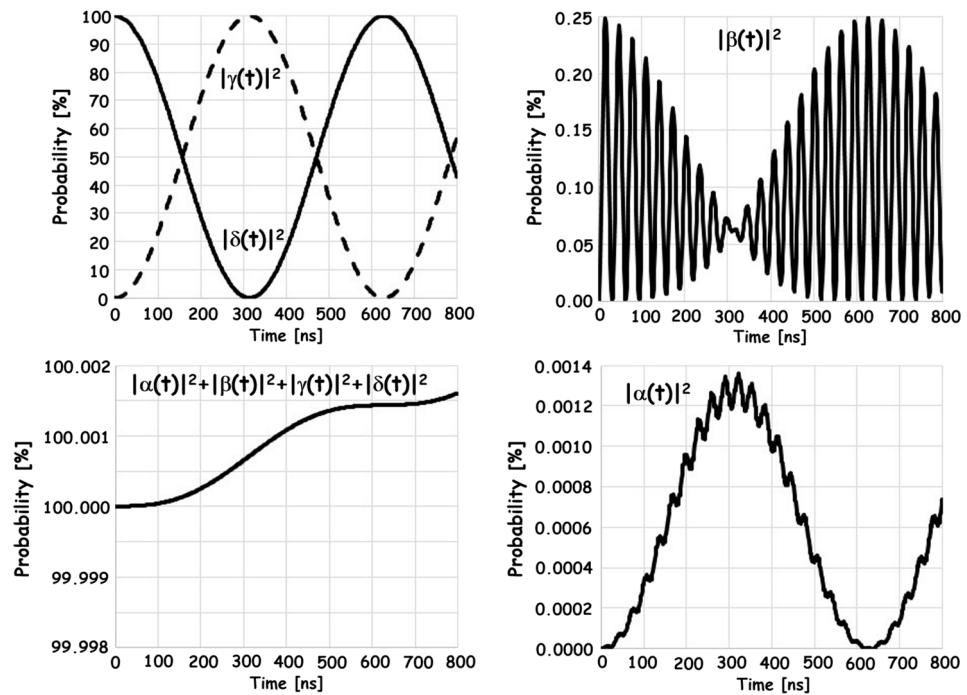


**Figure 12.** State occupation probabilities for an electromagnetic frequency  $\omega = \omega_{R1}$  and initial state  $|\psi_4\rangle$  for  $\omega_{01} = 0.6$  GHz,  $\omega_{02} = 0.5$  GHz,  $J = 0.3$  GHz, and  $\omega_1 = 5$  MHz.

Figure 12 depicts the obtained state occupation probabilities for a two-qubit system in the initial state  $|\psi_0\rangle = |\psi_4\rangle$ . The frequency  $\omega_1$  was kept equal to 5 MHz. In Figure 12, it was considered that, in force of Equation (91),  $|\alpha(t)|^2 = |x(t)|^2$ ,  $|\beta(t)|^2 = |y(t)|^2$ ,  $|\gamma(t)|^2 = |z(t)|^2$ , and  $|\delta(t)|^2 = |w(t)|^2$ .

In the upper left corner, because of Equation (81), the figure shows that the two-qubit system oscillates between the two states  $|\psi_3\rangle$  and  $|\psi_4\rangle$  with an oscillation period of 628 ns, corresponding to the Rabi frequency, while the occupation probabilities  $|\alpha(t)|^2$  and  $|\beta(t)|^2$  of the other two states remain very small. In the lower left corner, the figure shows that the condition  $|\alpha(t)|^2 + |\beta(t)|^2 + |\gamma(t)|^2 + |\delta(t)|^2 = 1$  is fulfilled, even if with a very small numerical error, which slowly increases, because it is time-integrated. The numerical results in Figure 12 therefore support the picture that the two-qubit system transits between two states when excited with an electromagnetic field at a resonance frequency. The same results are obtained for  $|\psi_0\rangle = |\psi_3\rangle$  and  $\omega = \omega_{R1}$ .

These considerations suggest an approximation for the last two differential equations in Equation (90) as follows:

$$\begin{cases} \frac{\partial \gamma(t)}{\partial t} = -j(\omega_{02} - \omega_{01} - J)\gamma(t) - j\omega_1 \delta(t)e^{-j\omega t} \\ \frac{\partial \delta(t)}{\partial t} = -j\omega_1 \gamma(t)e^{j\omega t} + j(\omega_{01} + \omega_{02} - J)\delta(t) \end{cases} \quad (97)$$

Equation (97) is formally identical to Equation (39). Consequently, the results reported in Table 1 can be used by replacing  $\omega_0$  with  $\omega_{R1}/2$ , because the resonance frequency for the one

qubit is  $2\omega_0$ , and the states  $|\psi_0\rangle$  and  $|\psi_1\rangle$  with the states  $|\psi_3\rangle$  and  $|\psi_4\rangle$ , respectively. Table 2 depicts the resulting equations.

**Table 2.** Time evolution of the two-qubit state as a function of the carrier phase and the initial condition for an electromagnetic frequency  $\omega = \omega_{R1}$ .

<b>In-phase carrier (Rotation around x-axis)</b>	Initial qubit state $ \psi_1\rangle$	$ \psi\rangle =  \psi_1\rangle$
	Initial qubit state $ \psi_2\rangle$	$ \psi\rangle =  \psi_2\rangle$
	Initial qubit state $ \psi_3\rangle$	$ \psi\rangle = e^{-j\frac{\omega_{R1}}{2}t} [\cos(\omega_1 t) \psi_3\rangle + e^{-j\frac{\pi}{2}} \sin(\omega_1 t) \psi_4\rangle]$
	Initial qubit state $ \psi_4\rangle$	$ \psi\rangle = e^{-j\frac{\omega_{R1}}{2}t} [e^{-j\frac{\pi}{2}} \sin(\omega_1 t) \psi_3\rangle + \cos(\omega_1 t) \psi_4\rangle]$
<b>In-quadrature carrier (Rotation around y-axis)</b>	Initial qubit state $ \psi_1\rangle$	$ \psi\rangle =  \psi_1\rangle$
	Initial qubit state $ \psi_2\rangle$	$ \psi\rangle =  \psi_2\rangle$
	Initial qubit state $ \psi_3\rangle$	$ \psi\rangle = e^{-j\frac{\omega_{R1}}{2}t} [\cos(\omega_1 t) \psi_3\rangle + \sin(\omega_1 t) \psi_4\rangle]$
	Initial qubit state $ \psi_4\rangle$	$ \psi\rangle = e^{-j\frac{\omega_{R1}}{2}t} [e^{-j\pi} \sin(\omega_1 t) \psi_3\rangle + \cos(\omega_1 t) \psi_4\rangle]$

Figure 13 shows the numerically calculated state occupation probabilities for a two-qubit system in the initial state  $|\psi_0\rangle = |\psi_4\rangle$  and the electromagnetic pulse frequency  $\omega = \omega_{R2}$ . As in the case of Figure 12,  $\omega_{01} = 0.6$  GHz,  $\omega_{02} = 0.5$  GHz,  $J = 0.3$  GHz, and  $\omega_1 = 5$  MHz were kept. Again, in agreement with Figure 11, the two-qubit system transits between the two states  $|\psi_4\rangle$  and  $|\psi_2\rangle$  while, similarly to the previous case, the occupation probabilities  $|\alpha(t)|^2$  and  $|\gamma(t)|^2$  of the other two states remain very small. Also, in Figure 13, the condition  $|\alpha(t)|^2 + |\beta(t)|^2 + |\gamma(t)|^2 + |\delta(t)|^2 = 1$  is fulfilled unless there is a very small numerical error. The same results are obtained for  $|\psi_0\rangle = |\psi_2\rangle$  and  $\omega = \omega_{R2}$ . Also in the present case, it is therefore possible to approximate the second and fourth differential equations in Equation (90) as follows:

$$\begin{cases} \frac{\partial\beta(t)}{\partial t} = -j(\omega_{01} - \omega_{02} - J)\beta(t) - j\omega_1\delta(t)e^{-j\omega t} \\ \frac{\partial\delta(t)}{\partial t} = -j\omega_1\beta(t)e^{j\omega t} + j(\omega_{01} + \omega_{02} - J)\delta(t) \end{cases} \quad (98)$$

Again, the couple of differential equations obtained in Equation (98) are formally identical to Equation (39) describing the dynamic of one qubit with  $\omega_{R2}/2$  replacing  $\omega_0$  and the states  $|\psi_2\rangle$  and  $|\psi_4\rangle$  in the place of the states  $|\psi_0\rangle$  and  $|\psi_1\rangle$ , respectively. Consequently, from Table 1, the equations describing the dynamic of the two-qubit system excited with an electromagnetic field oscillating at the resonance frequency  $\omega_{R2}$  are as reported in Table 3.

**Table 3.** Time evolution of the two-qubit state as a function of the carrier phase and the initial condition for an electromagnetic frequency  $\omega = \omega_{R2}$ .

<b>In-phase carrier (Rotation around x-axis)</b>	Initial qubit state $ \psi_1\rangle$	$ \psi\rangle =  \psi_1\rangle$
	Initial qubit state $ \psi_2\rangle$	$ \psi\rangle = e^{-j\frac{\omega_{R2}}{2}t} [\cos(\omega_1 t) \psi_2\rangle + e^{-j\frac{\pi}{2}} \sin(\omega_1 t) \psi_4\rangle]$
	Initial qubit state $ \psi_3\rangle$	$ \psi\rangle =  \psi_3\rangle$
	Initial qubit state $ \psi_4\rangle$	$ \psi\rangle = e^{-j\frac{\omega_{R2}}{2}t} [e^{-j\frac{\pi}{2}} \sin(\omega_1 t) \psi_2\rangle + \cos(\omega_1 t) \psi_4\rangle]$



Table 3. Cont.

<b>In-quadrature carrier (Rotation around y-axis)</b>	Initial qubit state $ \psi_1\rangle$	$ \psi\rangle =  \psi_1\rangle$
	Initial qubit state $ \psi_2\rangle$	$ \psi\rangle = e^{-j\frac{\omega_{R2}}{2}t} [\cos(\omega_1 t) \psi_2\rangle + \sin(\omega_1 t) \psi_4\rangle]$
	Initial qubit state $ \psi_3\rangle$	$ \psi\rangle =  \psi_3\rangle$
	Initial qubit state $ \psi_4\rangle$	$ \psi\rangle = e^{-j\frac{\omega_{R2}}{2}t} [e^{-j\pi} \sin(\omega_1 t) \psi_2\rangle + \cos(\omega_1 t) \psi_4\rangle]$

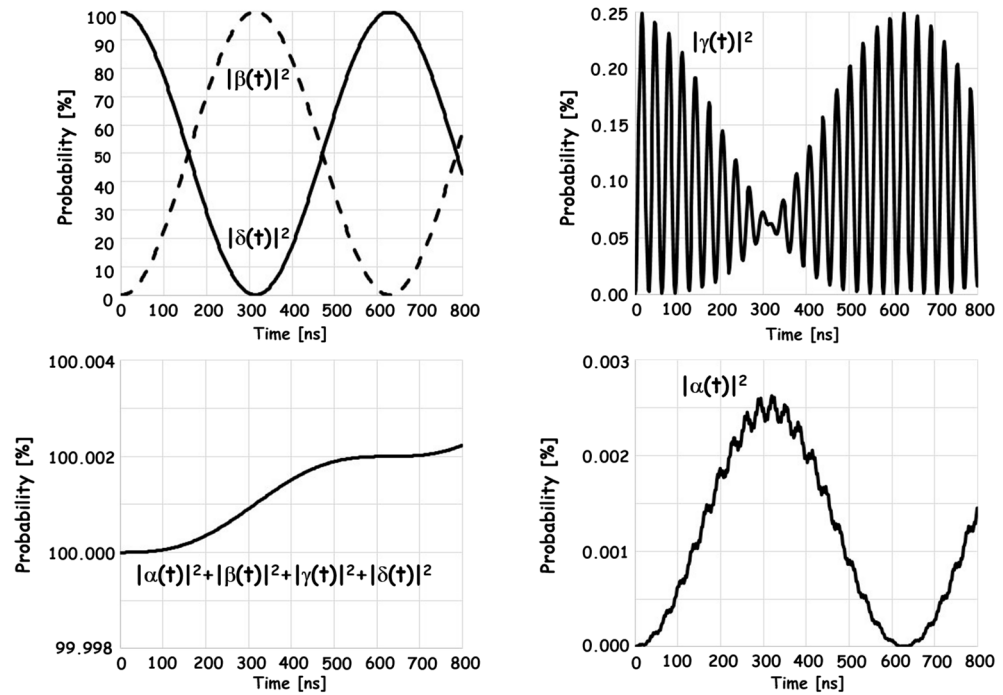


Figure 13. State occupation probabilities for an electromagnetic frequency  $\omega = \omega_{R2}$  and initial state  $|\psi_4\rangle$  for  $\omega_{01} = 0.6$  GHz,  $\omega_{02} = 0.5$  GHz,  $J = 0.3$  GHz, and  $\omega_1 = 5$  MHz.

Identical behavior of the state occupation probabilities, still in agreement with Figure 11, and the same considerations are found for the case of the two-qubit system in the initial state  $|\psi_1\rangle$  and excited with an electromagnetic frequency  $\omega = \omega_{R3}$  or  $\omega = \omega_{R4}$ . The following Tables 4 and 5 report the mathematical expressions describing the corresponding time evolution of the two-qubit state.

Table 4. Time evolution of the two-qubit state as a function of the carrier phase and the initial condition for an electromagnetic frequency  $\omega = \omega_{R3}$ .

<b>In-phase carrier (Rotation around x-axis)</b>	Initial qubit state $ \psi_1\rangle$	$ \psi\rangle = e^{-j\frac{\omega_{R3}}{2}t} [\cos(\omega_1 t) \psi_1\rangle + e^{-j\frac{\pi}{2}} \sin(\omega_1 t) \psi_3\rangle]$
	Initial qubit state $ \psi_2\rangle$	$ \psi\rangle =  \psi_2\rangle$
	Initial qubit state $ \psi_3\rangle$	$ \psi\rangle = e^{-j\frac{\omega_{R3}}{2}t} [e^{-j\frac{\pi}{2}} \sin(\omega_1 t) \psi_1\rangle + \cos(\omega_1 t) \psi_3\rangle]$
	Initial qubit state $ \psi_4\rangle$	$ \psi\rangle =  \psi_4\rangle$
<b>In-quadrature carrier (Rotation around y-axis)</b>	Initial qubit state $ \psi_1\rangle$	$ \psi\rangle = e^{-j\frac{\omega_{R3}}{2}t} [\cos(\omega_1 t) \psi_1\rangle + \sin(\omega_1 t) \psi_3\rangle]$
	Initial qubit state $ \psi_2\rangle$	$ \psi\rangle =  \psi_2\rangle$
	Initial qubit state $ \psi_3\rangle$	$ \psi\rangle = e^{-j\frac{\omega_{R3}}{2}t} [e^{-j\pi} \sin(\omega_1 t) \psi_1\rangle + \cos(\omega_1 t) \psi_3\rangle]$
	Initial qubit state $ \psi_4\rangle$	$ \psi\rangle =  \psi_4\rangle$

**Table 5.** Time evolution of the two-qubit state as a function of the carrier phase and the initial condition for an electromagnetic frequency  $\omega = \omega_{R4}$ .

<b>In-phase carrier (Rotation around x-axis)</b>	Initial qubit state $ \psi_1\rangle$	$ \psi\rangle = e^{-j\frac{\omega_{R4}}{2}t} [\cos(\omega_1 t) \psi_1\rangle + e^{-j\frac{\pi}{2}} \sin(\omega_1 t) \psi_2\rangle]$
	Initial qubit state $ \psi_2\rangle$	$ \psi\rangle = e^{-j\frac{\omega_{R4}}{2}t} [e^{-j\frac{\pi}{2}} \sin(\omega_1 t) \psi_1\rangle + \cos(\omega_1 t) \psi_2\rangle]$
	Initial qubit state $ \psi_3\rangle$	$ \psi\rangle =  \psi_3\rangle$
	Initial qubit state $ \psi_4\rangle$	$ \psi\rangle =  \psi_4\rangle$
<b>In-quadrature carrier (Rotation around y-axis)</b>	Initial qubit state $ \psi_1\rangle$	$ \psi\rangle = e^{-j\frac{\omega_{R4}}{2}t} [\cos(\omega_1 t) \psi_1\rangle + \sin(\omega_1 t) \psi_2\rangle]$
	Initial qubit state $ \psi_2\rangle$	$ \psi\rangle = e^{-j\frac{\omega_{R4}}{2}t} [e^{-j\pi} \sin(\omega_1 t) \psi_1\rangle + \cos(\omega_1 t) \psi_2\rangle]$
	Initial qubit state $ \psi_3\rangle$	$ \psi\rangle =  \psi_3\rangle$
	Initial qubit state $ \psi_4\rangle$	$ \psi\rangle =  \psi_4\rangle$

### 7. Two-Qubit Quantum Gates

As a single qubit can be exploited to implement one-qubit quantum gates, a couple of qubits can be exploited to realize two-qubit quantum gates. In particular, the present section addresses a specific two-qubit quantum gate, dubbed CNOT, together with its anti-form. The CNOT quantum gate is of particular interest because any arbitrary unitary operator on multiple qubits can be implemented by using one-qubit and CNOT gates [3]. In particular, the CNOT gate and the  $R_X$ ,  $R_Y$ , and  $R_Z$  gates in Sections 5.1–5.3 form a universal set [47].

#### 7.1. CNOT Quantum Gates

After Table 2, the application of an in-phase carrier microwave pulse at the resonance frequency  $\omega_{R1}$  for a time duration such that  $2\omega_1 t = \theta$  leaves the input states  $|\psi_1\rangle$  and  $|\psi_2\rangle$  unchanged so that the output state  $|\psi_{OUT}\rangle$  is as follows:

$$|\psi_{OUT}\rangle = |\psi_1\rangle = e^{-j\frac{\pi}{2}} |\psi_1\rangle \tag{99}$$

$$|\psi_{OUT}\rangle = |\psi_2\rangle = e^{-j\frac{\pi}{2}} |\psi_2\rangle \tag{100}$$

where the global phase  $-\pi/2$  has been added for reasons that will become clear later. On the other hand, if the input state is  $|\psi_3\rangle$ , the output state  $|\psi_{OUT}\rangle$  is as follows:

$$|\psi_{OUT}\rangle = e^{-j\frac{\omega_{R1}}{2} \frac{\theta}{2\omega_1}} \left[ \cos\left(\frac{\theta}{2}\right) |\psi_3\rangle + e^{-j\frac{\pi}{2}} \sin\left(\frac{\theta}{2}\right) |\psi_4\rangle \right] \tag{101}$$

and the output state is

$$|\psi_{OUT}\rangle = e^{-j\frac{\omega_{R1}}{2} \frac{\theta}{2\omega_1}} \left[ e^{-j\frac{\pi}{2}} \sin\left(\frac{\theta}{2}\right) |\psi_3\rangle + \cos\left(\frac{\theta}{2}\right) |\psi_4\rangle \right] \tag{102}$$

if the input state is  $|\psi_4\rangle$ .

Since  $\langle\psi_i|\psi_j\rangle$  is 1 if  $i = j$  and 0 otherwise, the resulting operator  $\hat{A}_{\omega_{R1},I}$  is as follows:

$$\begin{aligned} \hat{A}_{\omega_{R1},I} = e^{-j\frac{\pi}{2}} & |\psi_1\rangle\langle\psi_1| + e^{-j\frac{\pi}{2}} |\psi_2\rangle\langle\psi_2| + \cos\left(\frac{\theta}{2}\right) |\psi_3\rangle\langle\psi_3| + e^{-j\frac{\pi}{2}} \sin\left(\frac{\theta}{2}\right) |\psi_4\rangle\langle\psi_3| + e^{-j\frac{\pi}{2}} \sin\left(\frac{\theta}{2}\right) |\psi_3\rangle\langle\psi_4| \\ & + \cos\left(\frac{\theta}{2}\right) |\psi_4\rangle\langle\psi_4| \end{aligned} \tag{103}$$

The substitution of Equations (73)–(80) into Equation (103) leads to the matrix formulation of  $\hat{A}_{\omega R1,I}$ :

$$\begin{aligned} \hat{A}_{\omega R1,I} &= e^{-j\frac{\pi}{2}} \begin{bmatrix} 1 \\ 0 \\ 0 \\ 0 \end{bmatrix} [ 1 \ 0 \ 0 \ 0 ] + e^{-j\frac{\pi}{2}} \begin{bmatrix} 0 \\ 1 \\ 0 \\ 0 \end{bmatrix} [ 0 \ 1 \ 0 \ 0 ] + \cos \cos\left(\frac{\theta}{2}\right) \begin{bmatrix} 0 \\ 0 \\ 1 \\ 0 \end{bmatrix} [ 0 \ 0 \ 1 \ 0 ] \\ &+ e^{-j\frac{\pi}{2}} \sin\left(\frac{\theta}{2}\right) \begin{bmatrix} 0 \\ 0 \\ 0 \\ 1 \end{bmatrix} [ 0 \ 0 \ 1 \ 0 ] + e^{-j\frac{\pi}{2}} \sin\left(\frac{\theta}{2}\right) \begin{bmatrix} 0 \\ 0 \\ 1 \\ 0 \end{bmatrix} [ 0 \ 0 \ 0 \ 1 ] \\ &+ \cos\left(\frac{\theta}{2}\right) \begin{bmatrix} 0 \\ 0 \\ 0 \\ 1 \end{bmatrix} [ 0 \ 0 \ 0 \ 1 ] \\ &= e^{-j\frac{\pi}{2}} \begin{bmatrix} 1 & 0 & 0 & 0 \\ 0 & 0 & 0 & 0 \\ 0 & 0 & 0 & 0 \\ 0 & 0 & 0 & 0 \end{bmatrix} + e^{-j\frac{\pi}{2}} \begin{bmatrix} 0 & 0 & 0 & 0 \\ 0 & 1 & 0 & 0 \\ 0 & 0 & 0 & 0 \\ 0 & 0 & 0 & 0 \end{bmatrix} + \cos\left(\frac{\theta}{2}\right) \begin{bmatrix} 0 & 0 & 0 & 0 \\ 0 & 0 & 0 & 0 \\ 0 & 0 & 1 & 0 \\ 0 & 0 & 0 & 0 \end{bmatrix} \\ &+ e^{-j\frac{\pi}{2}} \sin\left(\frac{\theta}{2}\right) \begin{bmatrix} 0 & 0 & 0 & 0 \\ 0 & 0 & 0 & 0 \\ 0 & 0 & 0 & 0 \\ 0 & 0 & 1 & 0 \end{bmatrix} + e^{-j\frac{\pi}{2}} \sin\left(\frac{\theta}{2}\right) \begin{bmatrix} 0 & 0 & 0 & 0 \\ 0 & 0 & 0 & 0 \\ 0 & 0 & 0 & 1 \\ 0 & 0 & 0 & 0 \end{bmatrix} \\ &+ \cos\left(\frac{\theta}{2}\right) \begin{bmatrix} 0 & 0 & 0 & 0 \\ 0 & 0 & 0 & 0 \\ 0 & 0 & 0 & 0 \\ 0 & 0 & 0 & 1 \end{bmatrix} = \begin{bmatrix} e^{-j\frac{\pi}{2}} & 0 & 0 & 0 \\ 0 & e^{-j\frac{\pi}{2}} & 0 & 0 \\ 0 & 0 & \cos\left(\frac{\theta}{2}\right) & e^{-j\frac{\pi}{2}} \sin\left(\frac{\theta}{2}\right) \\ 0 & 0 & e^{-j\frac{\pi}{2}} \sin\left(\frac{\theta}{2}\right) & \cos\left(\frac{\theta}{2}\right) \end{bmatrix} \end{aligned}$$

In the case  $\theta = \pi$ , you obtain the following:

$$\hat{A}_{\omega R1,I}|_{\theta=\pi} = \begin{bmatrix} e^{-j\frac{\pi}{2}} & 0 & 0 & 0 \\ 0 & e^{-j\frac{\pi}{2}} & 0 & 0 \\ 0 & 0 & 0 & e^{-j\frac{\pi}{2}} \\ 0 & 0 & e^{-j\frac{\pi}{2}} & 0 \end{bmatrix} = -j \begin{bmatrix} 1 & 0 & 0 & 0 \\ 0 & 1 & 0 & 0 \\ 0 & 0 & 0 & 1 \\ 0 & 0 & 1 & 0 \end{bmatrix} = -j\hat{A}_{CNOT} \quad (104)$$

Note that the global phase introduced in Equations (99) and (100) allowed the term  $e^{-j\pi/2} = -j$  to be gathered. By coding the four states as  $|\psi_1\rangle = |00\rangle$ ,  $|\psi_2\rangle = |01\rangle$ ,  $|\psi_3\rangle = |10\rangle$ , and  $|\psi_4\rangle = |11\rangle$ , the matrix in Equation (104) describes the operator  $\hat{A}_{CNOT}$  of the CNOT quantum gate depicted in Figure 14. The truth table, which can be calculated by multiplying the matrix of the CNOT gate by the state vectors in Equations (73)–(76), shows that if the left qubit is “1” (“0”), the CNOT gate changes (does not change) the right qubit. The left (right) qubit is thus the control (target) qubit.

The CNOT gate acts on two qubits, performing the NOT operation on the second qubit only when the first qubit is  $|1\rangle$ .

After Table 3, the application of an in-phase carrier microwave pulse at the resonance frequency  $\omega_{R2}$  for a time duration such that  $2\omega_1 t = \theta$  leaves the input states  $|\psi_1\rangle$  and  $|\psi_3\rangle$  unchanged so that the output state  $|\psi_{OUT}\rangle$  is as follows:

$$|\psi_{OUT}\rangle = |\psi_1\rangle = e^{-j\frac{\pi}{2}} |\psi_1\rangle \quad (105)$$

$$|\psi_{OUT}\rangle = |\psi_3\rangle = e^{-j\frac{\pi}{2}} |\psi_3\rangle \quad (106)$$

where the global phase  $-\pi/2$  has been introduced for the same reasons as above. On the other hand, if the input state is  $|\psi_2\rangle$ , the output state  $|\psi_{OUT}\rangle$  is as follows:

$$|\psi_{OUT}\rangle = e^{-j\frac{\omega R_2}{2} \frac{\theta}{2\omega_1}} \left[ \cos\left(\frac{\theta}{2}\right) |\psi_2\rangle + e^{-j\frac{\pi}{2}} \sin\left(\frac{\theta}{2}\right) |\psi_4\rangle \right]$$

and the output state is

$$|\psi_{OUT}\rangle = e^{-j\frac{\omega R_2}{2} \frac{\theta}{2\omega_1}} \left[ e^{-j\frac{\pi}{2}} \sin\left(\frac{\theta}{2}\right) |\psi_2\rangle + \cos\left(\frac{\theta}{2}\right) |\psi_4\rangle \right]$$

if the input state is  $|\psi_4\rangle$ . Since  $\langle\psi_i|\psi_j\rangle$  is 1 if  $i = j$  and 0 otherwise, the resulting operator  $\hat{A}_{\omega R_2, I}$  is as follows:

$$\hat{A}_{\omega R_2, I} = e^{-j\frac{\pi}{2}} |\psi_1\rangle\langle\psi_1| + \cos\left(\frac{\theta}{2}\right) |\psi_2\rangle\langle\psi_2| + e^{-j\frac{\pi}{2}} \sin\left(\frac{\theta}{2}\right) |\psi_4\rangle\langle\psi_2| + e^{-j\frac{\pi}{2}} |\psi_3\rangle\langle\psi_3| + e^{-j\frac{\pi}{2}} \sin\left(\frac{\theta}{2}\right) |\psi_2\rangle\langle\psi_4| + \cos\left(\frac{\theta}{2}\right) |\psi_4\rangle\langle\psi_4| \tag{107}$$

The substitution of Equations (73)–(80) into Equation (107) leads to the matrix formulation of  $\hat{A}_{\omega R_2, I}$ :

$$\begin{aligned} \hat{A}_{\omega R_2, I} &= e^{-j\frac{\pi}{2}} \begin{bmatrix} 1 \\ 0 \\ 0 \\ 0 \end{bmatrix} \begin{bmatrix} 1 & 0 & 0 & 0 \end{bmatrix} + \cos\left(\frac{\theta}{2}\right) \begin{bmatrix} 0 \\ 1 \\ 0 \\ 0 \end{bmatrix} \begin{bmatrix} 0 & 1 & 0 & 0 \end{bmatrix} \\ &+ e^{-j\frac{\pi}{2}} \sin\left(\frac{\theta}{2}\right) \begin{bmatrix} 0 \\ 0 \\ 1 \\ 0 \end{bmatrix} \begin{bmatrix} 0 & 1 & 0 & 0 \end{bmatrix} + e^{-j\frac{\pi}{2}} \begin{bmatrix} 0 \\ 0 \\ 1 \\ 0 \end{bmatrix} \begin{bmatrix} 0 & 0 & 1 & 0 \end{bmatrix} \\ &+ e^{-j\frac{\pi}{2}} \sin\left(\frac{\theta}{2}\right) \begin{bmatrix} 0 \\ 1 \\ 0 \\ 0 \end{bmatrix} 0001 + \cos\left(\frac{\theta}{2}\right) \begin{bmatrix} 0 \\ 0 \\ 0 \\ 1 \end{bmatrix} \begin{bmatrix} 0 & 0 & 0 & 1 \end{bmatrix} \\ &= e^{-j\frac{\pi}{2}} \begin{bmatrix} 1 & 0 & 0 & 0 \\ 0 & 0 & 0 & 0 \\ 0 & 0 & 0 & 0 \\ 0 & 0 & 0 & 0 \end{bmatrix} + \cos\left(\frac{\theta}{2}\right) \begin{bmatrix} 0 & 0 & 0 & 0 \\ 0 & 1 & 0 & 0 \\ 0 & 0 & 0 & 0 \\ 0 & 0 & 0 & 0 \end{bmatrix} \\ &+ e^{-j\frac{\pi}{2}} \sin\left(\frac{\theta}{2}\right) \begin{bmatrix} 0 & 0 & 0 & 0 \\ 0 & 0 & 0 & 0 \\ 0 & 0 & 0 & 0 \\ 0 & 1 & 0 & 0 \end{bmatrix} + e^{-j\frac{\pi}{2}} \begin{bmatrix} 0 & 0 & 0 & 0 \\ 0 & 0 & 0 & 0 \\ 0 & 0 & 1 & 0 \\ 0 & 0 & 0 & 0 \end{bmatrix} \\ &+ e^{-j\frac{\pi}{2}} \sin\left(\frac{\theta}{2}\right) \begin{bmatrix} 0 & 0 & 0 & 0 \\ 0 & 0 & 0 & 1 \\ 0 & 0 & 0 & 0 \\ 0 & 0 & 0 & 0 \end{bmatrix} + \cos\left(\frac{\theta}{2}\right) \begin{bmatrix} 0 & 0 & 0 & 0 \\ 0 & 0 & 0 & 0 \\ 0 & 0 & 0 & 0 \\ 0 & 0 & 0 & 1 \end{bmatrix} \\ &= \begin{bmatrix} e^{-j\frac{\pi}{2}} & 0 & 0 & 0 \\ 0 & \cos\left(\frac{\theta}{2}\right) & 0 & e^{-j\frac{\pi}{2}} \sin\left(\frac{\theta}{2}\right) \\ 0 & 0 & e^{-j\frac{\pi}{2}} & 0 \\ 0 & e^{-j\frac{\pi}{2}} \sin\left(\frac{\theta}{2}\right) & 0 & \cos\left(\frac{\theta}{2}\right) \end{bmatrix} \end{aligned}$$

which, for  $\theta = \pi$ , reduces to

$$\hat{A}_{\omega_{R2,I}} = \begin{bmatrix} e^{-j\frac{\pi}{2}} & 0 & 0 & 0 \\ 0 & 0 & 0 & e^{-j\frac{\pi}{2}} \\ 0 & 0 & e^{-j\frac{\pi}{2}} & 0 \\ 0 & e^{-j\frac{\pi}{2}} & 0 & 0 \end{bmatrix} = -j \begin{bmatrix} 1 & 0 & 0 & 0 \\ 0 & 0 & 0 & 1 \\ 0 & 0 & 1 & 0 \\ 0 & 1 & 0 & 0 \end{bmatrix} = -j\hat{A}_{CNOT} \quad (108)$$

By coding the four states as  $|\psi_1\rangle = |00\rangle$ ,  $|\psi_2\rangle = |01\rangle$ ,  $|\psi_3\rangle = |10\rangle$ , and  $|\psi_4\rangle = |11\rangle$ , the matrix in Equation (108) describes the operator  $\hat{A}_{CNOT}$  of the CNOT quantum gate depicted in Figure 15. The truth table, which can be calculated by multiplying the matrix of the CNOT gate by the state vectors in Equations (73)–(76), shows that if the right qubit is “1” (“0”), the CNOT gate changes (does not change) the left qubit. Unlike the CNOT gate in Figure 14, the left (right) qubit is thus the target (control) qubit.

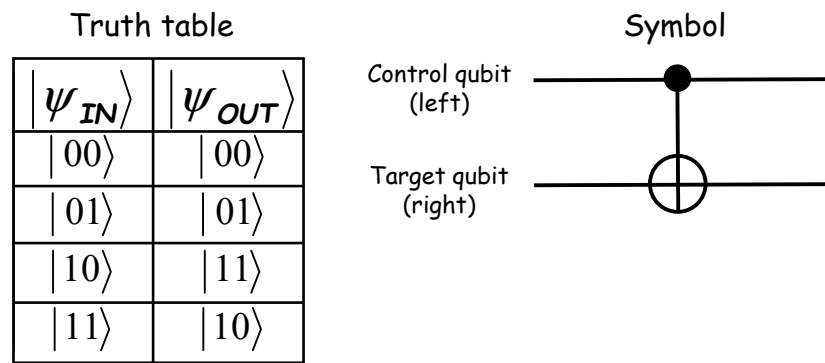


**Figure 14.** Truth table and symbol of the CNOT gate for the in-phase carrier microwave pulse at frequency  $\omega_{R1}$  and state coding  $|\psi_1\rangle = |00\rangle$ ,  $|\psi_2\rangle = |01\rangle$ ,  $|\psi_3\rangle = |10\rangle$ , and  $|\psi_4\rangle = |11\rangle$ . The left qubit is the control, and the right qubit is the target.

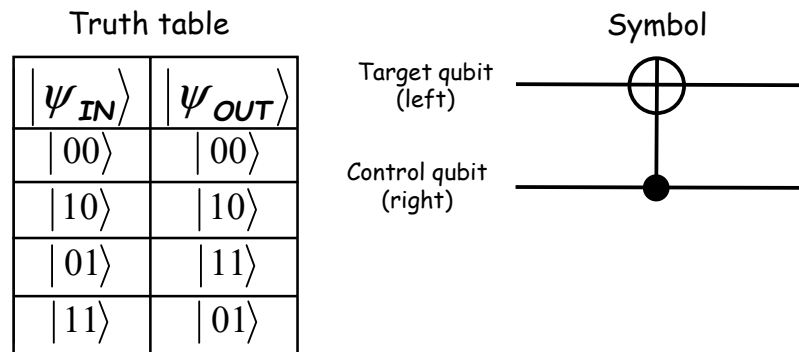


**Figure 15.** Truth table and symbol of the CNOT gate for the in-phase carrier microwave pulse at frequency  $\omega_{R2}$  and state coding  $|\psi_1\rangle = |00\rangle$ ,  $|\psi_2\rangle = |01\rangle$ ,  $|\psi_3\rangle = |10\rangle$ , and  $|\psi_4\rangle = |11\rangle$ . The right qubit is the control, and the left qubit is the target.

In the present case, the CNOT gate performs the NOT operation on the first qubit only when the second qubit is |1>.

### 7.2. Anti-CNOT Quantum Gates

After Table 4, the application of an in-phase carrier microwave pulse at the resonance frequency  $\omega_{R3}$  for a time duration such that  $2\omega_1 t = \theta$  leaves the input states  $|\psi_2\rangle$  and  $|\psi_4\rangle$  unchanged so that  $|\psi_{OUT}\rangle$  is as follows:

$$|\psi_{OUT}\rangle = |\psi_2\rangle = e^{-j\frac{\pi}{2}}|\psi_2\rangle \quad (109)$$

$$|\psi_{OUT}\rangle = |\psi_4\rangle = e^{-j\frac{\pi}{2}}|\psi_4\rangle \tag{110}$$

with the usual global phase  $-\pi/2$ . On the other hand, if the input state is  $|\psi_1\rangle$ , the output state  $|\psi_{OUT}\rangle$  is as follows:

$$|\psi_{OUT}\rangle = e^{-j\frac{\omega_{R3}}{2} \frac{\theta}{2\omega_1}} \left[ \cos\left(\frac{\theta}{2}\right)|\psi_1\rangle + e^{-j\frac{\pi}{2}}\sin\left(\frac{\theta}{2}\right)|\psi_3\rangle \right]$$

and the output state is

$$|\psi_{OUT}\rangle = e^{-j\frac{\omega_{R3}}{2} \frac{\theta}{2\omega_1}} \left[ e^{-j\frac{\pi}{2}}\sin\left(\frac{\theta}{2}\right)|\psi_1\rangle + \cos\left(\frac{\theta}{2}\right)|\psi_3\rangle \right]$$

if the input state is  $|\psi_3\rangle$ . Since  $\langle\psi_i|\psi_j\rangle$  is 1 if  $i = j$  and 0 otherwise, the resulting operator  $\hat{A}_{\omega R3,I}$  is as follows:

$$\begin{aligned} \hat{A}_{\omega R3,I} &= \cos\left(\frac{\theta}{2}\right)|\psi_1\rangle\langle\psi_1| + e^{-j\frac{\pi}{2}}\sin\left(\frac{\theta}{2}\right)|\psi_3\rangle\langle\psi_1| + e^{-j\frac{\pi}{2}}|\psi_2\rangle\langle\psi_2| + e^{-j\frac{\pi}{2}}\sin\left(\frac{\theta}{2}\right)|\psi_1\rangle\langle\psi_3| \\ &\quad + \cos\left(\frac{\theta}{2}\right)|\psi_3\rangle\langle\psi_3| + e^{-j\frac{\pi}{2}}|\psi_4\rangle\langle\psi_4| \end{aligned} \tag{111}$$

The substitution of Equations (73)–(80) into Equation (111) leads to the matrix formulation of  $\hat{A}_{\omega R3,I}$ :

$$\begin{aligned} \hat{A}_{\omega R3,I} &= \cos\left(\frac{\theta}{2}\right) \begin{bmatrix} 1 \\ 0 \\ 0 \\ 0 \end{bmatrix} \begin{bmatrix} 1 & 0 & 0 & 0 \end{bmatrix} + e^{-j\frac{\pi}{2}}\sin\left(\frac{\theta}{2}\right) \begin{bmatrix} 0 \\ 0 \\ 1 \\ 0 \end{bmatrix} \begin{bmatrix} 1 & 0 & 0 & 0 \end{bmatrix} \\ &\quad + e^{-j\frac{\pi}{2}} \begin{bmatrix} 0 \\ 1 \\ 0 \\ 0 \end{bmatrix} \begin{bmatrix} 0 & 1 & 0 & 0 \end{bmatrix} + e^{-j\frac{\pi}{2}}\sin\left(\frac{\theta}{2}\right) \begin{bmatrix} 1 \\ 0 \\ 0 \\ 0 \end{bmatrix} \begin{bmatrix} 0 & 0 & 1 & 0 \end{bmatrix} \\ &\quad + \cos\left(\frac{\theta}{2}\right) \begin{bmatrix} 0 \\ 0 \\ 1 \\ 0 \end{bmatrix} \begin{bmatrix} 0 & 0 & 1 & 0 \end{bmatrix} + e^{-j\frac{\pi}{2}} \begin{bmatrix} 0 \\ 0 \\ 0 \\ 1 \end{bmatrix} \begin{bmatrix} 0 & 0 & 0 & 1 \end{bmatrix} \\ &= \cos\left(\frac{\theta}{2}\right) \begin{bmatrix} 1 & 0 & 0 & 0 \\ 0 & 0 & 0 & 0 \\ 0 & 0 & 0 & 0 \\ 0 & 0 & 0 & 0 \end{bmatrix} + e^{-j\frac{\pi}{2}}\sin\left(\frac{\theta}{2}\right) \begin{bmatrix} 0 & 0 & 0 & 0 \\ 0 & 0 & 0 & 0 \\ 1 & 0 & 0 & 0 \\ 0 & 0 & 0 & 0 \end{bmatrix} \\ &\quad + e^{-j\frac{\pi}{2}} \begin{bmatrix} 0 & 0 & 0 & 0 \\ 0 & 1 & 0 & 0 \\ 0 & 0 & 0 & 0 \\ 0 & 0 & 0 & 0 \end{bmatrix} + e^{-j\frac{\pi}{2}}\sin\left(\frac{\theta}{2}\right) \begin{bmatrix} 0 & 0 & 1 & 0 \\ 0 & 0 & 0 & 0 \\ 0 & 0 & 0 & 0 \\ 0 & 0 & 0 & 0 \end{bmatrix} \\ &\quad + \cos\left(\frac{\theta}{2}\right) \begin{bmatrix} 0 & 0 & 0 & 0 \\ 0 & 0 & 0 & 0 \\ 0 & 0 & 1 & 0 \\ 0 & 0 & 0 & 0 \end{bmatrix} + e^{-j\frac{\pi}{2}} \begin{bmatrix} 0 & 0 & 0 & 0 \\ 0 & 0 & 0 & 0 \\ 0 & 0 & 0 & 0 \\ 0 & 0 & 0 & 1 \end{bmatrix} \\ &= \begin{bmatrix} \cos\left(\frac{\theta}{2}\right) & 0 & e^{-j\frac{\pi}{2}}\sin\left(\frac{\theta}{2}\right) & 0 \\ 0 & e^{-j\frac{\pi}{2}} & 0 & 0 \\ e^{-j\frac{\pi}{2}}\sin\left(\frac{\theta}{2}\right) & 0 & \cos\left(\frac{\theta}{2}\right) & 0 \\ 0 & 0 & 0 & e^{-j\frac{\pi}{2}} \end{bmatrix} \end{aligned}$$

For  $\theta = \pi$ , you obtain the following:

$$\hat{A}_{\omega R3,I} = \begin{bmatrix} 0 & 0 & e^{-j\frac{\pi}{2}} & 0 \\ 0 & e^{-j\frac{\pi}{2}} & 0 & 0 \\ e^{-j\frac{\pi}{2}} & 0 & 0 & 0 \\ 0 & 0 & 0 & e^{-j\frac{\pi}{2}} \end{bmatrix} = -j \begin{bmatrix} 0 & 0 & 1 & 0 \\ 0 & 1 & 0 & 0 \\ 1 & 0 & 0 & 0 \\ 0 & 0 & 0 & 1 \end{bmatrix} = -j\hat{A}_{anti-CNOT} \quad (112)$$

By coding the four states as  $|\psi_1\rangle = |00\rangle$ ,  $|\psi_2\rangle = |01\rangle$ ,  $|\psi_3\rangle = |10\rangle$ , and  $|\psi_4\rangle = |11\rangle$ , the matrix in Equation (112) describes the operator  $\hat{A}_{anti-CNOT}$  of the anti-CNOT quantum gate depicted in Figure 16. The truth table, which can be calculated by multiplying the matrix of the CNOT gate by the state vectors in Equations (73)–(76), shows that if the right qubit is “0” (“1”), the CNOT gate changes (does not change) the left qubit. For this reason, the gate is dubbed anti-CNOT. As in the case of the CNOT gate in Figure 15, the left (right) qubit is thus the target (control) qubit.

The anti-CNOT quantum gate performs the NOT operation on the first qubit only when the second one is  $|0\rangle$ .

After Table 5, the application of an in-phase carrier microwave pulse at the resonance frequency  $\omega_{R4}$  for a time duration such that  $2\omega_1 t = \theta$  leaves the input states  $|\psi_3\rangle$  and  $|\psi_4\rangle$  unchanged so that  $|\psi_{OUT}\rangle$  is as follows:

$$|\psi_{OUT}\rangle = |\psi_3\rangle = e^{-j\frac{\pi}{2}}|\psi_3\rangle \quad (113)$$

$$|\psi_{OUT}\rangle = |\psi_4\rangle = e^{-j\frac{\pi}{2}}|\psi_4\rangle \quad (114)$$

with the usual global phase  $-\pi/2$ . On the other hand, if the input state is  $|\psi_1\rangle$ , the output state  $|\psi_{OUT}\rangle$  is as follows:

$$|\psi_{OUT}\rangle = e^{-j\frac{\omega_{R4}}{2} \frac{\theta}{2\omega_1}} \left[ \cos\left(\omega_1 \frac{\theta}{2\omega_1}\right) |\psi_1\rangle + e^{-j\frac{\pi}{2}} \sin\left(\omega_1 \frac{\theta}{2\omega_1}\right) |\psi_2\rangle \right] = e^{-j\frac{\omega_{R4}}{2} \frac{\theta}{2\omega_1}} \left[ \cos\left(\frac{\theta}{2}\right) |\psi_1\rangle + e^{-j\frac{\pi}{2}} \sin\left(\frac{\theta}{2}\right) |\psi_2\rangle \right]$$

and the output state is

$$|\psi_{OUT}\rangle = e^{-j\frac{\omega_{R4}}{2} \frac{\theta}{2\omega_1}} \left[ e^{-j\frac{\pi}{2}} \sin\left(\omega_1 \frac{\theta}{2\omega_1}\right) |\psi_1\rangle + \cos\left(\omega_1 \frac{\theta}{2\omega_1}\right) |\psi_2\rangle \right] = e^{-j\frac{\omega_{R4}}{2} \frac{\theta}{2\omega_1}} \left[ e^{-j\frac{\pi}{2}} \sin\left(\frac{\theta}{2}\right) |\psi_1\rangle + \cos\left(\frac{\theta}{2}\right) |\psi_2\rangle \right]$$

if the input state is  $|\psi_2\rangle$ . Since  $\langle\psi_i|\psi_j\rangle$  is 1 if  $i = j$  and 0 otherwise, the resulting operator  $\hat{A}_{\omega R4,I}$  is as follows:

$$\hat{A}_{\omega R4,I} = \cos\left(\frac{\theta}{2}\right) |\psi_1\rangle\langle\psi_1| + e^{-j\frac{\pi}{2}} \sin\left(\frac{\theta}{2}\right) |\psi_2\rangle\langle\psi_1| + e^{-j\frac{\pi}{2}} \sin\left(\frac{\theta}{2}\right) |\psi_1\rangle\langle\psi_2| + \cos\left(\frac{\theta}{2}\right) |\psi_2\rangle\langle\psi_2| + e^{-j\frac{\pi}{2}} |\psi_3\rangle\langle\psi_3| + e^{-j\frac{\pi}{2}} |\psi_4\rangle\langle\psi_4| \quad (115)$$

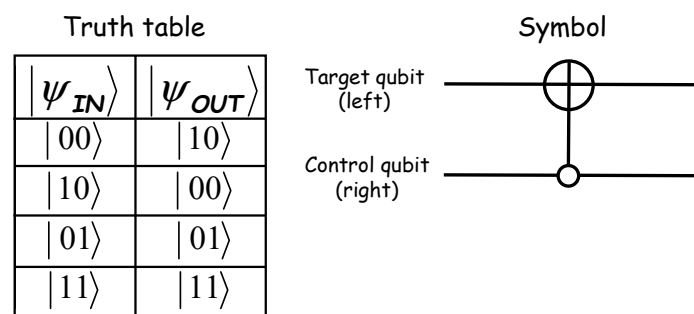


**Figure 16.** Truth table and symbol of the anti-CNOT gate for the in-phase carrier microwave pulse at frequency  $\omega_{R3}$  and state coding  $|\psi_1\rangle = |00\rangle$ ,  $|\psi_2\rangle = |01\rangle$ ,  $|\psi_3\rangle = |10\rangle$ , and  $|\psi_4\rangle = |11\rangle$ . The right qubit is the control, and the left qubit is the target.

The substitution of Equations (73)–(80) into Equation (115) leads to the matrix formulation of  $\hat{A}_{\omega R4,I}$ :

$$\begin{aligned} \hat{A}_{\omega R4,I} &= \cos\left(\frac{\theta}{2}\right) \begin{bmatrix} 1 \\ 0 \\ 0 \\ 0 \end{bmatrix} [1 \ 0 \ 0 \ 0] + e^{-j\frac{\pi}{2}} \sin\left(\frac{\theta}{2}\right) \begin{bmatrix} 0 \\ 1 \\ 0 \\ 0 \end{bmatrix} [1 \ 0 \ 0 \ 0] \\ &+ e^{-j\frac{\pi}{2}} \sin\left(\frac{\theta}{2}\right) \begin{bmatrix} 1 \\ 0 \\ 0 \\ 0 \end{bmatrix} [0 \ 1 \ 0 \ 0] + \cos\left(\frac{\theta}{2}\right) \begin{bmatrix} 0 \\ 1 \\ 0 \\ 0 \end{bmatrix} [0 \ 1 \ 0 \ 0] \\ &+ e^{-j\frac{\pi}{2}} \begin{bmatrix} 0 \\ 0 \\ 1 \\ 0 \end{bmatrix} [0 \ 0 \ 1 \ 0] + e^{-j\frac{\pi}{2}} \begin{bmatrix} 0 \\ 0 \\ 0 \\ 1 \end{bmatrix} [0 \ 0 \ 0 \ 1] \\ &= \cos\left(\frac{\theta}{2}\right) \begin{bmatrix} 1 & 0 & 0 & 0 \\ 0 & 0 & 0 & 0 \\ 0 & 0 & 0 & 0 \\ 0 & 0 & 0 & 0 \end{bmatrix} + e^{-j\frac{\pi}{2}} \sin\left(\frac{\theta}{2}\right) \begin{bmatrix} 0 & 0 & 0 & 0 \\ 1 & 0 & 0 & 0 \\ 0 & 0 & 0 & 0 \\ 0 & 0 & 0 & 0 \end{bmatrix} \\ &+ e^{-j\frac{\pi}{2}} \sin\left(\frac{\theta}{2}\right) \begin{bmatrix} 0 & 1 & 0 & 0 \\ 0 & 0 & 0 & 0 \\ 0 & 0 & 0 & 0 \\ 0 & 0 & 0 & 0 \end{bmatrix} + \cos\left(\frac{\theta}{2}\right) \begin{bmatrix} 0 & 0 & 0 & 0 \\ 0 & 1 & 0 & 0 \\ 0 & 0 & 0 & 0 \\ 0 & 0 & 0 & 0 \end{bmatrix} \\ &+ e^{-j\frac{\pi}{2}} \begin{bmatrix} 0 & 0 & 0 & 0 \\ 0 & 0 & 0 & 0 \\ 0 & 0 & 1 & 0 \\ 0 & 0 & 0 & 0 \end{bmatrix} + e^{-j\frac{\pi}{2}} \begin{bmatrix} 0 & 0 & 0 & 0 \\ 0 & 0 & 0 & 0 \\ 0 & 0 & 0 & 0 \\ 0 & 0 & 0 & 1 \end{bmatrix} \\ &= \begin{bmatrix} \cos\left(\frac{\theta}{2}\right) & e^{-j\frac{\pi}{2}} \sin\left(\frac{\theta}{2}\right) & 0 & 0 \\ e^{-j\frac{\pi}{2}} \sin\left(\frac{\theta}{2}\right) & \cos\left(\frac{\theta}{2}\right) & 0 & 0 \\ 0 & 0 & e^{-j\frac{\pi}{2}} & 0 \\ 0 & 0 & 0 & e^{-j\frac{\pi}{2}} \end{bmatrix} \end{aligned}$$

In the case  $\theta = \pi$ , you obtain the following:

$$\hat{A}_{\omega R4,I} = \begin{bmatrix} 0 & e^{-j\frac{\pi}{2}} & 0 & 0 \\ e^{-j\frac{\pi}{2}} & 0 & 0 & 0 \\ 0 & 0 & e^{-j\frac{\pi}{2}} & 0 \\ 0 & 0 & 0 & e^{-j\frac{\pi}{2}} \end{bmatrix} = e^{-j\frac{\pi}{2}} \begin{bmatrix} 0 & 1 & 0 & 0 \\ 1 & 0 & 0 & 0 \\ 0 & 0 & 1 & 0 \\ 0 & 0 & 0 & 1 \end{bmatrix} = -j\hat{A}_{anti-CNOT} \quad (116)$$

By coding the four states as  $|\psi_1\rangle = |00\rangle$ ,  $|\psi_2\rangle = |01\rangle$ ,  $|\psi_3\rangle = |10\rangle$ , and  $|\psi_4\rangle = |11\rangle$ , the matrix in Equation (116) describes the operator  $\hat{A}_{anti-CNOT}$  of the anti-CNOT quantum gate depicted in Figure 17. The truth table, which can be calculated by multiplying the matrix of the CNOT gate by the state vectors in Equations (73)–(76), shows that if the left qubit is “0” (“1”), the CNOT gate changes (does not change) the right qubit. For this reason, the gate is dubbed anti-CNOT. As in the case of the CNOT gate in Figure 14, the left (right) qubit is thus the control (target) qubit.



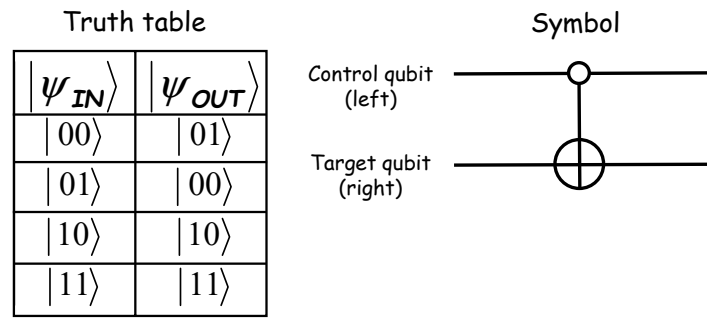


**Figure 17.** Truth table and symbol of the anti-CNOT gate for the in-phase carrier microwave pulse at frequency  $\omega_{R4}$  and state coding  $|\psi_1\rangle = |00\rangle$ ,  $|\psi_2\rangle = |01\rangle$ ,  $|\psi_3\rangle = |10\rangle$ , and  $|\psi_4\rangle = |11\rangle$ . The right qubit is the control, and the left qubit is the target.

In the present case, the anti-CNOT quantum gate performs the NOT operation on the second qubit only when the first qubit is  $|0\rangle$ .

### 7.3. Double-CNOT and SWAP Quantum Gates

A CNOT quantum gate with the control qubit on the left followed by a CNOT quantum gate with the control qubit on the right yields the so-called Double-CNOT quantum gate. After Figures 14 and 15, its operator  $\hat{A}_{\text{Double-CNOT}}$  is given by

$$\hat{A}_{\text{Double-CNOT}} = \begin{bmatrix} 1 & 0 & 0 & 0 \\ 0 & 0 & 0 & 1 \\ 0 & 0 & 1 & 0 \\ 0 & 1 & 0 & 0 \end{bmatrix} \begin{bmatrix} 1 & 0 & 0 & 0 \\ 0 & 1 & 0 & 0 \\ 0 & 0 & 0 & 1 \\ 0 & 0 & 1 & 0 \end{bmatrix} = \begin{bmatrix} 1 & 0 & 0 & 0 \\ 0 & 0 & 1 & 0 \\ 0 & 0 & 0 & 1 \\ 0 & 1 & 0 & 0 \end{bmatrix} \quad (117)$$

Following Section 7.1, the Double-CNOT quantum gate is obtained by applying an in-phase microwave pulse at the resonance frequency  $\omega_{R1}$  followed by another in-phase microwave pulse at the resonance frequency  $\omega_{R2}$ . Both the pulses should be applied for a time duration equal to  $\pi/2\omega_1$ . Figure 18 shows the symbol and truth table of the Double-CNOT quantum gate.

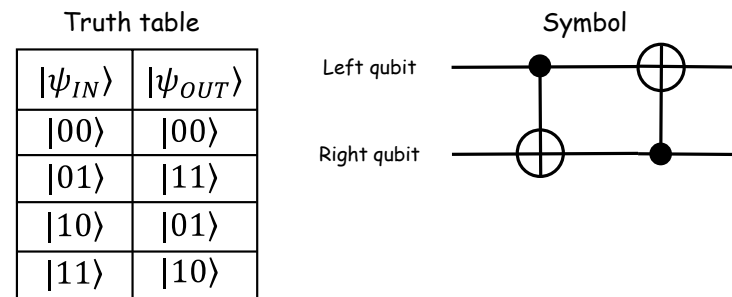


**Figure 18.** Truth table and symbol of the Double-CNOT quantum gate for the state coding  $|\psi_1\rangle = |00\rangle$ ,  $|\psi_2\rangle = |01\rangle$ ,  $|\psi_3\rangle = |10\rangle$ , and  $|\psi_4\rangle = |11\rangle$ .

The Double-CNOT quantum gate calculates the second output qubit as the XOR of the two input qubits, and it sets the first output qubit equal to the second input qubit.

The application of a further in-phase microwave pulse at the resonance frequency  $\omega_{R1}$ , still for a time duration  $\pi/2\omega_1$ , leads to the SWAP quantum gate, whose operator  $\hat{A}_{\text{SWAP}}$  is thus given by

$$\hat{A}_{\text{SWAP}} = \begin{bmatrix} 1 & 0 & 0 & 0 \\ 0 & 1 & 0 & 0 \\ 0 & 0 & 0 & 1 \\ 0 & 0 & 1 & 0 \end{bmatrix} \begin{bmatrix} 1 & 0 & 0 & 0 \\ 0 & 0 & 0 & 1 \\ 0 & 0 & 1 & 0 \\ 0 & 1 & 0 & 0 \end{bmatrix} \begin{bmatrix} 1 & 0 & 0 & 0 \\ 0 & 1 & 0 & 0 \\ 0 & 0 & 0 & 1 \\ 0 & 0 & 1 & 0 \end{bmatrix} = \begin{bmatrix} 1 & 0 & 0 & 0 \\ 0 & 0 & 1 & 0 \\ 0 & 1 & 0 & 0 \\ 0 & 0 & 0 & 1 \end{bmatrix} \quad (118)$$

Figure 19 shows the symbol and truth table of the SWAP quantum gate.

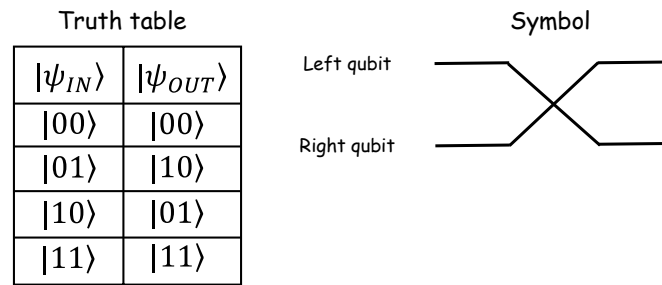


**Figure 19.** Truth table and symbol of the SWAP quantum gate for the state coding  $|\psi_1\rangle = |00\rangle$ ,  $|\psi_2\rangle = |01\rangle$ ,  $|\psi_3\rangle = |10\rangle$ , and  $|\psi_4\rangle = |11\rangle$ .

The SWAP quantum gate swaps the two input qubits.

#### 7.4. Further Remarks on the CNOT and Anti-CNOT Quantum Gates

Table 6 shows that the interpretation of the matrix in Equations (104), (108), (112), and (116) with the state coding  $|\psi_1\rangle = |11\rangle$ ,  $|\psi_2\rangle = |10\rangle$ ,  $|\psi_3\rangle = |01\rangle$ , and  $|\psi_4\rangle = |00\rangle$ , which is complementary to that used before, still leads to CNOT and anti-CNOT quantum gates but in a different order.

**Table 6.** CNOT and anti-CNOT quantum gates for the state coding  $|\psi_1\rangle = |00\rangle$ ,  $|\psi_2\rangle = |01\rangle$ ,  $|\psi_3\rangle = |10\rangle$ ,  $|\psi_4\rangle = |11\rangle$  and  $|\psi_1\rangle = |11\rangle$ ,  $|\psi_2\rangle = |10\rangle$ ,  $|\psi_3\rangle = |01\rangle$ ,  $|\psi_4\rangle = |00\rangle$ .

Operator	Resonance Frequency	States Coding			
		$ \psi_1\rangle =  00\rangle$ $ \psi_2\rangle =  01\rangle$	$ \psi_3\rangle =  10\rangle$ $ \psi_4\rangle =  11\rangle$	$ \psi_1\rangle =  11\rangle$ $ \psi_2\rangle =  10\rangle$	$ \psi_3\rangle =  01\rangle$ $ \psi_4\rangle =  00\rangle$
$\begin{bmatrix} 1 & 0 & 0 & 0 \\ 0 & 1 & 0 & 0 \\ 0 & 0 & 0 & 1 \\ 0 & 0 & 1 & 0 \end{bmatrix}$	$\omega_{R1}$	CNOT (left qubit: control) (right qubit: target)		Anti-CNOT (left qubit: control) (right qubit: target)	
$\begin{bmatrix} 1 & 0 & 0 & 0 \\ 0 & 0 & 0 & 1 \\ 0 & 0 & 1 & 0 \\ 0 & 1 & 0 & 0 \end{bmatrix}$	$\omega_{R2}$	CNOT (left qubit: target) (right qubit: control)		Anti-CNOT (left qubit: target) (right qubit: control)	
$\begin{bmatrix} 0 & 0 & 1 & 0 \\ 0 & 1 & 0 & 0 \\ 1 & 0 & 0 & 0 \\ 0 & 0 & 0 & 1 \end{bmatrix}$	$\omega_{R3}$	Anti-CNOT (left qubit: target) (right qubit: control)		CNOT (left qubit: target) (right qubit: control)	
$\begin{bmatrix} 0 & 1 & 0 & 0 \\ 1 & 0 & 0 & 0 \\ 0 & 0 & 1 & 0 \\ 0 & 0 & 0 & 1 \end{bmatrix}$	$\omega_{R4}$	Anti-CNOT (left qubit: control) (right qubit: target)		CNOT (left qubit: control) (right qubit: target)	

### 8. A Simple Quantum Algorithm: Deutsch’s Algorithm

The analogy between the quantum microprocessor and the double-slit experiment in Section 2 pointed out that a quantum algorithm makes solutions that are not accessible to a classical algorithm possible. To provide evidence of this statement, let us consider the physical system (oracle) depicted in Figure 20. It operates, by means of the unitary operator  $U$ , on the input two-qubit state  $|x_{in}\rangle \otimes |y_{in}\rangle$ , and it generates the output two-qubit state  $|x_{out}\rangle \otimes |y_{out}\rangle$  with  $|x_{out}\rangle = |x_{in}\rangle$ . In addition, let  $f$  be a scalar function  $f: \{0,1\} \rightarrow \{0,1\}$  such that  $|y_{out}\rangle = |y_{in} \oplus f(x_{in})\rangle$ , where  $y_{in} = 0$  ( $y_{in} = 1$ ) if  $|y_{in}\rangle = |0\rangle$  ( $|y_{in}\rangle = |1\rangle$ ),  $x_{in} = 0$  ( $x_{in} = 1$ ) if  $|x_{in}\rangle = |0\rangle$  ( $|x_{in}\rangle = |1\rangle$ ), and  $\oplus$  is the XOR operation.

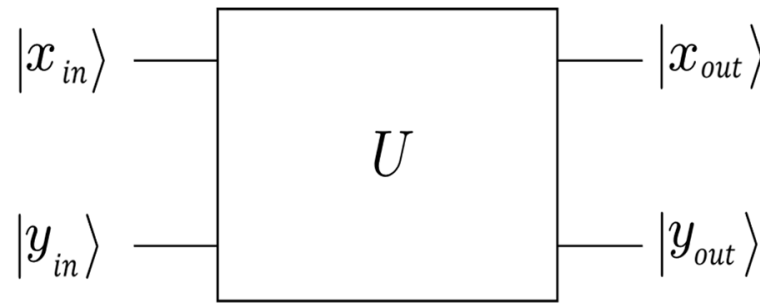


Figure 20. Oracle operating on the input two-qubit state  $|x_{in}\rangle \otimes |y_{in}\rangle$ .

Let us introduce the problem of determining if the above function  $f$  is constant, that is,  $f(0) = f(1)$ , or balanced, that is,  $f(0) \neq f(1)$ . To solve this problem for a given oracle, you need to calculate, for both  $|x_{in}\rangle = |0\rangle$  and  $|x_{in}\rangle = |1\rangle$ , first  $|x_{out}\rangle \otimes |y_{out}\rangle$  and then  $f(x_{in})$  from  $|y_{out}\rangle = |y_{in} \oplus f(x_{in})\rangle$ . For the sake of clarity, let us address the oracles in Figure 21.

Table 7 details the calculation for the case (a) for which  $U = I \otimes I$ , where  $I$  is the unitary operator used for Equations (82)–(87). Since  $|y_{out}\rangle = |y_{in}\rangle$ , by forcing  $|y_{out}\rangle = |y_{in} \oplus f(x_{in})\rangle$ , you obtain  $f(0) = f(1) = 0$ . For the oracle in Figure 21a, the function  $f$  is thus constant.

Table 7. Calculation for the oracle in Figure 21a.

$ x_{in}\rangle$	$ y_{in}\rangle$	$ x_{out}\rangle$	$ y_{out}\rangle$	$ y_{in} \oplus f(x_{in})\rangle$	$f(x_{in})$
$ 0\rangle$	$ 0\rangle$	$ 0\rangle$	$ 0\rangle$	$ 0 \oplus f(0)\rangle$	$0 = f(0)$
$ 0\rangle$	$ 1\rangle$	$ 0\rangle$	$ 1\rangle$	$ 1 \oplus f(0)\rangle$	$0 = f(0)$
$ 1\rangle$	$ 0\rangle$	$ 1\rangle$	$ 0\rangle$	$ 0 \oplus f(1)\rangle$	$0 = f(1)$
$ 1\rangle$	$ 1\rangle$	$ 1\rangle$	$ 1\rangle$	$ 1 \oplus f(1)\rangle$	$0 = f(1)$

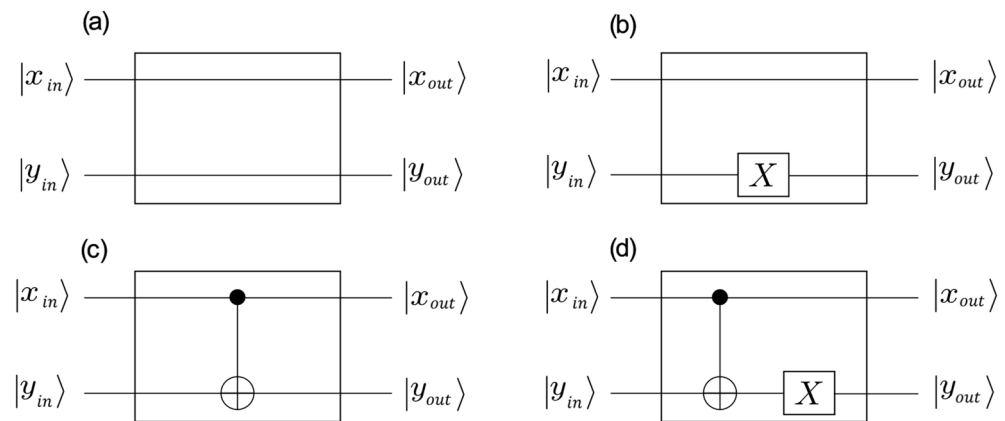


Figure 21. Four oracle implementations: (a)  $U = I \otimes I$ , (b)  $U = I \otimes \hat{A}_X$ , (c)  $U = \hat{A}_{CNOT}$ , (d)  $U = (I \otimes \hat{A}_X) \hat{A}_{CNOT}$ .

For the oracle in Figure 21b,  $U = I \otimes \hat{A}_X$ , where  $\hat{A}_X$  is the Pauli X gate operator in Equation (52). Table 8 provides the detailed calculation. The rightmost column shows that also in the present case, the function  $f$  is constant but with  $f(0) = f(1) = 1$ .

On the other hand, for the oracle in Figure 21c, for which  $U$  is the CNOT operator  $\hat{A}_{CNOT}$  in Equation (104), the calculation in Table 9 shows that the function  $f$  is balanced. Table 10 shows that also for the oracle in Figure 21d, for which  $U = I \otimes \hat{A}_X$ , the function  $f$  is balanced.

**Table 8.** Calculation for the oracle in Figure 21b.

$ x_{in}\rangle$	$ y_{in}\rangle$	$ x_{out}\rangle$	$ y_{out}\rangle$	$ y_{in} \oplus f(x_{in})\rangle$	$f(x_{in})$
$ 0\rangle$	$ 0\rangle$	$ 0\rangle$	$ 1\rangle$	$ 0 \oplus f(0)\rangle$	$1 = f(0)$
$ 0\rangle$	$ 1\rangle$	$ 0\rangle$	$ 0\rangle$	$ 1 \oplus f(0)\rangle$	$1 = f(0)$
$ 1\rangle$	$ 0\rangle$	$ 1\rangle$	$ 1\rangle$	$ 0 \oplus f(1)\rangle$	$1 = f(1)$
$ 1\rangle$	$ 1\rangle$	$ 1\rangle$	$ 0\rangle$	$ 1 \oplus f(1)\rangle$	$1 = f(1)$

**Table 9.** Calculation for the oracle in Figure 21c.

$ x_{in}\rangle$	$ y_{in}\rangle$	$ x_{out}\rangle$	$ y_{out}\rangle$	$ y_{in} \oplus f(x_{in})\rangle$	$f(x_{in})$
$ 0\rangle$	$ 0\rangle$	$ 0\rangle$	$ 0\rangle$	$ 0 \oplus f(0)\rangle$	$0 = f(0)$
$ 0\rangle$	$ 1\rangle$	$ 0\rangle$	$ 1\rangle$	$ 1 \oplus f(0)\rangle$	$0 = f(0)$
$ 1\rangle$	$ 0\rangle$	$ 1\rangle$	$ 1\rangle$	$ 0 \oplus f(1)\rangle$	$1 = f(1)$
$ 1\rangle$	$ 1\rangle$	$ 1\rangle$	$ 0\rangle$	$ 1 \oplus f(1)\rangle$	$1 = f(1)$

**Table 10.** Calculation for the oracle in Figure 21d.

$ x_{in}\rangle$	$ y_{in}\rangle$	$ x_{out}\rangle$	$ y_{out}\rangle$	$ y_{in} \oplus f(x_{in})\rangle$	$f(x_{in})$
$ 0\rangle$	$ 0\rangle$	$ 0\rangle$	$ 1\rangle$	$ 0 \oplus f(0)\rangle$	$1 = f(0)$
$ 0\rangle$	$ 1\rangle$	$ 0\rangle$	$ 0\rangle$	$ 1 \oplus f(0)\rangle$	$1 = f(0)$
$ 1\rangle$	$ 0\rangle$	$ 1\rangle$	$ 0\rangle$	$ 0 \oplus f(1)\rangle$	$0 = f(1)$
$ 1\rangle$	$ 1\rangle$	$ 1\rangle$	$ 1\rangle$	$ 1 \oplus f(1)\rangle$	$0 = f(1)$

All the above examples in Tables 7–10 share the need to calculate the function  $f$  twice, that is, for  $|x_{in}\rangle = |0\rangle$  and  $|x_{in}\rangle = |1\rangle$ , before concluding whether the function is constant or balanced.

Deutsch’s quantum algorithm, depicted in Figure 22, allows the same information to be obtained, but by performing just a single measurement. For the sake of formal brevity, the short notation  $|xy\rangle$  for the tensorial product  $|x\rangle \otimes |y\rangle$  is adopted in the following.

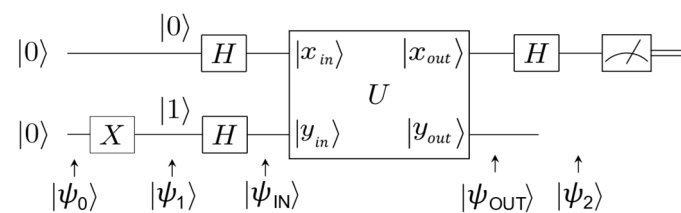


**Figure 22.** Quantum circuit implementing Deutsch’s algorithm.

First, you apply the operator  $I \otimes \hat{A}_X$  to the initial state  $|\psi_0\rangle = |00\rangle$  to obtain the state  $|\psi_1\rangle = |01\rangle$  that then is subjected to the operator  $\hat{A}_H \otimes \hat{A}_H$ , where  $\hat{A}_H$  is the Hadamard operator in Equation (69). In this way, the state  $|\psi_{IN}\rangle$  at the input of the oracle is as follows:

$$|\psi_{IN}\rangle = \left[ \frac{|0\rangle + |1\rangle}{\sqrt{2}} \right] \otimes \left[ \frac{|0\rangle - |1\rangle}{\sqrt{2}} \right] = \frac{1}{2}(|00\rangle - |01\rangle + |10\rangle - |11\rangle) \tag{119}$$

As  $|x_{out}\rangle = |x_{in}\rangle$ , the state  $|\psi_{OUT}\rangle$  at the output of the oracle is thus

$$|\psi_{OUT}\rangle = |x_{out}\rangle \otimes |y_{in} \oplus f(x_{in})\rangle = |x_{in}\rangle \otimes |y_{in} \oplus f(x_{in})\rangle = \frac{1}{2}|0\rangle \otimes (|0 \oplus f(0)\rangle - |1 \oplus f(0)\rangle) + \frac{1}{2}|1\rangle \otimes (|0 \oplus f(1)\rangle - |1 \oplus f(1)\rangle) \tag{120}$$

or, by separating for  $f$  constant or balanced,

$$|\psi_{OUT}\rangle = \begin{cases} \pm\frac{1}{2}(|0\rangle+|1\rangle) \otimes (|0\rangle-|1\rangle) & \text{if } f(0) = f(1) \\ \pm\frac{1}{2}(|0\rangle-|1\rangle) \otimes (|0\rangle-|1\rangle) & \text{if } f(0) \neq f(1) \end{cases} \quad (121)$$

Eventually, the application of the operator

$$\hat{A}_H \otimes I = \frac{1}{\sqrt{2}} \begin{bmatrix} 1 & 0 & 1 & 0 \\ 0 & 1 & 0 & 1 \\ 1 & 0 & -1 & 0 \\ 0 & 1 & 0 & -1 \end{bmatrix} \quad (122)$$

to the output state  $|\psi_{OUT}\rangle$  yields

$$|\psi_2\rangle = \begin{cases} \pm\frac{1}{\sqrt{2}}|0\rangle \otimes (|0\rangle-|1\rangle) & \text{if } f(0) = f(1) \\ \pm\frac{1}{\sqrt{2}}|1\rangle \otimes (|0\rangle-|1\rangle) & \text{if } f(0) \neq f(1) \end{cases} \quad (123)$$

which can be expressed in a more compact form, since  $f(0) \oplus f(1) = 0$  if  $f(0) = f(1)$ , and  $f(0) \oplus f(1) = 1$  if  $f(0) \neq f(1)$ :

$$|\psi_2\rangle = \pm\frac{1}{\sqrt{2}}|f(0) \oplus f(1)\rangle \otimes (|0\rangle - |1\rangle) \quad (124)$$

Equations (123) and (124) show that measuring the first qubit is sufficient to draw conclusions about the function  $f$ . The Deutsch quantum algorithm therefore speeds up the solution of the problem under investigation because a single measurement is required instead of two as in Tables 7–10.

## 9. Conclusions

The core of the present paper has been the mathematical–physical description of one- and two-qubit quantum gates, in the case of qubits encoded by using spin states of electrons confined within quantum dots. The matrices representing these quantum gates have been deduced from the solution of the Schrödinger equation by employing a mathematical formalism designed to be as accessible as possible for electronics engineers who do not enjoy the more speculative formalism of theoretical physics.

The deduction clearly reveals that, from a physical standpoint, quantum gates are obtained by applying a microwave pulse with the appropriate frequency and duration to manipulate the electron spins. This understanding holds significant importance as it provides the conceptual foundation for electronics engineers responsible for designing the radio frequency integrated circuits that control the qubits.

In addition, the paper has also described the nature of a quantum microprocessor within the frame of a finite-state machine, a common notion to any electronics engineer. In particular, the analogy between the behavior of a quantum finite-state machine and the historical experiment of the fringe patterns clearly points out the quantum nature of the quantum microprocessor. The considerations carried out in Section 2, together with the contents of Sections 5 and 7, suggest that a quantum microprocessor can be considered as a very sophisticated interferometric engine that is controlled by a precise sequence of microwave pulses operating on the same qubit network. From this point of view, a quantum microprocessor is similar to a musical instrument. It is the sequence (quantum algorithm) with which you excite the instrument (the qubit network) that generates the musical motif (the output of the quantum microprocessor).

This simplifies the task for a designer, enabling a clearer understanding of the purpose of the circuits they are designing and how a quantum computation occurs at the physical level. These insights are crucial, as they empower a designer to gain a deeper understanding

and make informed judgments regarding the specifications under which they are tasked with designing cryogenic integrated circuitry for a quantum processor.

In conclusion, since, on the one hand, several textbooks on quantum computing introduce quantum gates as pure mathematical objects without providing their mathematical–physical background, while, on the other hand, physics textbooks address qubit physical systems with a mathematical formalism, which is challenging for electronics engineers to follow, it is the authors’ opinion that the present paper may contribute to demystifying quantum microprocessors for electronics engineers. It is also the authors’ opinion that the present paper may enhance the information exchange between engineers and physicists who collaborate in the development of quantum microprocessors, a research field of significant interest in microelectronics today.

As a final remark, it is worth observing that the methodology employed in the present paper for electron spin qubits may be extended to superconductive qubits. In the case of a single superconductive qubit, Bardin and colleagues have indeed presented a Hamiltonian in a matrix form that bears similarities to Equation (40) [48]. Similarly, in the case of two capacitive-coupled superconductive qubits, Krantz and collaborators have reported a Hamiltonian with a structure akin to the Hamiltonian for two spins coupled by an exchange interaction [49], which is similar to Equation (72). This leads to the conclusion that the methodology adopted in the present paper can be extended to other physical implementations of qubits.

**Author Contributions:** Conceptualization, methodology, software, validation, data curation, and supervision, M.B.; formal analysis, investigation, writing—review and editing, visualization, M.B. and A.B. All authors have read and agreed to the published version of the manuscript.

**Funding:** This research received no external funding.

**Data Availability Statement:** Data are contained within the article.

**Conflicts of Interest:** The authors declare no conflict of interest.

## Appendix A

The first equation in Equation (39) yields

$$\beta(t) = \frac{j}{\omega_1} \left[ \frac{\partial \alpha(t)}{\partial t} + j\omega_0 \alpha(t) \right] e^{j\omega t} \quad (\text{A1})$$

which, once replaced in the second equation, leads to the following differential equation in the unknown  $\alpha(t)$ :

$$\frac{\partial^2 \alpha(t)}{\partial t^2} + j\omega \frac{\partial \alpha(t)}{\partial t} + (\omega_0^2 + \omega_1^2 - \omega\omega_0) \alpha(t) = 0 \quad (\text{A2})$$

Possible solutions are of the form  $\alpha(t) = e^{j\lambda t}$ , so you obtain from Equation (A2) the following algebraic equation:

$$\lambda^2 + \omega\lambda - (\omega_0^2 + \omega_1^2 - \omega\omega_0) = 0 \quad (\text{A3})$$

whose two solutions  $\lambda_{1,2}$  are as follows:

$$\lambda_1 = -\frac{\omega}{2} - \sqrt{\omega_1^2 + \left(\omega_0 - \frac{\omega}{2}\right)^2} \quad (\text{A4})$$

$$\lambda_2 = -\frac{\omega}{2} + \sqrt{\omega_1^2 + \left(\omega_0 - \frac{\omega}{2}\right)^2} \quad (\text{A5})$$

The general solution of Equation (A2) is therefore

$$\alpha(t) = K_1 e^{j\lambda_1 t} + K_2 e^{j\lambda_2 t} \tag{A6}$$

where the two constants  $K_1$  and  $K_2$  are set by the initial conditions. The substitution of Equation (A6) into Equation (A1) yields

$$\beta(t) = -\frac{K_1 e^{j\lambda_1 t}(\lambda_1 + \omega_0) + K_2 e^{j\lambda_2 t}(\lambda_2 + \omega_0)}{\omega_1} \tag{A7}$$

with the generic initial conditions  $\alpha(t = 0) = \alpha_0$  and  $\beta(t = 0) = \beta_0$ . Equations (A6) and (A7) yield the following algebraic systems in the unknown  $K_1$  and  $K_2$ :

$$\begin{cases} \alpha_0 = K_1 + K_2 \\ \beta_0 = -\frac{K_1(\lambda_1 + \omega_0) + K_2(\lambda_2 + \omega_0)}{\omega_1} \end{cases} \tag{A8}$$

whose solutions are as follows:

$$K_1 = \frac{\alpha_0(\lambda_2 + \omega_0) + \omega_1 \beta_0}{\lambda_2 - \lambda_1} \tag{A9}$$

$$K_2 = \frac{\alpha_0(\lambda_1 + \omega_0) + \omega_1 \beta_0}{\lambda_1 - \lambda_2} \tag{A10}$$

For the initial conditions  $\alpha_0 = 0$  and  $\beta_0 = 1$ , Equations (A9) and (A10) yield

$$K_1 = \frac{\omega_1}{\lambda_2 - \lambda_1} \tag{A11}$$

$$K_2 = \frac{\omega_1}{\lambda_1 - \lambda_2} \tag{A12}$$

From which, in virtue of Equations (A4) and (A5), you obtain the following:

$$K_1 = -K_2 = \frac{\omega_1}{2\sqrt{\omega_1^2 + (\omega_0 - \frac{\omega}{2})^2}} \tag{A13}$$

Finally, the substitution of Equations (A4), (A5), and (A13) into Equations (A6) and (A7) leads to the wanted mathematical expressions of  $\alpha(t)$  and  $\beta(t)$ :

$$\alpha(t) = \frac{\omega_1 \left[ e^{-j\frac{\omega}{2}t} e^{-j\sqrt{\omega_1^2 + (\omega_0 - \frac{\omega}{2})^2}t} - e^{-j\frac{\omega}{2}t} e^{j\sqrt{\omega_1^2 + (\omega_0 - \frac{\omega}{2})^2}t} \right]}{2\sqrt{\omega_1^2 + (\omega_0 - \frac{\omega}{2})^2}} \tag{A14}$$

$$\beta(t) = \frac{\left[ -\frac{\omega}{2} + \sqrt{\omega_1^2 + (\omega_0 - \frac{\omega}{2})^2} + \omega_0 \right] e^{-j\frac{\omega}{2}t} e^{j\sqrt{\omega_1^2 + (\omega_0 - \frac{\omega}{2})^2}t} - \left[ -\frac{\omega}{2} - \sqrt{\omega_1^2 + (\omega_0 - \frac{\omega}{2})^2} + \omega_0 \right] e^{-j\frac{\omega}{2}t} e^{-j\sqrt{\omega_1^2 + (\omega_0 - \frac{\omega}{2})^2}t}}{2\sqrt{\omega_1^2 + (\omega_0 - \frac{\omega}{2})^2}} \tag{A15}$$

By gathering  $e^{-j\omega/2t}$  and  $(\omega/2 - \omega_0)$ , Equations (A14) and (A15) take the following forms:

$$\alpha(t) = \frac{\omega_1 e^{-j\frac{\omega}{2}t}}{\sqrt{\omega_1^2 + (\omega_0 - \frac{\omega}{2})^2}} \frac{e^{-j\sqrt{\omega_1^2 + (\omega_0 - \frac{\omega}{2})^2}t} - e^{j\sqrt{\omega_1^2 + (\omega_0 - \frac{\omega}{2})^2}t}}{2} \tag{A16}$$

$$\beta(t) = \frac{e^{-j\frac{\omega}{2}t}}{\sqrt{\omega_1^2 + (\omega_0 - \frac{\omega}{2})^2}} \left\{ (\frac{\omega}{2} - \omega_0) \frac{e^{-j\sqrt{\omega_1^2 + (\omega_0 - \frac{\omega}{2})^2}t} - e^{j\sqrt{\omega_1^2 + (\omega_0 - \frac{\omega}{2})^2}t}}{2} + \sqrt{\omega_1^2 + (\omega_0 - \frac{\omega}{2})^2} \frac{e^{j\sqrt{\omega_1^2 + (\omega_0 - \frac{\omega}{2})^2}t} + e^{-j\sqrt{\omega_1^2 + (\omega_0 - \frac{\omega}{2})^2}t}}{2} \right\} \tag{A17}$$

Equations (A16) and (A17) can be further compacted by remembering that  $\sin(x) = (e^{jx} - e^{-jx})/2j$  and  $\cos(x) = (e^{jx} + e^{-jx})/2$ :

$$\alpha(t) = -j \frac{\omega_1 e^{-j\frac{\omega}{2}t}}{\sqrt{\omega_1^2 + (\omega_0 - \frac{\omega}{2})^2}} \sin \left[ \sqrt{\omega_1^2 + (\omega_0 - \frac{\omega}{2})^2} t \right] \tag{A18}$$

$$\beta(t) = \frac{e^{-j\frac{\omega}{2}t}}{\sqrt{\omega_1^2 + (\omega_0 - \frac{\omega}{2})^2}} \left\{ j(\omega_0 - \frac{\omega}{2}) \sin \left[ \sqrt{\omega_1^2 + (\omega_0 - \frac{\omega}{2})^2} t \right] + \sqrt{\omega_1^2 + (\omega_0 - \frac{\omega}{2})^2} \cos \left[ \sqrt{\omega_1^2 + (\omega_0 - \frac{\omega}{2})^2} t \right] \right\} \tag{A19}$$

Under the resonance condition ( $\omega = 2\omega_0$ ), Equations (A18) and (A19) can be simplified into the following mathematical expressions:

$$\alpha(t) = -j e^{-j\omega_0 t} \sin(\omega_1 t) \tag{A20}$$

$$\beta(t) = e^{-j\omega_0 t} \cos(\omega_1 t) \tag{A21}$$

Their substitution into Equation (6) leads to Equation (41).

For the initial condition  $\alpha_0 = 1$  and  $\beta_0 = 0$ , Equations (A9) and (A10) yield

$$K_1 = \frac{\lambda_2 + \omega_0}{\lambda_2 - \lambda_1} \tag{A22}$$

$$K_2 = \frac{\lambda_1 + \omega_0}{\lambda_1 - \lambda_2} \tag{A23}$$

The substitution of Equations (A4), (A5), (A22), and (A23) into Equations (A6) and (A7) leads to the wanted mathematical expressions of  $\alpha(t)$  and  $\beta(t)$ :

$$\alpha(t) = \frac{\omega_0 - \frac{\omega}{2} + \sqrt{\omega_1^2 + (\omega_0 - \frac{\omega}{2})^2}}{2\sqrt{\omega_1^2 + (\omega_0 - \frac{\omega}{2})^2}} e^{-j[\frac{\omega}{2} + \sqrt{\omega_1^2 + (\omega_0 - \frac{\omega}{2})^2}]t} + \frac{-\omega_0 + \frac{\omega}{2} + \sqrt{\omega_1^2 + (\omega_0 - \frac{\omega}{2})^2}}{2\sqrt{\omega_1^2 + (\omega_0 - \frac{\omega}{2})^2}} e^{-j[\frac{\omega}{2} - \sqrt{\omega_1^2 + (\omega_0 - \frac{\omega}{2})^2}]t} \tag{A24}$$

$$\beta(t) = -\frac{\omega_0 - \frac{\omega}{2} + \sqrt{\omega_1^2 + (\omega_0 - \frac{\omega}{2})^2}}{2\omega_1 \sqrt{\omega_1^2 + (\omega_0 - \frac{\omega}{2})^2}} \left[ \omega_0 - \frac{\omega}{2} - \sqrt{\omega_1^2 + (\omega_0 - \frac{\omega}{2})^2} \right] e^{-j[\frac{\omega}{2} + \sqrt{\omega_1^2 + (\omega_0 - \frac{\omega}{2})^2}]t} - \frac{-\omega_0 + \frac{\omega}{2} + \sqrt{\omega_1^2 + (\omega_0 - \frac{\omega}{2})^2}}{2\omega_1 \sqrt{\omega_1^2 + (\omega_0 - \frac{\omega}{2})^2}} \left[ \omega_0 - \frac{\omega}{2} + \sqrt{\omega_1^2 + (\omega_0 - \frac{\omega}{2})^2} \right] e^{-j[\frac{\omega}{2} - \sqrt{\omega_1^2 + (\omega_0 - \frac{\omega}{2})^2}]t} \tag{A25}$$

and with a few operations, Equations (A24) and (A25) can be rewritten in the following forms:

$$\alpha(t) = \frac{e^{-j\frac{\omega}{2}t}}{2\sqrt{\omega_1^2 + (\omega_0 - \frac{\omega}{2})^2}} \left[ j(2\omega_0 - \omega) \frac{e^{-j\sqrt{\omega_1^2 + (\omega_0 - \frac{\omega}{2})^2}t} - e^{j\sqrt{\omega_1^2 + (\omega_0 - \frac{\omega}{2})^2}t}}{2j} + 2\sqrt{\omega_1^2 + (\omega_0 - \frac{\omega}{2})^2} \frac{e^{-j\sqrt{\omega_1^2 + (\omega_0 - \frac{\omega}{2})^2}t} + e^{j\sqrt{\omega_1^2 + (\omega_0 - \frac{\omega}{2})^2}t}}{2} \right] \tag{A26}$$

$$\beta(t) = \frac{j\omega_1^2 e^{-j\frac{\omega}{2}t}}{\omega_1 \sqrt{\omega_1^2 + (\omega_0 - \frac{\omega}{2})^2}} \frac{e^{-j\sqrt{\omega_1^2 + (\omega_0 - \frac{\omega}{2})^2}t} - e^{j\sqrt{\omega_1^2 + (\omega_0 - \frac{\omega}{2})^2}t}}{2j} \tag{A27}$$



By remembering that  $\sin(x) = (e^{jx} - e^{-jx})/2j$  and  $\cos(x) = (e^{jx} + e^{-jx})/2$ , you obtain the following:

$$\alpha(t) = \frac{e^{-j\frac{\omega}{2}t}}{2\sqrt{\omega_1^2 + (\omega_0 - \frac{\omega}{2})^2}} \left[ -j(2\omega_0 - \omega)\sin\sqrt{\omega_1^2 + (\omega_0 - \frac{\omega}{2})^2}t + 2\sqrt{\omega_1^2 + (\omega_0 - \frac{\omega}{2})^2}\cos\sqrt{\omega_1^2 + (\omega_0 - \frac{\omega}{2})^2}t \right] \tag{A28}$$

$$\beta(t) = -\frac{j\omega_1 e^{-j\frac{\omega}{2}t}}{\sqrt{\omega_1^2 + (\omega_0 - \frac{\omega}{2})^2}} \sin\sqrt{\omega_1^2 + (\omega_0 - \frac{\omega}{2})^2}t \tag{A29}$$

Under resonance condition ( $\omega = 2\omega_0$ ), Equations (A28) and (A29) reduce to

$$\alpha(t) = e^{-j\omega_0 t} \cos\omega_1 t \tag{A30}$$

$$\beta(t) = e^{-j\omega_0 t} e^{-j\frac{\pi}{2}} \sin\omega_1 t \tag{A31}$$

Their substitution into Equation (6) leads to Equation (42).

### Appendix B

Remembering Euler’s formula  $e^{jx} = \cos x + j\sin x$ , Equation (44) takes the following form:

$$\begin{cases} \frac{\partial \alpha(t)}{\partial t} = -j\omega_0 \alpha(t) - \omega_1 \beta(t) e^{-j\omega t} \\ \frac{\partial \beta(t)}{\partial t} = \omega_1 e^{j\omega t} \alpha(t) + j\omega_0 \beta(t) \end{cases} \tag{A32}$$

The first equation in the system (A32) yields

$$\beta(t) = \frac{\frac{\partial \alpha(t)}{\partial t} + j\omega_0 \alpha(t)}{-\omega_1 e^{-j\omega t}} = -\frac{1}{\omega_1} \left[ \frac{\partial \alpha(t)}{\partial t} + j\omega_0 \alpha(t) \right] e^{j\omega t} \tag{A33}$$

which, in its turn, once replaced in the second equation, leads to Equation (A2). Also, for the magnetic field with the components  $B_x$  and  $B_y$  at the quadrature,  $\alpha(t)$  takes the form of Equation (A6). On the other hand, since Equation (A33) can be obtained from Equation (A1) by multiplying by  $j$ , you obtain the following from Equation (A7):

$$\beta(t) = -j \frac{K_1 e^{j\lambda_1 t} (\lambda_1 + \omega_0) + K_2 e^{j\lambda_2 t} (\lambda_2 + \omega_0)}{\omega_1} \tag{A34}$$

with the generic initial conditions  $\alpha(t = 0) = \alpha_0$  and  $\beta(t = 0) = \beta_0$ . Equations (A6) and (A34) yield the following algebraic systems in the unknown  $K_1$  and  $K_2$ :

$$\begin{cases} \alpha_0 = K_1 + K_2 \\ \beta_0 = -j \frac{K_1 (\lambda_1 + \omega_0) + K_2 (\lambda_2 + \omega_0)}{\omega_1} \end{cases} \tag{A35}$$

whose solutions are as follows:

$$K_1 = \frac{j\alpha_0 (\lambda_2 + \omega_0) + \omega_1 \beta_0}{j(\lambda_2 - \lambda_1)} \tag{A36}$$

$$K_2 = \frac{j\alpha_0 (\lambda_1 + \omega_0) + \omega_1 \beta_0}{j(\lambda_1 - \lambda_2)} \tag{A37}$$

For the initial conditions  $\alpha_0 = 0$  and  $\beta_0 = 1$ , Equations (A36) and (A37) yield

$$K_1 = \frac{\omega_1}{j(\lambda_2 - \lambda_1)} \tag{A38}$$

$$K_2 = \frac{\omega_1}{j(\lambda_1 - \lambda_2)} \tag{A39}$$

Equations (A38) and (A39) are identical to Equations (A11) and (A12) but divided by  $j$ . Since, in virtue of Equation (A6),  $\alpha(t)$  is proportional to  $K_1$  and  $K_2$ , and  $\lambda_1$  and  $\lambda_2$  are given by Equations (A4) and (A5), which are calculated before the introduction of the in-phase or in-quadrature conditions for the components  $B_x$  and  $B_y$ , the mathematical expression of  $\alpha(t)$  for the in-quadrature condition can be derived by dividing Equation (A18) by  $j$ :

$$\alpha(t) = -\frac{\omega_1 e^{-j\frac{\omega}{2}t}}{\sqrt{\omega_1^2 + (\omega_0 - \frac{\omega}{2})^2}} \sin \left[ \sqrt{\omega_1^2 + (\omega_0 - \frac{\omega}{2})^2} t \right] \tag{A40}$$

On the other hand, since Equation (A34) was obtained from Equation (A1) by multiplying by  $j$  and Equation (A34) also shows that  $\beta(t)$  is proportional to  $K_1$  and  $K_2$ , the mathematical expression of  $\beta(t)$  is given by Equation (A19). At the resonance ( $\omega = 2\omega_0$ ), Equations (A40) and (A19) reduce to

$$\alpha(t) = -e^{-j\omega_0 t} \sin(\omega_1 t) \tag{A41}$$

$$\beta(t) = e^{-j\omega_0 t} \cos(\omega_1 t) \tag{A42}$$

The substitution of Equations (A41) and (A42) into Equation (6) yields Equation (45). For the initial conditions  $\alpha_0 = 1$  and  $\beta_0 = 0$ , Equations (A36) and (A37) yield

$$K_1 = \frac{\lambda_2 + \omega_0}{\lambda_2 - \lambda_1} \tag{A43}$$

$$K_2 = \frac{\lambda_1 + \omega_0}{\lambda_1 - \lambda_2} \tag{A44}$$

These equations are identical to Equations (A22) and (A23). Consequently, since, as previously remarked, Equation (A6) yields the mathematical form of  $\alpha(t)$  for the in-phase and the in-quadrature condition for  $B_x$  and  $B_y$ , Equation (A28) is the wanted mathematical expression of  $\alpha(t)$ . Similarly, since Equation (A34) was obtained from Equation (A2) by multiplying by  $j$ , Equations (A23) and (A24) imply that the mathematical expression of  $\beta(t)$  is given by Equation (A29) multiplied by  $j$ :

$$\beta(t) = -j \frac{j\omega_1 e^{-j\frac{\omega}{2}t}}{\sqrt{\omega_1^2 + (\omega_0 - \frac{\omega}{2})^2}} \sin \sqrt{\omega_1^2 + (\omega_0 - \frac{\omega}{2})^2} t \tag{A45}$$

At the resonance ( $\omega = 2\omega_0$ ), Equations (A28) and (A45) reduce to

$$\alpha(t) = e^{-j\omega_0 t} \cos \omega_1 t \tag{A46}$$

$$\beta(t) = e^{-j\omega_0 t} \sin \omega_1 t \tag{A47}$$

The substitution of Equations (A46) and (A47) into Equation (6) yields Equation (46).

### Appendix C

The Fourier transform is performed on the envelope signals to assess their spectral content:

$$\mathcal{F}\{x(t)\} = X(f) = \int_{-\infty}^{+\infty} x(t) e^{-2\pi i f t} dt \tag{A48}$$

After Equation (A48), the corresponding Fourier  $X(f)$  transforms for the sinusoidal, rectangular, and Gaussian envelopes are calculated as follows:

Appendix C.1 Sinusoidal Envelope

$$x(t) = \begin{cases} \cos\left(\frac{\pi t}{2T}\right), & \text{if } -T < t < T \\ 0 & \text{otherwise} \end{cases} \tag{A49}$$

with  $f_0 = \frac{1}{4T}$ .

Its  $X(f)$  is as follows:

$$\begin{aligned} X(f) &= \int_{-T}^T \cos\left(\frac{\pi t}{2T}\right) e^{-2\pi i f t} dt \\ &= \int_{-T}^T \cos(2\pi f_0 t) e^{-2\pi i f t} dt \\ &= \int_{-T}^T \frac{e^{2\pi i f_0 t} + e^{-2\pi i f_0 t}}{2} e^{-2\pi i f t} dt \\ &= \frac{1}{2} \left[ \int_{-T}^T e^{-2\pi i (f-f_0)t} dt + \int_{-T}^T e^{-2\pi i (f+f_0)t} dt \right] \\ &= \frac{1}{2} \left[ \frac{e^{-2\pi i (f-f_0)T} - e^{-2\pi i (f-f_0)(-T)}}{-2\pi i (f-f_0)} + \frac{e^{-2\pi i (f+f_0)T} - e^{-2\pi i (f+f_0)(-T)}}{-2\pi i (f+f_0)} \right] \\ &= \frac{1}{2} \left[ \frac{e^{2\pi i (f-f_0)T} - e^{-2\pi i (f-f_0)T}}{2\pi i (f-f_0)} + \frac{e^{2\pi i (f+f_0)T} - e^{-2\pi i (f+f_0)T}}{2\pi i (f+f_0)} \right] \\ &= \frac{\sin[2\pi (f-f_0)T]}{2\pi (f-f_0)} + \frac{\sin[2\pi (f+f_0)T]}{2\pi (f+f_0)} \\ &= T \operatorname{sinc}[2\pi (f-f_0)T] + T \operatorname{sinc}[2\pi (f+f_0)T] \\ &= T \operatorname{sinc}\left[2\pi \left(f - \frac{1}{4T}\right)T\right] + T \operatorname{sinc}\left[2\pi \left(f + \frac{1}{4T}\right)T\right] \end{aligned} \tag{A50}$$

Appendix C.2 Rectangular Envelope

$$x(t) = \begin{cases} 1, & \text{if } -T < t < T \\ 0, & \text{otherwise} \end{cases} \tag{A51}$$

whose  $X(f)$  is as follows:

$$\begin{aligned} zX(f) &= \int_{-T}^T e^{-2\pi i f t} dt \\ &= \left[ \frac{e^{-2\pi i f t}}{-2\pi i f} \right]_{-T}^T \\ &= \left( \frac{e^{2\pi i f T} - e^{-2\pi i f T}}{2\pi i f} \right) \\ &= \frac{\sin(2\pi f T)}{\pi f} \\ &= 2T \operatorname{sinc}(2\pi f T) \end{aligned} \tag{A52}$$

Appendix C.3 Gaussian Envelope

$$x(t) = \begin{cases} e^{-bt^2}, & \text{if } -T < t < T \\ 0, & \text{otherwise} \end{cases} \tag{A53}$$

whose  $X(f)$  is as follows:

$$\begin{aligned} X(f) &= \int_{-T}^T e^{-bt^2} e^{-2\pi i f t} dt \\ &= e^{-\frac{\pi^2 f^2}{b}} \int_{-T}^T e^{-(\sqrt{bt} + i\frac{\pi f}{\sqrt{b}})^2} dt \\ &= \frac{\sqrt{\pi}}{2} e^{-\frac{\pi^2 f^2}{b}} \left[ \frac{2}{\sqrt{\pi}} \int_0^T e^{-(\sqrt{bt} + i\frac{\pi f}{\sqrt{b}})^2} dt - \frac{2}{\sqrt{\pi}} \int_0^{-T} e^{-(\sqrt{bt} + i\frac{\pi f}{\sqrt{b}})^2} dt \right] \\ &= \frac{1}{2} \sqrt{\frac{\pi}{b}} e^{-\frac{\pi^2 f^2}{b}} \left[ \operatorname{erf}\left(\frac{bT + i\pi f}{\sqrt{b}}\right) - \operatorname{erf}\left(\frac{-bT + i\pi f}{\sqrt{b}}\right) \right] \\ &= \frac{i}{2} \sqrt{\frac{\pi}{b}} e^{-\frac{\pi^2 f^2}{b}} \left[ \operatorname{erfi}\left(\frac{\pi f - ibT}{\sqrt{b}}\right) - \operatorname{erfi}\left(\frac{\pi f + ibT}{\sqrt{b}}\right) \right] \end{aligned} \tag{A54}$$

where

$$\operatorname{erf}(x) = \frac{2}{\sqrt{\pi}} \int_0^x e^{-t^2} dt$$

$$\operatorname{erfi}(x) = -i \operatorname{erf}(ix)$$

In Figure A1, the extended integration window with  $T \rightarrow +\infty$  was assumed for simplicity, in order to plot the spectrum. Under this assumption, Equation (A54) reduces to

$$X(f) = \sqrt{\frac{\pi}{b}} e^{-\frac{\pi^2 f^2}{b}} \quad (\text{A55})$$

whose module squared is simply

$$|X(f)|^2 = \frac{\pi}{b} e^{-\frac{2\pi^2 f^2}{b}} \quad (\text{A56})$$

Figure A1 shows that the rectangular envelope exhibits the broadest spectrum.

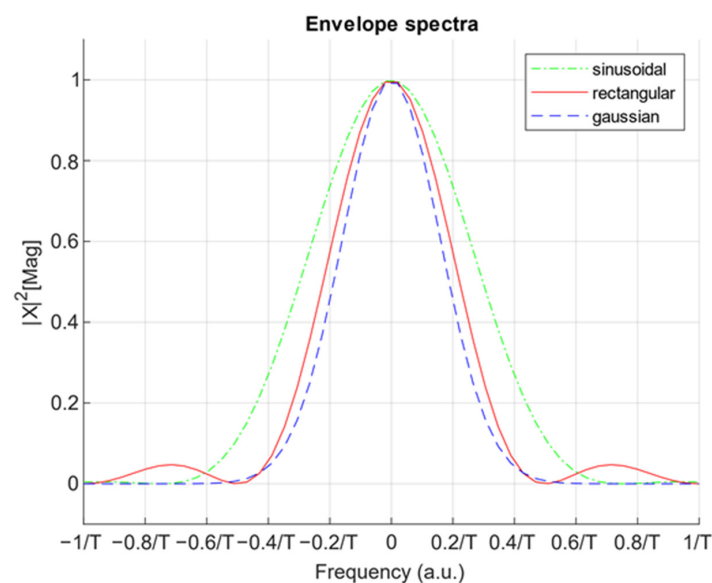


Figure A1. Sinusoidal, rectangular, and Gaussian ( $b = 1$ ) pulse spectra. All amplitudes normalized.

## References

1. Murphy, A.; Tucker, H. The Global 2000. *Forbes*. 8 June 2023. Available online: <https://www.forbes.com/lists/global2000/> (accessed on 31 July 2023).
2. Faggin, F.; Hoff, M.E., Jr.; Mazor, S.; Shima, M. The History of the 4004. *IEEE Micro* **1996**, *16*, 10–20. [CrossRef]
3. Nielsen, M.A.; Chuang, I.L. *Quantum Computation and Quantum Information*, 7th ed.; Cambridge University Press: New York, NY, USA, 2010; ISBN 978-1-10700-217-3.
4. Shor, P.W. Algorithms for Quantum Computation: Discrete Logarithms and Factoring. In Proceedings of the 35th Annual Symposium on Foundation of Computer Science, Washington, DC, USA, 20–22 November 1994. [CrossRef]
5. Harrow, A.W.; Hassidim, A.; Lloyd, A. Quantum Algorithm for Linear Systems of Equations. *Phys. Rev. Lett.* **2009**, *103*, 150502. [CrossRef] [PubMed]
6. Shapiro, A. NVIDIA, Rolls-Royce and Classiq Announce Quantum Computing Breakthrough for Computational Fluid Dynamics in Jet Engines. July 2023. Available online: <https://nvidianews.nvidia.com/news/nvidia-rolls-royce-and-classiq-announce-quantum-computing-breakthrough-for-computational-fluid-dynamics-in-jet-engines> (accessed on 31 July 2023).
7. Shaikh, T.A.; Ali, R. Quantum Computing in Big Data Analytics: A Survey. In Proceedings of the IEEE International Conference on Computer and Information Technology, Nadi, Fiji, 8–10 December 2016. [CrossRef]
8. Zhang, X.; Zhao, Y.Q.; Li, R.G.; Li, X.L.; Guo, Z.H.; Zhu, X.M.; Dong, G. The Quantum Shor Algorithm Simulated on FPGA. In Proceedings of the IEEE Intl Conf on Parallel & Distributed Processing with Applications, Big Data & Cloud Computing, Sustainable Computing & Communications, Social Computing & Networking, Xiamen, China, 16–18 December 2019. [CrossRef]
9. Rodriguez, A.G.; Padilla, A.M.; Siudak, R. *Post-Quantum International Security*; Kosciuszko Institute Policy Brief; Kosciuszko Institute: Kraków, Poland, 2020; pp. 1–11.
10. IBM's Roadmap for Scaling Quantum Technology. Available online: <https://research.ibm.com/blog/ibm-quantum-roadmap> (accessed on 31 July 2023).

11. First Quantum Computer to Pack 100 Qubits Enters Crowded Race. Available online: <https://www.nature.com/articles/d41586-021-03476-5> (accessed on 31 July 2023).
12. IBM's New 53-Qubit Quantum Computer Is Its Biggest Yet. Available online: <https://www.cnet.com/tech/computing/ibm-new-53-qubit-quantum-computer-is-its-biggest-yet/> (accessed on 31 July 2023).
13. Kandala, A.; Mezzacapo, A.; Temme, K.; Takita, M.; Brink, M.; Chow, J.M.; Gambetta, J.M. Hardware-efficient variational quantum eigensolver for small molecules and quantum magnets. *Nat. Lett.* **2017**, *549*, 242–246. [CrossRef] [PubMed]
14. Get to Know Honeywell's Latest Quantum Computer System Model H1. Available online: <https://www.honeywell.com/us/en/news/2020/10/get-to-know-honeywell-s-latest-quantum-computer-system-model-h1> (accessed on 31 July 2023).
15. What Intel Is Planning for the Future of Quantum Computing: Hot Qubits, Cold Control Chips, and Rapid Testing. Available online: <https://spectrum.ieee.org/intels-quantum-computing-plans-hot-qubits-cold-control-chips-and-rapid-testing> (accessed on 31 July 2023).
16. Intel's Horse Ridge II Improves the Control of Quantum Computing. Available online: <https://www.eetimes.com/intels-horse-ridge-ii-improves-the-control-for-quantum-computing/> (accessed on 31 July 2023).
17. Hsu, J. CES2018: Intel's 49-Qubit Chips Shoots for Quantum Supremacy. *IEEE Spectrum*. 2018. Available online: <https://spectrum.ieee.org/intels-49qubit-chip-aims-for-quantum-supremacy> (accessed on 31 July 2023).
18. Intel Presents 17-Qubit Superconducting Chip with Advanced Packaging. 2017. Available online: <https://phys.org/news/2017-10-intel-qubit-superconducting-chip-advanced.html> (accessed on 31 July 2023).
19. Google Wants to Build a Useful Quantum Computer by 2029. Available online: <https://www.theverge.com/2021/5/19/22443453/google-quantum-computer-2029-decade-commercial-useful-qubits-quantum-transistor> (accessed on 31 July 2023).
20. Quantum possibilities. *Nat. Phys.* **2018**, *14*, 321. [CrossRef]
21. Arute, F.; Arya, K.; Babbush, R.; Bacon, D.; Bardin, J.C.; Barends, R.; Biswas, R.; Boixo, S.; Brandao, F.G.S.L.; Buell, D.A.; et al. Quantum supremacy using a programmable superconducting processor. *Nature* **2019**, *574*, 505–511. [CrossRef]
22. IonQ Says Its Record-Breaking Quantum Computer Is Most Powerful Ever. Available online: <https://www.newscientist.com/article/2256004-ionq-says-its-record-breaking-quantum-computer-is-most-powerful-ever/> (accessed on 31 July 2023).
23. Wright, K.; Beck, K.M.; Debnath, S.; Amini, J.M.; Nam, Y.; Grzesiak, N.; Chen, J.-S.; Pienti, N.C.; Chmielewski, M.; Collins, C.; et al. Benchmarking an 11-qubit quantum computer. *Nat. Commun.* **2019**, *10*, 5464. [CrossRef] [PubMed]
24. Proctor, T.; Rudinger, K.; Young, K.; Nielsen, E.; Blume-Kohout, R. Measuring the Capabilities of Quantum Computers. *Nat. Phys.* **2022**, *18*, 75–79. [CrossRef]
25. Castelvechi, D. IBM Quantum Computer passes Calculation Milestone. *Nature* **2023**, *618*, 656–657. [CrossRef]
26. Nikandish, R.; Blokhina, E.; Leipold, D.; Staszewski, R.B. Semiconductor Quantum Computing: Towards a CMOS Quantum Computer on Chip. *IEEE Nanotechnol. Mag.* **2021**, *15*, 8–20. [CrossRef]
27. Loss, F.; DiVincenzo, D.P. Quantum computation with quantum dots. *Phys. Rev. A* **1998**, *57*, 120–126. [CrossRef]
28. Kjaergaard, M.; Schwartz, M.E.; Braumuller, J.; Krantz, P.; Wang, J.I.J.; Gustavsson, S.; Olivier, W.D. Superconducting Qubits: Current State of Play. *Annu. Rev. Condens. Matter* **2020**, *11*, 369–395. [CrossRef]
29. Bruzewicz, C.D.; Chiaverini, J.; McConnell, R.; Sage, J.M. Trapped-ion quantum computing: Progress and challenges. *Appl. Phys. Rev.* **2019**, *6*, 021314. [CrossRef]
30. Reilly, D.J. Engineering the quantum-classical interface of solid-states qubits. *NPJ Nat. Quantum Inf.* **2015**, *1*, 15011. [CrossRef]
31. Charbon, E.; Sebastiano, F.; Babaie, M.; Vladimirescu, A.; Shahmohammadi, M.; Staszewski, R.B.; Homulle, H.A.R.; Patra, B.; van Dijk, J.P.G.; Incadela, R.M.; et al. Cryo-CMOS Circuits and Systems for Scalable Quantum Computing. In Proceedings of the IEEE International Solid State Circuits Conference, San Francisco, CA, USA, 5–9 February 2017; pp. 264–266. [CrossRef]
32. Anders, J.; Babaie, M.; Bardin, J.C.; Bashir, I.; Billiot, G.; Blokhina, E.; Bonen, S.; Charbon, E.; Chiaverini, J.; Chuang, I.L.; et al. CMOS Integrated Circuits for the Quantum Information Sciences. *IEEE Trans. Quantum Eng.* **2023**, *4*, 1–30. [CrossRef]
33. Knox Bassett, R. *To the Digital Age*; Johns Hopkins University Press: Baltimore, MD, USA, 2007; ISBN 978-0-80188-639-3.
34. Riordan, M.; Hoddeson, L. *Crystal Fire*; Norton & Company: New York, NY, USA, 1998; ISBN 978-0-39331-851-7.
35. Born, M. Zur Quantenmechanik der Stoßvorgänge. *Z. Phys.* **1926**, *38*, 803–827. [CrossRef]
36. Zettili, N. *Quantum Mechanics: Concepts and Applications*, 3rd ed.; John Wiley & Sons: Hoboken, NJ, USA, 2022; ISBN 978-1-11830-789-2.
37. Susskind, L.; Friedman, A. *Quantum Mechanics. The Theoretical Minimum*; Penguin: London, UK, 2015; ISBN 978-0-14197-781-2.
38. Merli, P.G.; Missiroli, G.F.; Pozzi, G. On the statistical aspect of electron interference phenomena. *Am. J. Phys.* **1976**, *44*, 306–307. [CrossRef]
39. Lambert, K.; Brittan, G.B. *An Introduction to the Philosophy of Science*; Ridgeview Publication Company: Atascadero, CA, USA, 1979; ISBN 978-0-91793-017-1.
40. Dirac, P.A.M. *The Principles of Quantum Mechanics*, 4th ed.; Cambridge University Press: Cambridge, UK, 1988; ISBN 978-0-19852-011-5.
41. Pais, A. George Uhlenbeck and the Discovery of Electron Spin. *Phys. Today* **1989**, *42*, 34–40. [CrossRef]
42. Yu, X.-T.; Zhang, Q.; Ban, Y.; Chen, X. Fast and robust control of two interacting spins. *Phys. Rev. A* **2018**, *97*, 062317. [CrossRef]
43. Albertini, F.; D'Alessandro, D. The Lie algebra structure and controllability of spin systems. *Linear Algebra Its Appl.* **2002**, *350*, 213–235. [CrossRef]
44. Dumoulin Stuyck, N.I.; Mohiyaddin, F.A.; Li, R.; Heyns, M.; Govoreanu, B.; Radu, I.P. Low dephasing and robust micromagnet designs for silicon spin qubits. *Appl. Phys. Lett.* **2021**, *119*, 094001. [CrossRef]

45. Laucht, A.; Muhonen, J.T.; Mohiyaddin, F.A.; Kalra, R.; Dehollain, J.P.; Freer, S.; Hudson, F.E.; Veldhorst, M.; Rahman, R.; Klimeck, G.; et al. Electrically controlling single-spin qubits in a continuous microwave field. *Sci. Adv.* **2015**, *1*, e1500022. [[CrossRef](#)]
46. Giannantoni, C. *Linear Differential Equations with Variable Coefficients: The Fundamental Theorem of the Solving Kernel*; ENEA Technical Report RT/ERG/95/07; ENEA: Kista, Sweden, 1995.
47. Bergou, J.A.; Hillery, M. *Introduction to the Theory of Quantum Information Processing*; Springer: Berlin/Heidelberg, Germany, 2015; ISBN 978-1-48999-843-8.
48. Bardin, J.C.; Sank, D.; Naaman, O.; Jeffrey, E. Quantum Computing. *IEEE Microw. Mag.* **2020**, *21*, 24–44. [[CrossRef](#)]
49. Krantz, P.; Kjaergaard, M.; Yan, F.; Orlando, T.P.; Gustavsson, S.; Oliver, W.D. A quantum engineer's guide to superconducting qubits. *Appl. Phys. Rev.* **2019**, *6*, 021318. [[CrossRef](#)]

**Disclaimer/Publisher's Note:** The statements, opinions and data contained in all publications are solely those of the individual author(s) and contributor(s) and not of MDPI and/or the editor(s). MDPI and/or the editor(s) disclaim responsibility for any injury to people or property resulting from any ideas, methods, instructions or products referred to in the content.